1977

Polariton effects in naphthalene crystals

Susan Louise Robinette
Iowa State University

INFORMATION TO USERS

This material was produced from a microfilm copy of the original document. While the most advanced technological means to photograph and reproduce this document have been used, the quality is heavily dependent upon the quality of the original submitted.

The following explanation of techniques is provided to help you understand markings or patterns which may appear on this reproduction.

1. The sign or "target" for pages apparently lacking from the document photographed is "Missing Page(s)". If it was possible to obtain the missing page(s) or section, they are spliced into the film along with adjacent pages. This may have necessitated cutting thru an image and duplicating adjacent pages to insure you complete continuity.

2. When an image on the film is obliterated with a large round black mark, it is an indication that the photographer suspected that the copy may have moved during exposure and thus cause a blurred image. You will find a good image of the page in the adjacent frame.

3. When a map, drawing or chart, etc., was part of the material being photographed the photographer followed a definite method in "sectioning" the material. It is customary to begin photoing at the upper left hand corner of a large sheet and to continue photoing from left to right in equal sections with a small overlap. If necessary, sectioning is continued again – beginning below the first row and continuing on until complete.

4. The majority of users indicate that the textual content is of greatest value, however, a somewhat higher quality reproduction could be made from "photographs" if essential to the understanding of the dissertation. Silver prints of "photographs" may be ordered at additional charge by writing the Order Department, giving the catalog number, title, author and specific pages you wish reproduced.

5. PLEASE NOTE: Some pages may have indistinct print. Filmed as received.

University Microfilms International
300 North Zeeb Road
Ann Arbor, Michigan 48106 USA
St. John's Road, Tyler's Green
High Wycombe, Bucks, England HP10 8HR

Polariton effects in naphthalene crystals

by

Susan Louise Robinette

A Dissertation Submitted to the
Graduate Faculty in Partial Fulfillment of
The Requirements for the Degree of
DOCTOR OF PHILOSOPHY

Department: Chemistry
Major: Physical Chemistry

Approved:

Signature was redacted for privacy.

In Charge of Major Work

Signature was redacted for privacy.

For the Major Department

Signature was redacted for privacy.

For the Graduate College

Iowa State University
Ames, Iowa

1977

TABLE OF CONTENTS

	Page
QUOTATION	viii
INTRODUCTION	1
THEORY AND DISCUSSION	14
Preface	14
Language	14
Exciton State Viewpoint	15
Electromagnetic Modes of Media	19
Lorentz Model	26
Retardation	29
Polariton Models	33
Volume and anisotropy effects	36
Spatial vs. temporal damping	38
Spatial dispersion	41
Boundary conditions	45
Second quantization formalism	46
Exciton-Phonon and Polariton-Phonon Interactions	58
Exciton-phonon coupling in crystals with two molecules per unit cell	58
Thermal broadening and exciton-phonon interaction	62
Urbach rule behavior	66
Polariton-phonon coupling	67
EXPERIMENTAL	72
Liquid Helium Cryostats and Spectrometers	72
Light Sources, Filters and Polarizers	73
Calibration and Intensity Measurements	74
Sample Handling	74

Strain-Free Mounting 76

Sample Preparation 78

Purification 78
Crystal growth 78
Mixed crystals 83

RESULTS AND DISCUSSION 85

Computer Spectra 85

Interference modes 113

Pure Crystal Spectra 118

Temperature dependence 122
Band shapes 143
Strained, pure crystals 144

Doped Crystals 147

β-methylnaphthalene 147
Anthracene 151
Depolarization spectra 154

Emission Experiments 159

Exciton-phonon coupling parameters 160

CONCLUSIONS 164

REFERENCES 166

ACKNOWLEDGMENTS 183

LIST OF FIGURES

		Page
Figure 1.	Coulomb exciton and polariton dispersion relations	32
Figure 2.	Effect of spatial vs temporal damping on polariton dispersion curves	40
Figure 3.	Exciton-phonon and polariton-phonon scattering processes	70
Figure 4.	Strain-free sample holder	77
Figure 5.	Covered beaker sublimation apparatus	79
Figure 6.	Covered beaker sublimation apparatus	80
Figure 7.	Vacuum sublimation apparatus	82
Figure 8.	Computer generated reflection, transmission and absorption for a 0.3 μ crystal	87
Figure 9.	Computer generated reflection, transmission and absorption for a 0.6 μ crystal	88
Figure 10.	Computer generated reflection, transmission and absorption for a 1.3 μ crystal	89
Figure 11.	Computer generaged reflection, transmission and absorption for a 3.2 μ crystal	91
Figure 12.	Computer generated reflection, transmission and absorption for a 5 μ crystal	94
Figure 13.	Computer generated reflection, transmission and absorption for a 6.3 μ crystal	97
Figure 14.	Computer generated reflection, transmission and absorption for a 10 μ crystal	100
Figure 15.	Computer generated reflection, transmission and absorption for a 12.7 μ crystal	103
Figure 16.	Computer generated reflection, transmission and absorption	105

Figure 17.	Computer generated reflection, transmission and absorption	106
Figure 18.	Computer generated reflection, transmission and absorption	108
Figure 19.	Computer generated reflection, transmission and absorption	109
Figure 20.	Idealized dielectric slab of thickness 2a	110
Figure 21.	Computer generated interference modes	114
Figure 22.	Polarized transmission 0.94 μ strain-free naphthalene crystal	116
Figure 23.	Thickness dependent interference modes in the $\underset{\sim}{b}(0,0)$ region	117
Figure 24.	$S_{1\leftarrow 0}$ absorption in perfect naphthalene crystal	119
Figure 25.	Enlargement of the "M" band region in perfect crystal	121
Figure 26.	Spectral profile of the naphthalene $\underset{\sim}{a}(0,0)$ band as a function of temperature	123
Figure 27.	Spectral profile of the naphthalene $\underset{\sim}{a}(0,0)$ band as a function of temperature	126
Figure 28.	Spectral profile of the naphthalene $\underset{\sim}{a}(0,0)$ band as a function of temperature	128
Figure 29.	Spectral profile of the naphthalene $\underset{\sim}{a}(0,0)$ band as a function of temperature	129
Figure 30.	Area of $\underset{\sim}{a}(0,0)$ in perfect, strain-free $\sim$2.5 μ naphthalene crystal as a function of temperature	132
Figure 31.	Area of $\underset{\sim}{a}(0,0)$ in perfect, strain-free $\geq$ 10 μ naphthalene crystal as a function of temperature	134

Figure 32.	Area of $\underset{\sim}{a}(0,0)$ for several perfect crystals as a function of temperature	135
Figure 33.	Area of $\underset{\sim}{a}(0,0)$ and 370 cm^{-1} band as a function of temperature for 2.3 μ crystals	136
Figure 34.	$\underset{\sim}{a}(0,0)$ full width-half maxima for several pure strain-free naphthalene crystals	138
Figure 35.	$\underset{\sim}{a}(0,0)$ full width-half maxima for several pure strain-free naphthalene crystals	139
Figure 36.	$\underset{\sim}{a}(0,0)$ full width-half maxima for >5 μ pure strain-free naphthalene crystal	140
Figure 37.	Comparison of FWHM of $\underset{\sim}{a}(0,0)$ and 370 cm^{-1} bands in pure, strain-free naphthalene crystal	141
Figure 38.	Energy shift of $\underset{\sim}{a}(0,0)$ vs temperature for two perfect crystals	142
Figure 39.	Temperature dependence of $\underset{\sim}{a}(0,0)$ area in pure crystals	145
Figure 40.	FWHM behavior in pure, strained crystals	146
Figure 41.	Comparison of heavily doped and highly strained crystals	148
Figure 42.	$\underset{\sim}{a}(0,0)$ area increase in 10^{-4} m/m βMN doped naphthalene crystal	149
Figure 43.	FWHM behavior for 10^{-4} m/m βMN doped naphthalene crystal	150
Figure 44.	$\underset{\sim}{a}(0,0)$ area increase with temperature for anthracene crystals	152
Figure 45.	FWHM behavior for anthracene doped naphthalene crystals	153
Figure 46.	Depolarization effect in $S_{0\leftarrow 1}$ naphthalene spectrum	156

Figure 47. Depolarization effect in perfect crystal a(0,0) as function of temperature 157

Figure 48. Comparison of experimental band broadening to phonon occupation number curves 162

QUOTATION

"We are now entering/in the age of Aquarius with the complementary sign of Leo. Aquarius is an air sign, signifying waves, especially of vibration or electricity."

The 1977 Lunar Calendar

INTRODUCTION

Two different approaches are frequently used to describe the interaction of light with crystal exciton states: one is macroscopic and based essentially on classical optics (Maxwell's equations) and the other, quantum mechanical. When spatial dispersion effects are included, the classical model should yield the same results as the quantum mechanical but to date this has not been easy to demonstrate and workers have used either one or the other approach depending on the problem being addressed.

The essential point of this dissertation is that the polariton model is not a further refinement of the existing microscopic quantum mechanical theory but requires a discontinuous and rather basic shift in emphasis. The problem lies in the nature of the coupling to the photon field. Most early exciton work (Frenkel or Wannier-Mott) simply considered the coupling weak (manageable by perturbation theory) and got on with the business of spectroscopically measuring or calculating effects in "crystal exciton states". The polariton model on the other hand presumes a strong coupling between resonant crystal states and the radiation field (i.e., perturbation treatments not allowed) which always exists. Other interactions such as exciton-phonon or exciton-defect must then be considered as strong or weak relative to this "primary" interaction.

Over the past 30 years interest in exciton states (1-9) (here defined as electronic resonance states weakly coupled to the radiation field) has flourished. Naphthalene and anthracene have become prototype molecular crystals much as CdS is a prototype semiconductor. They have been studied by a variety of spectroscopic methods and have given rise to a host of theoretical treatments. Although the first theoretical description of exciton states in molecular crystals was introduced in 1931 by Frenkel (10), nearly twenty years passed before the formalism began to be used by spectroscopists to explain stationary state (Coulomb exciton) properties such as the formation of exciton bands and the gas to crystal energy shifts of spectral lines. The experimental confirmation (11,12,13) in the 1950's of the theoretical predictions by Davydov (14) concerning factor group (Davydov) splittings was a major triumph for the microscopic approach.

Today, interest in aromatic molecular crystals seems far from exhausted (4,15). Indeed, in many respects, it appears we have hardly scratched the surface. Current research addresses a number of problems of which most continue to focus on exciton as opposed to polariton effects. An overview here of some of the more pertinent exciton work seems, therefore, in order.

Exciton phenomena can be loosely classified as static (stationary state effects for which the exciton may be treated as delocalized over the entire crystal or dynamic (rate processes describing the migration and scattering of a quasiparticle)). For stationary states, much effort has been expended on the measurement and calculation of exciton energies, factor group splittings, oscillator strengths and polarization ratios. In this regard, the earliest theoretical treatments employed perturbation theory (16,17) followed by finite basis set methods (9) which are still considered useful for weak and very weak transitions ($f \lesssim 10^{-3}$). For large oscillator strengths ($f \gtrsim 0.1$), classical dipole theory or the second quantization approach is required (9). The second quantization method which was first introduced by Agranovich (18) has the advantage of describing (within the one formalism) excitons interacting with phonons or impurity molecules, as well as excitons in perfect crystals. A few calculations for molecules with very large oscillator strengths ($f \gtrsim 3$) have been performed (19,20). Philpott (9,21) has discussed the dipole sum method at length and commented on several causes of error in it's application by other workers. In addition, he has pointed out that from an appropriate choice of gauge (Lorentz rather than Coulomb) the polariton dispersion relations arise naturally in the theory (9). A simplified dipole sum

method has recently been used by Sceats and Rice (22) to obtain the exciton band dispersion for anthracene. Earlier calculations on this system were done by Craig and Dissado (23), Philpott (21) and Schroeder and Silbey (24). The addition of higher multipole (e.g., octapole-octapole, etc.) and charge transfer terms to the calculations is difficult and is in most cases probably not a significant contribution to the energy for moderate to intense transitions ($f \gtrsim 0.1$) but may be quite important for crystals such as naphthalene. Some newer methods have been devised to take into account higher multipole terms (25).

It is well known that symmetry arguments often provide microscopic insight and may greatly simplify quantum mechanical calculations (1,2). The first definitive discussion of the uses of group theory in constructing exciton wave functions was by Winston and Halford (26). More recently, Hoshen and coworkers (27) have treated the problem and brief synopses of space group symmetry considerations appear in several review articles (4,5,6,9).

A number of experimental determinations of exciton band structure have appeared. Energy denominator studies have been used to locate the lower energy band edge in anthracene (28) and naphthalene (29). The spectrum of the exciton density-of-states in naphthalene has been obtained by a direct hot band method (30), by exciton superexchange (31)

and by the use of nontotally symmetric phonon bands (32). The exciton density of states in anthracene and benzene have also derived by the hot band method (30,33) and for anthracene from reflectance (34) data. In the case of naphthalene (and benzene) the agreement between the calculated and the experimentally determined density-of-states of Colson and coworkers (30) is reasonably good for the calculation in which parameters were modified to fit experimental data. At this point all calculated and experimental curves can only be considered approximate.

There is naturally a great deal of interest in the phonon modes of molecular crystals (35-42) since these provide information on ground state intermolecular interactions and because exciton-phonon (and more recently polariton-phonon) coupling effects are often very important and remain far from being completely understood. Coherent neutron scattering with fully deuterated crystals would yield true phonon dispersion curves but these experiments have not yet been done. At present only rather incomplete knowledge of the phonon modes in molecular crystals can be said to exist. Raman and infrared experiments (43-49) can provide data on the small fraction of modes which are optically allowed. A few incoherent neutron scattering studies (50-52) which measure a weighted phonon density-of-states have been performed. For naphthalene and benzene,

phonon side-bands in the electronic spectra have proved useful in assigning the phonon density-of-states. The utility of the phonon side-band method was first discussed by Small (53) for chemically mixed crystal systems and has been applied by Hochstrasser and Prasad (54) and Kopelman and coworkers (55,56) and Sheka and Terenetskaya (57) with some success to isotopically mixed naphthalene crystals. Pawley (58-60) was the first to discuss the nature of phonons in molecular crystals and to attempt to calculate phonon dispersion curves. More recently, Prasad and Kopelman (61) have reexamined these types of phonons.

An immense amount of labor has gone into understanding exciton-phonon interaction (62-65) in both pure and mixed molecular crystals. Several reviews of the field by Hochstrasser and Prasad (15), Kopelman (4), Levinson and Rashba (66), and Toyozawa (67) have appeared. A number of diverse aspects of the problem have been examined, such as, polarons (68-71), charge carrier-lattice interaction and photoconductivity (72-74), weakly allowed transitions (75-76), coupling in one-dimensional chains (77,78), retarded interactions (79), Urbach rule effects (80-86) and line shapes (87-100). Strong and weak coupling models (101-109) for Frenkel excitons and phonons have been discussed at length. For higher vibronic transitions in crystals such as naphthalene the concept of two-particle states (states in which vibrational and electronic excitation are located on

different sites) has proven useful in interpreting spectral data (110-117).

Most current approaches to exciton-phonon coupling make use of the statistical methods of quantum field theory and the second quantization method. A density matrix averaging procedure for the phonon bath and the Green's function-mass operator formalism is employed to derive energies, band shapes and line widths (118-130). An advantage of this method is that it is readily extended to mixed crystal systems. Along these lines, Prasad (131), Sumi (132), and Hong and Kopelman (133) have examined the utility of the coherent potential approximation (CPA) for treating exciton-phonon interactions in both pure and isotopically mixed crystals.

The dynamic nature of excitons (134-151) is revealed by exciton migration and scattering events. These aspects of excitons as quasiparticles have also been rather extensively studied. A number of papers have appeared on exciton-exciton interactions such as triplet-triplet annihilation (152,153), singlet-triplet fusion (154), singlet decay into triplets (155). Exciton diffusion rates (both singlet and triplet) have been calculated and measured experimentally in a number of crystals (156-166). Kopelman (167) and Kopelman and coworkers (168) have used the model of excitonic percolation for a thorough study of energy

transfer in isotopically mixed naphthalene crystals. Numerous theoretical models for coherent and incoherent energy transfer in both pure and mixed crystals have appeared (169-179). The case of impurity or defect trapping has also been described in a rather thorough fashion (180-190).

In addition to the already mentioned dynamic studies, triplet states (191-196) have also been probed extensively by magnetic resonance experiments (197-202). Since the sizable realm of triplet exciton work really lies beyond the scope of the dissertation, no attempt will be made to discuss it. However, a number of references on triplet states including reviews (203-207) are included.

For completeness it should be noted that while in most of the proceeding work the effect of finite crystal size and surfaces was neglected, surface exciton phenomena (and more recently polariton phenomena) are beginning to be actively studied (208-216).

As mentioned above, the bulk of molecular crystal work has dealt with exciton effects. The potential power of an almost classical treatment of optical absorption (which the polariton model basically is) was simply not recognized in chemical physics until quite recently when a handful of papers brought the polariton concept into the spotlight. The existence of a mixed state of the polarization field and the photon field, which has come to be known as a

polariton state (217-223), was first proposed by Hopfield in his Ph.D. thesis. Work along similar lines by Fano (224), Agranovich (18) and Pekar (225-227) appeared at about the same time. Actually, Hopfield coined the term "polariton" in his 1958 paper (217) to designate any particle in the polarization field (e.g., excitons, phonons, magnons) which could couple strongly with the photon field. Later Russian workers took "polariton" to mean the mixed state resulting from the interaction between excitons and photons and this usage has come to be standard.

The polariton model generates a unique dependence of wave vector, $\vec{k}$, on frequency (the dispersion curves) corresponding to two states having both quasiparticle and photon character (217,219). The nature of the exciton-polariton dispersion curves predicts the existence of new processes such as downward phonon scattering at absolute zero temperature. Hopfield (217) was first to point out an additional consequence of the model: the absorption of photon energy by the crystal should be viewed as a two-step process. Previously, absorption in solids was considered a one step process -- the creation of a quasiparticle by a photon. In the polariton picture, however, a photon enters the crystal and forms a mixed state having both polarization field and photon character. In the idealization of an infinite perfectly ordered crystal, energy, initially

carried, by the photon is "stored" in the crystal. Absorption results when this polariton wave is damped, or equivalently when the polariton quasiparticle is scattered by a phonon, chemical impurity, or lattice defect. Absorption seen in this way is defined as an irreversible loss of photon energy to the lattice (heat bath) rather than the creation of a polarization state in the crystal.

The experimental verification of the two-step nature of energy dissipation, perhaps the most general manifestation of polariton effects, is the subject of this dissertation.

Another interesting prediction of the polariton model is that the coupling between polarization states and photons is proportional to the oscillator strength of the crystal transition (222,223). This dependence implies among other things, that transmission and reflection spectra for large oscillator strength transitions ($f \geq 0.1$) may be very different from the true absorption (defined by $A = 1-R-T$). So far, only for anthracene has this result been confirmed experimentally (228,229).

The polariton model proposed by Hopfield was recognized almost from it's inception as the correct model for explaining the behavior of optical phonons in semiconductors and ionic crystals. A number of infrared and Raman experiments (230,231), as well as theoretical treatments and calculations (230-235), were done on these systems from the

early sixties on. By 1975, two review volumes on phonon-polaritons had appeared (230,231).

While Hopfield's initial treatment specifically employed polarization states closely resembling Frenkel (tight binding) excitons (217), the model was not applied to either Frenkel or Wannier-Mott excitons for several years until in the late 1950's Agranovich and coworkers and Pekar began to publish what has become an extensive theoretical examination of polariton states in molecular crystals (225-227, 236-238). In the 1970's other important theoretical treatments by Davydov (222,223), Philpott (239-243), and Davydov and Serikov (244) appeared. Permogorov and Travnikov (245), Sumi (246), Tait and Weiher (247,248), and Tait (249) have examined the effect of phonon scattering on exciton polariton absorption and emission processes specifically for semiconductors and ionic crystals. However, much of the general formalism applies to molecular crystals as well.

Philpott and Sherman (250), Philpott and Turlet (251), and Kliewer and Fuchs (232) have examined surface polaritons for both Frenkel and Wannier-Mott exciton states, and commented on the fact that Frenkel excitons are more likely to form true surface states because of their small radii. Kovener and coworkers (252), Bishop and coworkers (253), and others (254,255) have treated the case of surface exciton-polaritons in semiconductor systems.

The first solid experimental evidence for exciton-polaritons did not appear until 1974 when Voigt (256) reported an increase in absorption intensity with temperature for the An = 1 exciton band in CdS. In the same year, Delyukov and Klimusheva (257) detected a similar anomolous temperature dependence in the (0,0) absorption of n-dichloro and n-dibromobenzene crystals. In 1975 Ferguson (228,229) described the first of a series of careful experiments designed to reveal true polariton absorption in very thin anthracene flakes (~500-4000 Å) and Kreingol'd and Makarov (258) observed polariton effects in the n = 1 quadrapole absorption of Cu_2O. Bosacchi et al. (259) reported similar polariton induced behavior for GaSe in 1976.

The first interpretation of molecular crystal emission (anthracene) in terms of polaritons (260) and experimental evidence of surface polariton states in semiconductor systems (261,262) appeared in 1976. At present these seem to be the only other experimental confirmations, besides the work reported here for naphthalene (263), for exciton-polariton states. The fact that very similar effects are seen for systems where the underlying exciton states are known to be quite different simply reaffirms the essentially classical nature of the phenomena.

Optical detection of polariton effects requires a crystal of extremely high purity and one which is free of

externally induced strain. Such a crystal is sometimes called "perfect" although they are far from that. The demands of purity and, probably more important, the necessity of strain-free mounting explain why even though a number of "exciton absorption" spectra of single crystals have been published by many workers, polariton induced temperature dependent effects have only recently been detected. One anticipates that excitonic-polariton phenomena will be encountered for a number of ionic, semiconductor and molecular crystal systems as further careful experiments are performed.

THEORY AND DISCUSSION

Preface

The treatment of polariton modes given here owes much to several excellent review articles on various aspects of the exciton-polariton problem (9,218,219,221). In addition a number of articles specifically dealing with phonon-polaritons (220, 230-235) have proved quite helpful. As mentioned in the Introduction, there exists a large body of literature on excitons (3-7, 264) (weak coupling to radiation field) in molecular crystals which is generally familiar to molecular spectroscopists. It will, however, only be selectively dealt with here since this discussion is to focus primarily on polaritons. Some discussion of the exciton state viewpoint (5,6,9,264) is necessary, of course, for a clearer understanding of the nature of the differences between the exciton and polariton pictures.

Language

Unfortunately, over the years a body of language pertaining to excitons has evolved which is difficult to completely translate into the polariton picture. "Excitons" are said to no longer exist (as correct descriptions of crystal states) once the radiation field is introduced into the problem. But the fact that the exciton concept

is so familiar makes it almost impossible not to use it in arguing for it's own nonexistence. Since we have said exciton-photon coupling is not to be treated by perturbation theory, it is mathematically incorrect to refer to excitons as "zeroth order states", vide infra. More accurately excitons are the "uncoupled states" of the crystal and for describing a few situations they prove quite adequate. (That in general spectroscopic processes are not included among these few processes is what this dissertation attempts to demonstrate.) Finally, throughout this work we use "polariton" as a generic term and "exciton-polariton" to mean "as distinguished from phonon-polariton", "magnon-polariton", etc.

Exciton State Viewpoint

The basic model of an exciton (uncoupled) state proposed in the 1930's by Frenkel (10), Peierls (265) and Wannier (266) is that of an electron in the conduction band bound by coulomb attraction to a hole in the valence band. (The model obviously implies insulators). Two limiting cases exist: Frenkel, also called tight binding or excitons of small radius, which correspond to the case of electron and hole remaining together on the same molecule and Wannier-Mott excitons, for which the electron may be thought of as orbiting the hole at discreet radii which can cover

several unit cells (8). In both cases the exciton may be described as either an (approximate) stationary state delocalized over the entire crystal or as a quasiparticle moving in the lattice potential, transferring energy, but not charge, between lattice sites.

A number of authors have discussed the formalism for describing Frenkel excitons. The following treatment parallels that of Philpott (9), Fischer (6), and Davydov (5). The notation is specifically for a naphthalene-like system with two translationally inequivalent molecules in a unit cell containing a center of inversion. As Fischer (6) has pointed out, this sort of treatment is nothing more than an extension of writing out the wave functions and energies for the dimer problem.

The Hamiltonian for a crystal composed of σN chemically equivalent molecules located at sites α, within N unit cells n, is

$$\mathcal{H} = \sum_{n\alpha} \mathcal{H}_{n\alpha} + \frac{1}{2} \sum_{n\alpha \neq m\beta} V_{n\alpha,m\beta} \tag{1}$$

Molecules with the same α index are translationally equivalent. Since the overlap of wavefunctions on adjacent molecules is known to be small, molecular wave functions may be constructed using the Heitler-London formalism. The crystal ground state wave function is given by

$$\Psi_G = A_{n,\alpha} \Pi \phi_{n\alpha} \tag{2}$$

where $\phi_{n\alpha}$ is a molecular wave function and A is the anti-symmetrizer. The additional energy terms describing intermolecular electron exchange which A introduces are neglected. The ground state energy is given by

$$E_G = N\sigma\varepsilon^\circ + \frac{1}{2} \sum_{n\alpha \neq m\beta} \langle \psi^\circ_{n\alpha}\psi^\circ_{m\beta} | V_{n\alpha,m\beta} | \psi^\circ_{n\alpha}\psi^\circ_{m\beta} \rangle \qquad (3)$$

The superscript zero denotes molecules in the electronic ground state. The simplest excited state wave function would be

$$\Psi^f_{n\alpha} = \psi^f_{n\alpha} \sum_{n\alpha \neq m\beta} \psi_{m\beta} \qquad (4)$$

However, (4) does not carry the translational symmetry of the crystal. This can be remedied by a change to the orthonormal functions

$$\Psi^f_\alpha(\vec{k}) = N^{-\frac{1}{2}} \sum_n \Psi^f_{n\alpha} \exp(i\vec{k}\cdot\vec{n}) \qquad (5)$$

Equation (5) must be further modified to describe two translationally inequivalent molecules per unit cell. This is accomplished by using coefficients from the character table of the interchange group. To construct the site symmetry adapted wave functions

$$|\Psi^f(\vec{k},\zeta)\rangle = (\sigma)^{-\frac{1}{2}} \sum_\alpha C_\alpha(\zeta) |\Psi^f_\alpha(\vec{k})\rangle \qquad (6)$$

For naphthalene there are two molecules in the unit cell $\sigma=2$, and two sites connected by a 2-fold screw operation,

so $\alpha = 1,2$. The proper interchange group is C_2. Therefore, the coefficients $C_\alpha(\zeta)$ may be taken directly from the character table:

$$\underset{\sim}{C} = \begin{pmatrix} 1 & 1 \\ 1 & -1 \end{pmatrix} \tag{7}$$

The excited state energies are given by the operator

$$\Delta\mathcal{H} = \mathcal{H} - E_G \tag{8}$$

$$\sum_{\alpha=1}^{\sigma} C_\alpha(\zeta)\langle\Psi_\beta^f(\vec{k})|\Delta H|\Psi_\alpha^f(\vec{k})\rangle = E_\alpha^f(\vec{k})C_\alpha(\zeta)\delta_{\alpha\beta} \tag{9}$$

Letting $L_{\alpha\beta}(k) = \langle\Psi_\beta^f(k)|\Delta H|\Psi_\alpha^f(k)\rangle$ equation (9) can be rewritten as the product of two matrices

$$\sum_{\alpha=1}^{\sigma} C_\alpha(\zeta)[L_{\alpha\beta}(\vec{k}) - E_\alpha^f(\vec{k})\delta_{\alpha\beta}] = 0 \tag{10}$$

Clearly nontrivial solutions require that

$$\det|L_{\alpha\beta}(\vec{k}) - E_\alpha^f(\vec{k})\delta_{\alpha\beta}| = 0 \tag{11}$$

One obtains

$$L_{\alpha\beta}(\vec{k}) = (\Delta\varepsilon^f + D^f)\delta_{\alpha\beta} - L_{\alpha\beta}^f(\vec{k}) \tag{12}$$

$\Delta\varepsilon^f$ is the free molecule excitation energy and D^f is the difference between the ground state van der Waals energy

and the van der Waals energy when one molecule is excited.

$$D^f = \sum_{n\alpha \neq m\beta} \{\langle \psi^\circ_{n\alpha}\psi^\circ_{m\beta} | V_{n\alpha,m\beta} | \psi^f_{n\alpha}\psi^\circ_{m\beta}\rangle - \langle \psi^\circ_{n\alpha}\psi^\circ_{m\beta} | V_{n\alpha,m\beta} | \psi^\circ_{n\alpha}\psi^\circ_{m\beta}\rangle\} \quad (13)$$

Both $\Delta\varepsilon^f$ and D^f are the same for all Davydov components. The last term $L^f_{\alpha\beta}(\vec{k})$ is a resonance term describing the transfer of energy between sites. For naphthalene when $\vec{k}=0$, or lies parallel or perpendicular to the $\underline{b}$ crystalographic axis, both the diagonal $L_{\alpha\alpha}$ and off diagonal terms $L_{\alpha\beta}$ in (12) are equal. The matrix form of (12) is then readily diagonalized to yield

$$\Delta E^f_{1,2}(\vec{k}) = \Delta\varepsilon^f + D^f + L^f_{11}(\vec{k}) \pm L^f_{12}(\vec{k}) \quad (14)$$

The two solutions of (14) correspond to the two Davydov or factor group states (to first order). The Davydov splitting is $2L_{12}(\vec{k})$. This treatment has been extended to include vibronic wavefunctions and mixed crystal states; these aspects are briefly reviewed by Fischer (6).

Electromagnetic Modes of Media

At this point a different approach to the description of electronic resonance states in crystals which has developed simultaneously and (until quite recently independently) from the exciton state picture will be discussed.

This is the so-called classical approach which forms the basis for all polariton treatments.

Maxwell's equations with appropriate boundary conditions suffice to characterize all observable linear phenomena in an optical experiment. This characterization is achieved by specifying a quantity called the dielectric function of a medium. When an electromagnetic wave of the form

$$E = E_o \, e^{i(\vec{k}\cdot\vec{r}-\omega t)} \quad [1] \tag{15}$$

propagates in a medium, it causes a polarization of the underlying resonance states. The effect can be expressed mathematically by a response function, with the dielectric function ε, as the kernel:

$$\vec{D}(\vec{r},t) = \int d^3\vec{r}' \int_{-\infty}^{t} dt' \; \varepsilon(\vec{r}-\vec{r}', \, t-t')E(\vec{r},t') \tag{16}$$

$\vec{D}$ is the dielectric displacement, a quantity proportional to the dielectric polarization $\vec{P}$:

$$\vec{D} = \vec{E} + 4\pi\vec{P} \tag{17}$$

---

[1] All E and M waves referred to in this dissertation will be of the form $\vec{Z} = \vec{Z}_o \, e^{i(\vec{k}\cdot\vec{r}-\omega t)}$. There are a number of equivalent but slightly different developments of the dielectric polarization in standard E&M texts in terms of either $\vec{D}$ or $\vec{P}$. Feynman's lectures (267) contain a nice explanation of the historical origins of the two quantities.

Expression (16) is completely general, ε=1 in the vacuum and is approximately constant and real away from absorption resonances and is a complex function of frequency and wave vector (or $\vec{r}$ and t) in a resonance region. In addition, in condensed media, ε is generally a nondiagonal tensor function due to spatial anisotropy. Note also: $\varepsilon=n^2$, where n is the refractive index.

Equation (16) is termed "nonlocal" in that the dielectric displacement $\vec{D}$ at some point $\vec{r}$ in space, depends on $\vec{E}$ in the vicinity of $\vec{r}$. Since it is generally more convenient to handle solid state problems in reciprocal space, equation (16) is Fourier transformed twice, first to

$$\vec{D}(\vec{r},\omega) = \int d^3\vec{r}' \; \varepsilon(\vec{r}-\vec{r}',\omega)\vec{E}(r,\omega). \tag{17}$$

Next, by making what is called the local approximation, i.e., that $\vec{D}(\vec{r})$ is influenced by $\vec{E}$ at $\vec{r}$ only, one can write

$$\varepsilon(\vec{r}-\vec{r}',\omega) = \varepsilon(\omega)\delta(\vec{r}-\vec{r}') \tag{18}$$

Fourier transforming a second time yields

$$\vec{D}(\vec{k}\omega) = \varepsilon(\vec{k},\omega)E(\vec{k}\omega) \tag{19}$$

or equivalently

$$\vec{D}_i = \varepsilon_{ij}(\vec{k}\omega)\vec{E}_j \tag{19'}$$

The dependence of ε on wave vector $\vec{k}$ is referred to as spatial dispersion, dependence on frequency ω, as temporal dispersion. Equation (19) is a linear relationship valid for the long wavelength limit where the wavelength of light used λ, is much larger than a unit cell dimension a and for moderate intensity sources (not high power lasers). The first requirement is realized for the exciton (and phonon) states of most crystals, e.g., for naphthalene a is $\sim$8-10 Å and λ $\sim$3000 Å for the lowest energy singlet transition.

The dielectric function $\varepsilon(\omega,\vec{k})$ may be related to the physically observable quantities frequency ω, wave vector $\vec{k}$, and the speed of light by the use of Maxwell's equations, rewritten in a slightly different form

$$\vec{\nabla}\cdot\vec{D} = 0 \qquad (20) \qquad \vec{k}\cdot\vec{D} = 0 \qquad (21)$$

$$\vec{\nabla}\cdot\vec{B} = 0 \qquad (22) \qquad \vec{k}\cdot\vec{B} = 0 \qquad (23)$$

(20-23) are completely general.

$$\vec{\nabla}\times\vec{H} = \frac{1}{c}\frac{\partial\vec{D}}{\partial t} \qquad (24) \qquad \vec{k}\times\vec{H} = -\frac{\omega}{c}\vec{D} \qquad (25)$$

$$\vec{\nabla}\times\vec{E} = -\frac{1}{c}\frac{\partial\vec{B}}{\partial t} \qquad (26) \qquad \vec{k}\times\vec{E} = \frac{\omega}{c}\vec{B} \qquad (27)$$

For a nonmagnetic media $\vec{B}=\vec{H}$, therefore one may write

$$\vec{k}\times[\frac{c}{\omega}\vec{k}\times\vec{E}] = -\frac{\omega}{c}\vec{D} \qquad (28)$$

$$\vec{k}x(\vec{k}x\vec{E}) = -(\frac{\omega}{c})^2\vec{D} \tag{29}$$

$$\vec{k}(\vec{k}\cdot\vec{E}) - \vec{E}k^2 = -(\frac{\omega}{c})^2\vec{D} \tag{30}$$

$$\vec{k}^2\vec{E} - \vec{k}(\vec{k}\cdot\vec{E}) = (\frac{\omega}{c})^2\vec{D} \tag{31}$$

Substituting equation (19') in equation (31) yields

$$k^2E_i - k_ik_\ell E_\ell - (\frac{\omega}{c})^2 \varepsilon_{i\ell}E_\ell = 0 \tag{32}$$

Since $k^2E_i = k^2\delta_{i\ell}E_\ell$

$$(\frac{\omega^2}{c} \varepsilon_{i\ell} + k_ik_\ell - k^2\delta_{i\ell})E_\ell = 0 \tag{33}$$

Equation (33) is often written as a quadratic in terms of the refractive index (recall $\varepsilon=n^2$).

$$(\varepsilon_{ij}s_is_j)n^4 - [(\varepsilon_{ij}s_is_j)\varepsilon_u - \varepsilon_{i\ell}\varepsilon_{\ell j}s_is_j]n^2$$

$$+ |\varepsilon_{ij}| = 0 \tag{34}$$

In this form it is called the Fresnel equation. s_i is defined by $\vec{s} = \vec{k}/k$. Equation (38) allows the calculation of the complex refractive index if the crystal dielectric function is known. It is instructive to consider equation (33) in matrix form, for i = x,y,z, ℓ = x,y,z.

$$\begin{bmatrix} (\frac{\omega}{c})^2\varepsilon_{xx}+k_x^2-k^2 & (\frac{\omega}{c})^2\varepsilon_{xy}+k_xk_y & (\frac{\omega}{c})^2\varepsilon_{xz}+k_xk_z \\ (\frac{\omega}{c})^2\varepsilon_{yx}+k_yk_x & (\frac{\omega}{c})^2\varepsilon_{yy}+k_y^2-k^2 & (\frac{\omega}{c})^2\varepsilon_{yz}+k_yk_z \\ (\frac{\omega}{c})^2\varepsilon_{zx}+k_zk_x & (\frac{\omega}{c})^2\varepsilon_{zy}+k_{zy} & (\frac{\omega}{c})^2\varepsilon_{zz}+k_z^2-k^2 \end{bmatrix} \begin{bmatrix} E_x \\ E_y \\ E_z \end{bmatrix} = 0 \quad (33')$$

For an isotropic, homogeneous media, equation (33') can be diagonalized by choosing and arbitrary orthogonal coordinate system for the medium and fixing $\vec{k}$ parallel to the $\vec{z}$ direction, i.e., consider a plane wave travelling in the $\vec{z}$ direction, such that $\vec{k} = \hat{z}k$. Then equation (33') becomes a set of three uncoupled equations

$$\begin{bmatrix} (\frac{\omega}{c})^2\varepsilon_{xx}-k^2 & 0 & 0 \\ 0 & (\frac{\omega}{c})^2\varepsilon_{yy}-k^2 & 0 \\ 0 & 0 & (\frac{\omega}{c})^2\varepsilon_{zz} \end{bmatrix} \begin{bmatrix} E_x \\ E_y \\ E_z \end{bmatrix} = 0 \quad (35)$$

Since $\vec{k}\cdot\vec{D} = 0$ by equation (21) $\vec{D}$ is required to lie in the xy plane, which implies

$$(\frac{\omega}{c})^2\varepsilon_{zz}E_z = 0 \quad (36)$$

Since in general $E_z \neq 0$, equation (36) requires $\varepsilon_{zz} = 0$.

The E_z mode is frequently termed longitudinal since E_z is parallel to $\vec{k}$.

The equations describing the x and y fields are

$$\left[\left(\frac{\omega}{c}\right)^2 \varepsilon_{xx} - k^2\right] E_x = 0 \tag{37}$$

$$\left[\left(\frac{\omega}{c}\right)^2 \varepsilon_{yy} - k^2\right] E_y = 0 \tag{38}$$

Equations (36) and (37) are satisfied when $\varepsilon_{xx} \neq 0$, $\varepsilon_{yy} \neq 0$ and $E_x \neq 0$, $E_y \neq 0$ and E_x and E_y are perpendicular to $\vec{k}$, with $\vec{D}$ and $\vec{E}$ lying in the xy plane (recall $\vec{k} \cdot \vec{D} = 0$). The E_x and E_y modes are called transverse. Equations (37) and (38) may be generalized. For any case where ε is non-zero

$$\left(\frac{\omega}{c}\right)^2 \varepsilon = k^2 \tag{39}$$

The calculation of the elements $\varepsilon_{ij}(\omega, \vec{k})$ is a microscopic problem that for real crystals is still far from a completely satisfactory solution (vide infra). However, the form of the tensor $\varepsilon_{ij}(\omega\vec{k})$ is governed by the crystal class. $\varepsilon(\omega, \vec{k})$ for a monoclinic crystal such as naphthalene, belonging to the space group $P_{2_1/a}$ has been derived by Koch and coworkers (268) as

$$\begin{bmatrix} \varepsilon_{xx}(\omega) & 0 & \varepsilon_{xz}(\omega) \\ 0 & \varepsilon_{yy}(\omega) & 0 \\ \varepsilon_{xz}(\omega) & 0 & \varepsilon_{zz}(\omega) \end{bmatrix} = \varepsilon(\omega,k) \qquad (40)$$

Equation (39) is valid only when spatial dispersion effects are neglected. It is obvious that the tensor (39) cannot be diagonalized by any choice of axis system.

Lorentz Model

A good introduction to the polaritons can be found in the work of Lorentz, who in 1931 derived an expression for $\varepsilon(\omega,k)$ at an absorption resonance (8). Lorentz considered the case of an ordered isotropic array of electric dipoles free to oscillate harmonically when pumped by an E&M wave of the form given in equation (15). The system is a sort of idealized "hydrogen crystal" in which a particle of mass m_e, charge e, vibrates about an equilibrium position at which a positive charge of equal and opposite magnitude is fixed. Because of the assumption of an isotropic medium, the dielectric constant obtained will be a scalar quantity. The equation of motion for the system is

$$m_e(\ddot{\vec{u}} + \gamma\dot{\vec{u}} + \omega_e^2\vec{u}) = e\vec{E} \qquad (41)$$

The solutions of equation (40) are

$$\vec{u}(\vec{r}t) = \frac{e\vec{E}(\vec{r}t)}{m_e}\left[\frac{1}{(\omega_o^2-\omega^2) + i\omega\gamma}\right] \tag{42}$$

γ here serves as a purely phenomenological damping parameter necessary to keep the system from diverging ($\vec{u} \to \infty$) as the frequency ω approaches the resonance frequency ω_o. If the density of the oscillators is taken to be η_o then the media polarization brought about by E can be written as

$$\vec{P} = \eta_o e\vec{u} \tag{43}$$

Substituting (41) and (42) into $\vec{D} = \vec{E} + 4\pi\vec{P}$ yields an expression for the Lorentzian dielectric function

$$\vec{D} = \vec{E} + 4\pi\eta_o e\vec{u} = \left[1 + \frac{4\pi\eta_o\, e^2/m_e}{(\omega_o{}^2-\omega^2+i\omega\gamma)}\right]\vec{E} \tag{44}$$

$$\varepsilon(\omega,\vec{k}) = \left[1 + \frac{4\pi\eta_o\, e^2/m_e}{(\omega_o{}^2-\omega^2+i\omega\gamma)}\right] \tag{45}$$

which describes the interaction of electromagnetic radiation with an infinite medium composed of microscopic electric dipoles. The model is actually very suggestive of polar phonon modes in ionic crystals, where the sublattices of

positive and negatively charged ions oscillate relative to one another.

The classical absorption coefficient K, can easily be obtained from the Lorentz model by assuming a complex form for the refractive index

$$n = n' + in'' \equiv \varepsilon^{\frac{1}{2}} = (\varepsilon' + i\varepsilon'')^{\frac{1}{2}} \tag{46}$$

By substituting equation (46) into equation (15) and letting r lie along the z direction, the direction of the plane wave propagation (z parallel to k), one obtains

$$\vec{E} = \vec{E}_o \exp[i\omega(\frac{n'z}{c} - t)] \exp[\frac{-n''\omega z}{c}] \tag{47}$$

Because the intensity of the wave is proportional to $|E|^2$, it will be attenuated in space by a factor

$$\exp[\frac{-2n''\omega z}{c}] \tag{48}$$

where the absorption coefficient K is defined as

$$K = \frac{2n''\omega}{c} \tag{49}$$

K can be rewritten in a form explicitly dependent on the Lorentzian dielectric function as

$$K(\omega)n'(\omega) = \frac{-\gamma}{c} \frac{(4\pi\eta_o e^2/m_e)}{(\omega_o{}^2-\omega^2)^2 + \omega^2\gamma^2}, \tag{50}$$

by making use of identity (44). The form of equation (49) gives rise to the familiar Lorentzian absorption profiles. Obviously the refractive index and the dielectric constant are both frequency dependent. From equations (49) and (50) it is clear that $n'(\omega)$ and $n''(\omega)$ are not independent. They are connected by a type of Hilbert transform called the Krammers-Kronig relation (269).

Besides providing a new macroscopic perspective on absorption processes, the chief pedagogical value of the Lorentz model is that this very simple formalism generates the so-called polariton dispersion curves. When equation (45) is substituted into equation (39) and the values of ω vs. $\vec{k}$ are plotted for the case $\gamma=0$ (no damping), Figure 1a is obtained. As in the previous section, the modes may be classified as either transverse or longitudinal. The true polariton modes correspond to the transverse modes ($\varepsilon\neq 0$). For the longitudinal mode ($\varepsilon=0$), there is no $\vec{k}$ dependence; this corresponds to the mode labelled || coulomb exciton in Figure 1a.

Retardation

At this point it is convenient to discuss the effect of retardation. Since the speed of light is not infinite some part of the interaction between charges in a media must be treated as a retarded one. Retardation implies causality, i.e., information cannot travel between points faster than

the speed of light in the medium. By the use of Maxwell's equations and equations (33) and (34) retarded interactions are built into the polariton (Lorentz) model. If for a longitudinal mode ($\vec{k}||\vec{E}$), one allows $c\to\infty$ in equation (36), the normal modes generated will account for only instantaneous Coulomb interactions between charges, which in turn depend on relative distances and not velocities. These modes are referred to as Coulomb excitons.

Actually, there are two cases possible for Coulomb excitons, which deserve a more detailed consideration.

1) $\vec{D} = 0$ since $\vec{D} = \vec{E} + 4\pi\vec{P}$

$$\vec{P} = \frac{-1}{4\pi}\vec{E} = \frac{-1}{4\pi}\frac{\vec{k}}{k}E \to \vec{P} \text{ is also longitudinal} \qquad (51)$$

these modes satisfy

$$|\varepsilon_{ij}(\omega,\vec{k})| = 0 \qquad (52)$$

2) $\vec{D} \neq 0$ $\vec{\nabla}\cdot\vec{D} = 0$ implies D is always transverse and

$$\vec{P} = \frac{1}{4\pi}\left[\vec{D} - \frac{\vec{k}}{k}E\right] \qquad (53)$$

This requires that $\vec{P}$ contain a transverse component, in the special case $\vec{E} = 0$, $\vec{P}$ is purely transverse, i.e.,

$$\vec{P}^{\perp} = \frac{\vec{D}}{4\pi} \qquad (54)$$

These pure transverse modes satisfy the equation

$$[\varepsilon_{ij}(\omega\vec{k})]^{-1} = 0 \tag{55}$$

Agranovich and Ginsberg term the case of $\vec{D} \neq \vec{E} \neq 0$ "fictitious" longitudinal waves and the second case, $\vec{D} \neq \vec{E} = 0$ "polarization waves". Both cases 1) and 2) are plotted in Figure 1b; 1) corresponds to modes labelled || Coulomb excitons and 2) to $\perp$ Coulomb excitons - $\perp$ here implying a transverse P component.

The differences between Figures 1a and 1b are the result of including retardation effects. One of the features of the polariton model is that retardation is always included in any determination of band energies.

Agranovich has pointed out that $\varepsilon(\omega\vec{k})$ must depend on retarded interactions as well and that at $c\to\infty$ $\varepsilon(\omega\vec{k})$ changes to a new tensor $\tilde{\varepsilon}(\omega,\vec{k})$. The difference between these two tensors should be especially large for the imaginary components of $\varepsilon(\omega\vec{k})$ near the long-wave length tail of exciton absorption bands of large oscillator strengths (219). Retardation does not influence the longitudinal electromagnetic modes but has a large influence on the transverse modes. Agranovich has also shown that retardation does not effect the energies of exciton lines but does effect the line shapes (219).

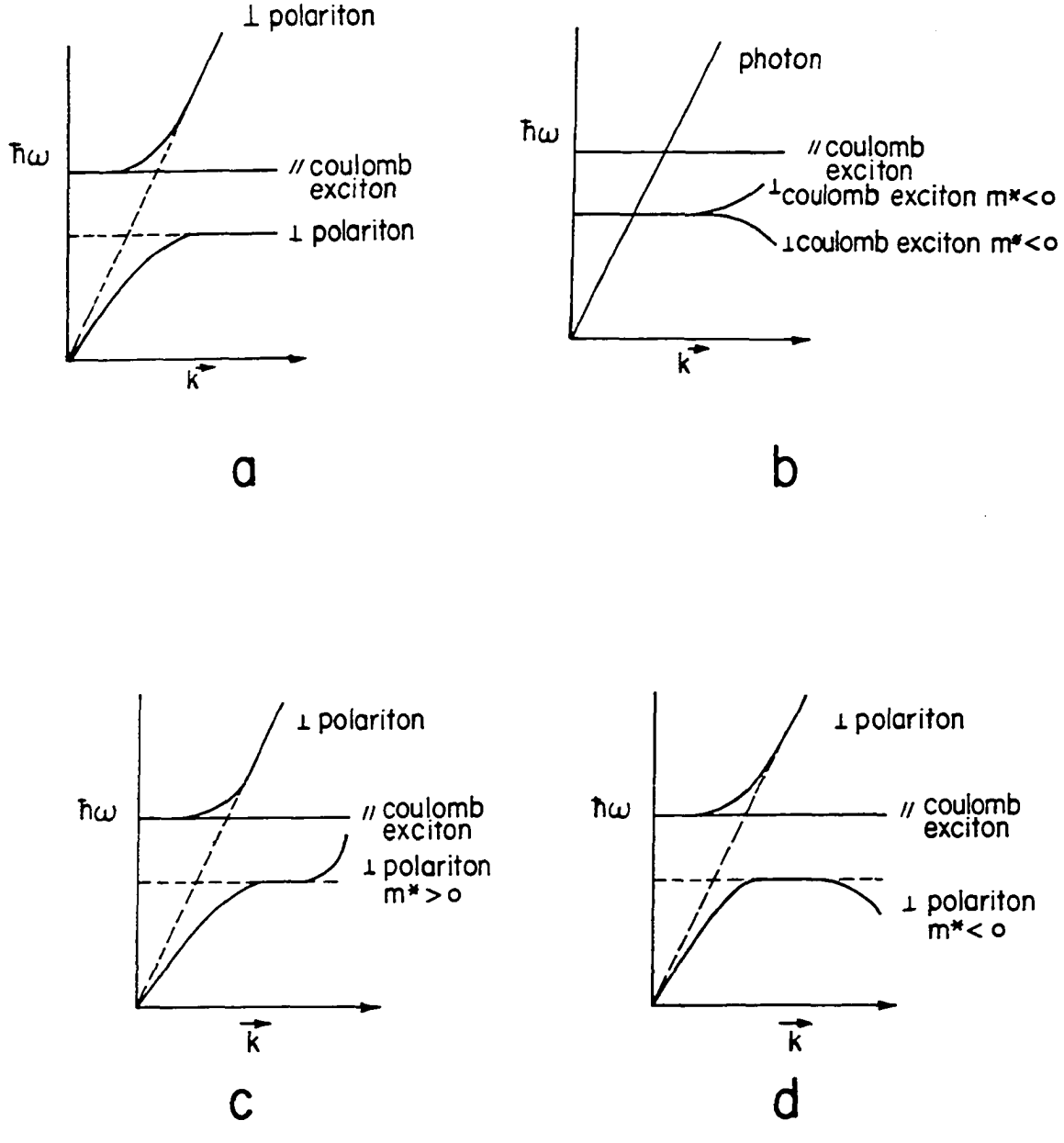

Figure 1. Coulomb exciton and polariton dispersion relations

Polariton Models

More recent polariton treatments of later workers such as Davydov (222), Philpott (239-243), and Agranovich (219) may be seen to evolve naturally from the model of Lorentz. The basic form for $\varepsilon(\omega,\vec{k})$ is retained and following Agranovich (219), the dielectric function for exciton states in an isotropic medium may be written

$$\varepsilon(\omega,\vec{k}) = \varepsilon_o + \frac{f\ \omega_p^2}{\omega_{EX}^2(\vec{k}) - \omega^2 - i\gamma\omega^2} \tag{56}$$

Where $\omega_{EX}(k)$ is the frequency of the resonant exciton state, $\omega_{EX(0)} = \varepsilon(0)/\hbar = \omega_{\perp}(0)$.

ε_o is a constant background dielectric contribution representing all nonresonance states, ω_p is the plasma frequency $\omega_o^2 = \frac{4\pi e^2 N}{m}$, N is the valence electron concentration, m and e the charge and mass of an electron, and f is the oscillator strength of the crystal transition. The quantity $f\ \omega_p^2$ is a measure of the strength of the coupling between excitons and photons and equivalently is also proportional to the energy splitting of the transverse and longitudinal polariton modes

$$\varepsilon_o(\omega_{||}^2(\vec{k}) - \omega_{EX}^2(\vec{k})) \simeq f\ \omega_p^2 \tag{57}$$

In classical optics $(\omega_{||}(0) - \omega_{\perp}(0))$ is called the stop band since for $\gamma=0$ it corresponds to the frequency region

where reflection becomes 1 (hence transmission becomes zero). Finally, there is the quantity γ included in the Lorentz model as a phenomological parameter to insure good mathematical behavior. γ in later models is seen as a measure of real microscopic attenuation processes. For phonon-polaritons γ is related to lattice anharmonicity, for exciton polaritons to scattering events, such as energy trapping by chemical impurities and defects and inelastic collisions with phonons. An important aspect of polariton treatments is the temperature dependence built into γ by its dependence on exciton-phonon interactions.

The temperature dependent nature of γ provides for an effect not predicted by exciton theory, namely that if the other contributions to γ from chemical impurities and crystal defects can be made sufficiently small, one may be able to observe an increase in absorption with increasing temperature due to the increasing phonon occupation number. This behavior appears to be an exception to Beer's law

$$I = I_o e^{-K\ell} \tag{58}$$

but actually Beer's law proves to be merely a limiting case of the polariton model, i.e., γ is already so large that any temperature dependent effects are negligible. Unfortunately, Davydov has introducted some language which

is at best confusing. He refers to the limit where Beer's law holds as weak-coupling with regard to excitons and photons

$$\omega_p^2 f << \varepsilon_o \gamma^2 \tag{59}$$

And the limit where Beer's law does not hold as strong exciton-photon coupling

$$\omega_p^2 f >> \varepsilon_o \gamma^2 \tag{60}$$

The coupling between the photon field and the polarization states is, however, fixed by equation (54) and is not temperature dependent. Therefore, in this dissertation the cases covered by equations (59) and (60) will be referred to as the case of large and small γ, respectively. One might conclude as Agranovich has stated that only for cases when $(\omega_{||}(0) - \omega_{\perp}(0))$ is much larger than the width of an exciton line will polariton effects become important. This is certainly true if polariton dispersion curve effects are being studied. However, the experimental data presented in this dissertation indicate that even for small oscillator strengths, the temperature dependent character of γ can be observed.

It is to be expected that any model proporting to describe real crystals should be more complicated than an infinite isotropic medium of harmonic oscillators and indeed

most present day work on polariton theory consists of attempts to incorporate more real crystal parameters into theoretical models. The important point is that while the simplest models are not very satisfying in terms of approximating most molecular crystal experiments, they do provide a great deal of basic insight into the physics of light absorption. Therefore, the modifications and additions to the theory to be introduced below should be seen as clarification and extension of a basically sound foundation.

Volume and anisotropy effects

An obvious discrepancy between theory and experiment is that real crystals are not infinitely large. Actually, the approximation is not as bad as it may seem since for a crystal composed of $N \sim 10^{23}$ unit cells for many theoretical applications is nearly infinite. It was pointed out by Hopfield (217) and later by others (6,270) that only for the case of an "infinitely" large crystal with the radiation field quantized in the same crystal volume will only one radiation state and one polarization state exist and hence for $\gamma=0$ the polariton modes persist forever in time. Whenever the radiation field is quantized in a volume larger than the crystal, a continuum of radiation states is created and the process of radiation damping becomes available.

To introduce the effect of surfaces into theory, two models have been used fairly extensively. Treating the crystal as a semi-infinite half sphere proves useful in most reflection and surface calculations since these experiments generally study only one face of rather thick crystals (243). For calculations involving transmission, reflection and absorption (A = 1-R-T), the infinite thin slab model is more suitable. Philpott (243) and other workers have considered the approach of considering the slab as composed of layers with each layer assigned its own dielectric function $\varepsilon_i(\omega k)$ in order to simulate the anisotropy encountered in going from surface to bulk. This dissertation includes a number of computer simulated R, T and A spectra generated from a simpler model of a homogeneous thin slab (cf., chapter four).

At present no authors have considered specifically the effect of crystal anisotropy on exciton-polariton dispersion curves. However, a number of treatments have appeared for phonon-polaritons (230,231). Dispersion curves for crystals of lower symmetry reveal a number of new modes occurring in the region $\omega_{||}(\vec{k}) - \omega_{\perp}(\vec{k})$. The general form of the dispersion relations is determined by crystal class and should be similar regardless of the type of polarization state, therefore, a study of the phonon-polariton curves such as given in Light Scattering by Phonon-Polaritons by Claus, Merten and Brandmuller (231) proves very suggestive for future work in molecular crystals.

Spatial vs. temporal damping

When the dielectric function (equations 44 or 55) is allowed to be complex ($\gamma \neq 0$), then equation (54) requires that either the wave vector or frequency also become complex, i.e.,

$$\vec{k} = \vec{k}' + i\vec{k}'' \tag{61}$$

or

$$\omega = \omega' + i\omega'' \tag{62}$$

The two cases correspond to spatial or temporal damping. That this is so can be easily shown by replacing either $\vec{k}$ or ω by its complex form in equation (15). It is becoming clearer that the two cases correspond to different experimental situations and in general should not be used interchangeably (vide infra). Obviously for the case $\gamma=0$ both approaches will yield the same result.

When equation (60) is used, one obtains what are generally referred to as the polariton modes. These are elementary excitations with an average lifetime $\tau = 1/\gamma$, which can be normalized to delta functions in an infinite volume (time fixed). Davydov calls the solutions obtained using equation (60) "normal electromagnetic waves" because they cannot be normalized in an infinite volume and hence are not true elementary excitations.

An extremely important point has been raised by Merten and Borstel (271), amplifying an earlier paper by Alfano and Giallorenzi (272). It is that markedly different types of polariton dispersion curves are generated depending on whether one assumes complex frequency or complex $\vec{k}$, and further that the choice is not arbitrary. For two photon experiments (they consider Raman active polar phonon modes) temporal damping is correct. Because the incident photons are not resonant with a crystal phonon frequency and hence cannot be spatially damped. In order to observe polariton effects, the phonon modes considered must be simultaneously infrared and Raman active -- i.e., the Raman photons merely prepare the one photon state. One photon experiments, such as conventional infrared, should be treated in the spatial damping picture where quantities such as the absorption coefficient appear naturally.

Shown in Figure 2 are three representative polariton dispersion curves for the case of no damping a), temporal damping b), and spatial damping c), in a simple isotropic system (after Alfano). There is striking difference between (2b) and (2c). For the case of spatial damping another polariton effect occurs, the dispersion curves now contain so-called turning points for the real (experimentally accessible) modes. Secondly, for the spatial damped (one photon) case there now exist solutions at the resonance

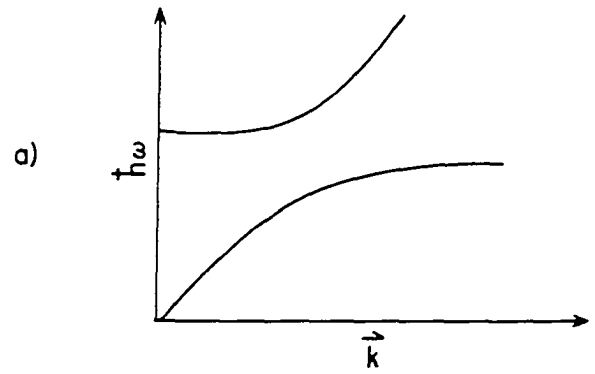

(a) no damping
$\gamma = 0$

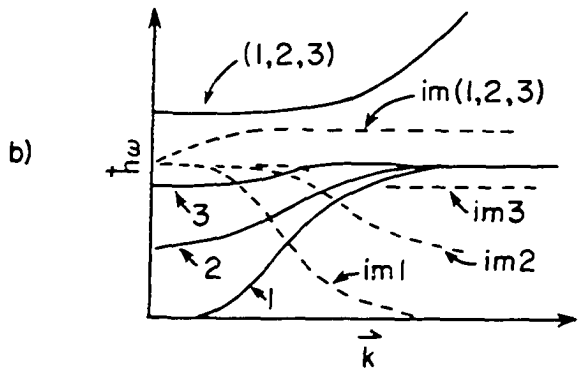

(b) temporal damping curves labeled 1,2,3 refer to $\gamma_1 > \gamma_2 > \gamma_3$

--- imaginary solutions

—— real solutions

i.e., curve 1 in (b) and (c) is most strongly damped

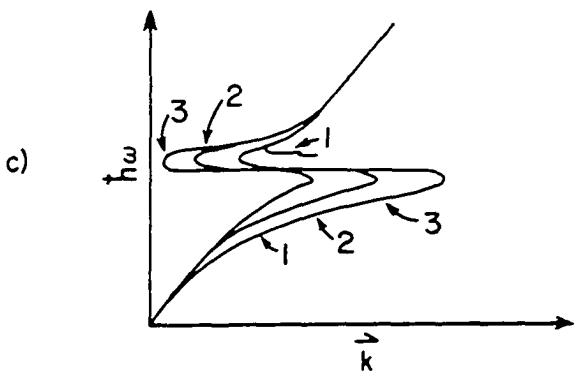

(c) spatial damping curves labeled 1,2,3 refer to $\gamma_1 > \gamma_2 > \gamma_3$

only real solutions shown

Figure 2. Effect of spatial vs temporal damping on polariton dispersion curves

point $\hbar\omega_{photon} = \hbar\omega_{exciton}$, $\vec{k}_{photon} = \vec{k}_{exciton}$. As might be expected, the lowering of crystal symmetry to cases such as uniaxial crystals causes the $\hbar\omega$ vs $\vec{k}$ to become much more complex, through the addition of new modes in the region between $\omega_{||} - \omega_{\perp}$. Merten and Borstel have calculated the phonon dispersion curves for the uniaxial crystal ZnF_2 (271). At present no calculations of spatial vs temporal damping exist either for exciton polaritons in general or for biaxial systems (such as naphthalene). It seems safe to assume, however, that such curves must bear a qualitative resemblance to the phonon-polariton modes, and hence at least theoretically there exists the possibility of obtaining quite different behavior for large $\vec{k}$ in one and two photon experiments on exciton systems.

Spatial dispersion

Spatial dispersion refers to the dependence of frequency ω for the exciton portion of the dispersion curve (i.e., $\vec{k} \geq \vec{k}$ resonance) on wave vector $\vec{k}$ and treatments where spatial dispersion is specifically included are generally termed "semiclassical". Spatial dispersion effects result when a dependence on the exciton effective mass, m*, is introduced into equation (54). (Note: quasiparticles are distinguished from real particles in that they have only "effective" masses which depend on the form

of the lattice potential energy). Generally, the energy of an "uncoupled" exciton band is expressed as a $\cos(\vec{k}\cdot\vec{r})$ dependence which is approximated by a series, the first two terms of which are retained. These terms give the standard quadratic dependence of energy on $\vec{k}$ and m^*. For a crystal with a center of symmetry

$$\varepsilon(\vec{k}) = h\omega_{EX}(\vec{k}) = \hbar\omega_{EX}(0) + \frac{\hbar^2 k^2}{2m^*(\vec{k})} \tag{63}$$

letting

$$\frac{\hbar\omega_{EX}}{m^*} = \alpha \tag{64}$$

The dielectric function, equation (54), is now rewritten as

$$\varepsilon(\omega\vec{k}) = \varepsilon_o + \frac{f\,\omega_o^2}{\omega_{\varepsilon(0)}^2 - \omega_{(\vec{k})}^2 + \alpha k^2} \tag{65}$$

The effective mass may be either positive ($\alpha > 0$) or negative ($\alpha < 0$). For the case $\alpha=0$, $m\to\infty$ and the dispersion curves have the form shown in Figure 1b. That this corresponds to a localized exciton can be seen from a simple argument. Spatial dispersion may also exist in the exciton of "uncoupled" regime as shown by Figure 1a. Here the effect only alters the energies of the $\vec{P}\perp$ Coulomb exciton modes.

The inclusion of spatial dispersion (αk^2) in this manner rectifies an omission made very early in our treatment, which was to adopt the local approximation for equation (17). In general, spatial dispersion in molecular crystals is sufficiently small that the effect can be neglected (219), as can be shown by a rule of thumb argument that $\vec{r}/\lambda$ should be small.

For a molecular crystal the region of space near r which can be considered to contribute to the integral (17) is on the order of a lattice constant a, the wave length of light λ considerably exceeds those dimensions, therefore

$$a/\lambda \approx \frac{5 \times 10^{-8}}{5 \times 10^{-5}} \approx 10^{-3}$$

There appear to be two situations where spatial dispersion effects can become important. The first is in the structure of reflectance bands and has been treated by Philpott (239) for an anthracene-like system, by Johnson and Rimbey (271) for semiconductors, and by Rimbey (19) for very large oscillator strength molecular crystals. The inclusion of the extra term in the denominator of equation (65) results in an asymmetric rounding off of reflection bands and may, depending on the system, introduce unique structure. So far, only the reflection spectrum of anthracene has been studied extensively (251) and no clear evidence of spatial dispersion effects has been shown. The second situation is

the creation of the so-called "anomalous" or "new waves" as discussed by Davydov (270), Pekar (226) and Agranovich (219). Pekar and Strashnikova claim to have unambiguous evidence for the existence of anomalous waves in CdS spectra (272). When spatial dispersion effects are small, the tensor elements $\varepsilon_{ij}(\omega\vec{k})$ may be replaced by

$$\varepsilon_{ij}(\omega\vec{k}) = \varepsilon_{ij}(\omega,0) + i\gamma_{ij\ell}(\omega)k_{\ell} + \alpha_{ij\ell m}(\omega)k_{\ell}k_{m} \qquad (66)$$

$$\varepsilon_{ij}^{-1}(\omega,\vec{k}) = \varepsilon_{ij}^{-1}(\omega,0) + i\delta_{ij\ell}(\omega)k_{\ell} + \beta_{ij\ell m}(\omega)k_{\ell}k_{m} \qquad (67)$$

For crystals with a center of symmetry (called non-gyrotropic), $\gamma = \delta = 0$ and spatial dispersion will be cetermined only by quadratic terms and only for non-gyrotropic crystals will anomalous waves be possible. The higher order terms in equations (66) and (67) bring about what is called optical anisotropy; that is, when higher order terms are included it has been shown that even for a cubic crystal $\varepsilon_{ij}(\omega\vec{k})$ will no longer be a scalar. Consider the relation

$$\tilde{\eta}^2 = \frac{k^2c^2}{\omega^2} = \varepsilon_o + \frac{F_s\omega_o^2}{\omega_{EX(0)}^2 - \omega^2 + \alpha k^2} \cdot \qquad (68)$$

For the case $\alpha \neq 0$, $\gamma = 0$, there are two values for the refractive index $\eta_{1,2}(\omega)$, which gives rise to a situation where for a given frequency ω there will exist two polariton waves. The wave with the larger value of the refractive index is called the anomalous wave.

Boundary conditions

With the introduction of a surface into polariton problems Maxwell's equations no longer are sufficient to completely characterize the system and additional boundary conditions (ABC's) are required. The form of these ABC's has been discussed by a number of authors (273). For an infinite half space with $\vec{z}$ normal to the surface and $\vec{z}$ and $\vec{k}$ defining a plane perpendicular to the surface the three most general ABC's are

$$\vec{P}_{(z=0)} = 0 \tag{69}$$

$$\frac{d\vec{P}}{dZ} (Z=0) = 0 \tag{70}$$

$$\vec{P}_{(Z=0)} + \frac{\lambda d\vec{P}}{dZ} (Z=0) = 0 \tag{71}$$

Equation (69) was first proposed by Pekar and continues to be favored for the case of Frenkel excitons. Equation (70) applies to metals, and equation (71) a linear combination of (69) and (70) is appropriate for semiconductor

systems containing Wannier-Mott states. Most work done in comparing the theoretical predictions derived using various boundary conditions (and dielectric functions) to experimental data has been for reflectance in systems of large ($f \sim 0.1$) to very large ($f \sim 3$) oscillator strengths where spatial dispersion effects are also expected to be important (19). In the case where spatial dispersion is not included, the form chosen for the boundary conditions is immaterial.

Second quantization formalism

Both the exciton and polariton pictures are nowadays generally expressed in the language of second quantization. The expressions presented here are common to most discussions of the model. A more detailed treatment may be found in Davydov's book (270), and in the papers of Agranovich (18) and Philpott (9).

Neglecting exciton-phonon coupling the Hamiltonian for the polariton system may be written as

$$H_{\text{polariton}} = H_{\text{coul}} + H_{\perp} + H_{\text{int}} \qquad (72)$$

where H_{coul} is the "uncoupled" exciton Hamiltonian given in equation (1), $H_{\perp}$ describes the transverse component of the photon field, and H_{int} the coupling of excitons with the transverse photon field. With the important stipulation that the transverse photon field is enclosed in the

volume of the crystal and is subject to the same boundary conditions as the excitons

$$H_{\perp} = \sum_{\vec{q}}^{\infty} \sum_{j=1,2} \hbar\omega(k) A^{+}_{\vec{q}j} A_{\vec{q}j} \tag{73}$$

$A^{+}_{\vec{q}j}$ and $A_{\vec{q}j}$ are the Bose creation and annihilation operators for photons of energy $\hbar\omega$, quasimomentum $\vec{q}$ and polarization $j = 1,2$. Excitons may be considered "approximate Bosons" subject to the following commutation rules, when B^{+}_{nf}, B_{nf} are defined as creation and annihilation operators for an exciton at site $n\equiv(n\alpha)$ of f^{th} electronic state.

$$[B_{nf}, B^{+}_{nf}] = 1 - 2N_{nf} \tag{74}$$

N_{nf} is the occupation number for the f^{th} state. For low intensity light sources and a large ($\sim 10^{23}$ molecules) crystal, N_{nf} is approximately zero, hence equation (74) may be written

$$[B_{nf}, B^{+}_{nf}] = 1 = \delta_{nn'}\delta_{ff'} \tag{75}$$

It is often convenient to rewrite the site excitation operators in a delocalized plane wave form dependent on the site ($\alpha=2$, $\rightarrow\alpha=1,2$)

$$B^{+}_{nf} = N^{-\frac{1}{2}} \sum_{k} e^{-i\vec{k}\cdot\vec{n}} B^{+}_{\alpha f}(\vec{k}) \tag{76a}$$

$$B_{nf} = N^{-\frac{1}{2}} \sum_{k} e^{i\vec{k}\cdot\vec{n}} B_{\alpha f}(\vec{k}) \tag{76b}$$

Equation (75) is now

$$[B_{\alpha' f'}(\vec{k}'),\ B_{\alpha f}(\vec{k})] = \delta_{\vec{k}\vec{k}'}\delta_{ff'}\delta_{\alpha\alpha'} \tag{77}$$

$B^{+}_{\alpha f}(\vec{k})$ now creates and $B_{\alpha f}(\vec{k})$ destroys a delocalized excitation of the entire crystal for translationally equivalent sites.

To simplify the following discussion we should consider only the case of a crystal containing one molecule per unit cell ($\rightarrow \alpha \equiv \beta$). Therefore, the α site index will be deleted, in addition the unit cell will be assumed to possess a center of symmetry. Equation (12) for $\alpha \equiv \beta$ may now be rewritten in the second quantized form as

$$H_{coul} = \sum_{n} (E_f + D_f)\, B^{+}_{nf} B_{nf} + \sum_{n+m} M^{f}_{nm} B^{+}_{mf} B_{nf} \tag{78}$$

M_{nm} is related to the term $L^{f}_{\alpha\beta}(\vec{k})$ given at the beginning of this chapter by

$$L^{f}_{\alpha\beta}(\vec{k}) = \sum_{n} M^{f}_{n\alpha,m\beta} \exp\{i\vec{k}(\vec{n}-\vec{m})\} = L^{f}(\vec{k}) \qquad \alpha \equiv \beta \tag{79}$$

$$M_{n\alpha,m\beta} = \langle \psi^{o}_{n\alpha}\psi^{f}_{m\beta} | V_{n\alpha,m\beta} | \psi^{f}_{n\alpha}\psi^{o}_{m\beta} \rangle = M_{n,m} \qquad \alpha \equiv \beta \tag{80}$$

Generally, $H_{polariton}$ is diagonalized in two steps. First, H_{coul} is made diagonal and secondly, $H_{polariton}$ which is then diagonal for H_{photon} and H_{coul} is diagonalized. By virtue of the choice of a one molecule per unit cell model, H_{coul} may be diagonalized simply by substituting equations (76a) and (76b) in equation (78). The result is

$$H_{coul} = \sum_{k} E^{f}(\vec{k}) B_{f}^{+}(\vec{k}) B_{f}(\vec{k}) \tag{81}$$

where $E^{f} = \Delta\varepsilon_{f} + D_{f} + L^{f}(\vec{k})$.

It now remains to state the explicit form for H_{int} and then to diagonalize $H_{polariton}$. H_{int} may be expressed in terms of the vector potential $A(\vec{r}_n)$ and the operator of the total momentum of the electrons in the molecule at site n, $\hat{J}$, as

$$H_{int} = -\sum_{n} \frac{e}{mc} A(\vec{r}_n)\hat{J}_n + \frac{e^2 S}{2mc^2} \sum_{n} A^2(\vec{r}_n) \tag{82}$$

where e and m are the mass and charge of the electron, c is the speed of light and S is defined by the sum rule on molecular oscillator strengths as

$$S = \sum_{f} F_{f} \tag{83}$$

where F is a molecular oscillator strength. (For atoms S = 1) $A(\vec{r}_n)$ is written in terms of the photon creation

and annihilation operators as

$$A(\vec{r}_n) = \sum_{k,j}^{\infty} \sqrt{\frac{2\Pi e}{V \cdot |k|}}\, \vec{U}_{kj}\, \hat{\gamma}_{kj}\, \exp(i\vec{k}\cdot\vec{r}) \tag{84}$$

where $\hat{\gamma}_{\vec{k},j} = \hat{\gamma}^{+}_{-\vec{k},j} = A_{\vec{k}j} + A_{-\vec{k}j}$, $j = 1,2$, and $\vec{U}_{\vec{k}j}$ is a unit vector describing the k sense and polarization of the photon.

$\hat{J}_n$ may be expressed in terms of the exciton creation and annihilation operators by making use of the following identities. First, any operator in the coordinate representation may be rewritten in the second quantization form as

$$\hat{J}_n = \sum_{f\neq 0} \{\langle f|\hat{J}_n|0\rangle B^{+}_{nf} + \langle 0|\hat{J}_n|f\rangle B_{nf}\} \tag{85}$$

secondly

$$\langle f|\hat{J}_n|0\rangle = \frac{im\omega_f}{e}\, \underset{\sim}{d}_{f\leftarrow 0} \tag{86}$$

$\underset{\sim}{d}_{f\leftarrow 0}$ is the molecular dipole moment for the transition $f\rightarrow 0$, occurring at frequency ω_f. By substituting equations (84), (85) and (86) into operator (82), a form for H_{int} which now contains the photon and exciton creation and annihilation operators but which is not yet diagonalized, is obtained

$$H_{int} = -\frac{i}{c} \sum_{n,f} \omega_f (A(\vec{r}_n)\underset{\sim}{d}_{f\leftarrow 0})(B^+_{nf} - B_{nf})$$

$$+ \frac{e^2 S}{2me^2} \sum A^2(\vec{r}_n) \quad (87)$$

At this point it is convenient to define two new quantities

$$D(\vec{k},j,f) = -i\omega_f(\vec{U}_{\vec{k}j} \cdot \underset{\sim}{d}_{f\leftarrow 0}) \sqrt{\frac{2\Pi}{vc|k|}}$$

$$\cdot [u_j k_f + v_j k_f] \quad (88)$$

$$\omega_o^2 = \frac{4\Pi e^2 S}{mv} = 4\Pi \sum_{f\neq 0} \omega_f (\underset{\sim}{d}_{f\leftarrow 0} \cdot \vec{U}_{kj})^2 \quad (89)$$

Note that ω_o^2 is nearly the plasma frequency ω_p, $\omega_p = \frac{4\Pi e^2}{mv}$; also that $(\vec{d}_f \cdot \vec{U}_{kj}) = 0$ for longitudinal excitons with $\vec{k}$ parallel $\underset{\sim}{d}_{f\leftarrow 0}$. Restricting the sums in the polariton operator to those values of $\vec{k}$ lying in the first Brillouin zone - $\frac{-\pi}{a} < k < \frac{\pi}{a}$, the quadratic form of $H_{polariton}$ may be written out explicitly as

$$H_{\vec{k}} = \sum_f E_f(\vec{k})[B^+_{\vec{k}f}B_{\vec{k}f} + B^+_{-\vec{k}f}B_{-\vec{k}f}] + \sum_j c|\vec{k}|(1 + \frac{\omega_o^2}{2c^2k^2})$$

$$[A^+_{\vec{k}j}A_{\vec{k}j} + A^+_{-\vec{k}j}A_{-\vec{k}j}] + \frac{\omega_o^2}{4c|\vec{k}|} \sum_j (A_{\vec{k}j}A_{-\vec{k}j}$$

$$+ A^+_{\vec{k}j}A^+_{-\vec{k}j}) + \sum_f D(\vec{k}_j f)\{\hat{Y}_{\vec{k}j}(B^+_{\vec{k}f} - B_{-\vec{k}f})$$

$$+ \hat{Y}_{-\vec{k}j}(B^+_{-\vec{k}f} - B_{\vec{k}f})\} \quad (90)$$

What one now wishes to do is to find a transformation to a set of new operators which will diagonalize $H_{polariton}$, and describe the new zero order states of the system the polaritons. To accomplish this the Tyablikov operators $\xi(\mu)$ are required. The photon and exciton operators may be rewritten in terms of $\xi^{+}(\mu)\xi(\mu)$ and the Tyablikov coefficients u and v as

$$B_{\vec{k}f} = \sum_{\mu} (\xi(\mu)u_{\vec{k}f\mu} + \overset{+}{\xi}(\mu)v_{\vec{k}f\mu}) \tag{91}$$

$$A_{\vec{k}j} = \sum_{\mu} (\xi(\mu)u_{\vec{k}jf} + \overset{+}{\xi}(\mu)v^{*}_{\vec{k}jf} \tag{92}$$

The μ's will later be seen to index the polariton branches. For one crystal transition such as described by the classical picture μ = 1,2,3; correspond to the two transverse and one longitudinal branch. The coefficients u and v are c numbers which must satisfy the following relations

$$\sum_{\ell} (u_{\ell\mu}u^{*}_{\ell\mu'} - v_{\ell\mu}v^{*}_{\ell\mu'}) = \delta_{\mu\mu'} \tag{93}$$

$$\sum_{\ell} (u_{\ell\mu}v_{\ell\mu'} - v_{\ell\mu'}u_{\ell\mu}) = 0 \tag{94}$$

$$\sum_{\ell} (u_{\ell\mu}v^{*}_{\ell\mu'} - v_{\ell\mu'}u_{\ell\mu}) = 0 \tag{95}$$

where $\ell = \vec{k}f, -\vec{k}f, kj, -kj$ at fixed k. In addition, after the substitution of equations (91) and (92) into equation

(90) four independent equations for the u's and v's are generated.

$$[E\mu(\vec{k}) - E]u_{\vec{k}f} + \sum_j D(\vec{k}jf)(u_{\vec{k}j} + v_{-\vec{k}j}) = 0 \qquad (96)$$

$$[E\mu(\vec{k}) + E]v_{-\vec{k}f} - \sum_j D(\vec{k}jf)(u_{\vec{k}j} + v_{-\vec{k}j}) = 0 \qquad (97)$$

$$(\hbar|\vec{k}|c - E)u_{\vec{k}j} - \sum_f D(\vec{k}jf)(u_{\vec{k}f} - v_{-\vec{k}f}) + \frac{\hbar\omega_o^2}{2|\vec{k}|c}(u_{\vec{k}j} + v_{-\vec{k}j}) = 0 \qquad (98)$$

$$(\hbar|\vec{k}|c - E)v_{-\vec{k}j} - \sum_f D(\vec{k}jf)(u_{\vec{k}f} - v_{-\vec{k}f}) + \frac{\hbar\omega_o^2}{2|\vec{k}|c}(u_{\vec{k}j} + v_{-\vec{k}j}) = 0 \qquad (99)$$

Comparing equation (96) to equation (97) and equation (98) to equation (99) it is found that

$$v_{-\vec{k}f} = \frac{E_f(\vec{k}) - E}{E_f(\vec{k}) + E} u_{\vec{k}f} \qquad (100)$$

and

$$v_{-\vec{k}j} = \frac{\hbar|\vec{k}|c - E}{\hbar|\vec{k}|c + E} u_{\vec{k}j} \qquad (101)$$

The quantity E appearing above represents the energy of the total system - the polariton energy. Expressing u_{kf}

in terms of $u_{\vec{k}j}$ for all states for which $(\vec{d}_f \cdot \vec{U}_{kj}) \neq 0$ - the transverse modes, and substituting this result into equation (90) one obtains two linearly independent equations for u_{kj}. When the determinant formed from these two equations is set equal to zero, a rather complicated equation for the polariton energies, E, is obtained.

$$(\hbar^2k^2c^2 + \hbar^2\omega_o^2 - E^2)^2 - (\hbar^2k^2c^2 + \hbar^2\omega_o^2 - E^2)$$

$$(T_{11} + T_{22}) + T_{11}T_{22} - T_{12}T_{21} = 0 \quad (102)$$

where

$$T_{ab} = T_{ba} = \sum_f D(a\vec{k}f)D(bkf) \quad \frac{4\hbar kc\ E_f(\vec{k})}{E^2 - E_f^2(\vec{k})} \quad (103)$$

Equation (102) does not determine the energies of elementary excitations without dipole moments nor does it provide the energies of longitudinal modes. Using the general relation between $\varepsilon(\omega k)$ and ω, $\varepsilon(\omega k) = \frac{\hbar^2k^2c^2}{E^2}$, equation (102) may be written as a function of the dielectric constant

$$\varepsilon(\omega\vec{k}) = 1 - \left(\frac{\omega_o}{\omega}\right)^2 + \frac{1}{2E^2}(T_{11} + T_{22})$$

$$\pm \tfrac{1}{2}\left[\left(\frac{T_{11} - T_{22}}{E^2}\right)^2 + 4\left(\frac{T_{12}}{E^2}\right)^2\right]^{\frac{1}{2}} \quad (104)$$

The T_{ab} terms may be eliminated by the introduction of an arbitrary coordinate system, $x \perp y$, and by the use of a

modified form of the operators introduced in equations (85) and (86). If the total crystal dipole moment is defined by $\hat{D}$

$$\hat{D} = \sum_{n\alpha} \hat{d}_{n\alpha} \tag{105}$$

where $\hat{d}_{n\alpha}$ is the dipole moment operator of the $n\alpha^{th}$ molecule, a conjugate operator to $\hat{D}$ is

$$\hat{\dot{D}} \equiv \hat{P} = \sum_{n\alpha} \hat{\dot{d}}_{n\alpha} \tag{106}$$

where $\hat{P}$ is the crystal momentum. (Both $\hat{D}$ and $\hat{P}$ lack a phase factor $\exp(i\vec{k}\cdot\vec{n})$. The following relations hold

$$\hat{P}_x\hat{D}_y - \hat{D}_y\hat{P}_x = -\frac{i\hbar e^2}{m} S \tag{107}$$

and

$$-i\hbar\hat{P}_x = H_{coul} D_x - D_x H_{coul} \tag{108}$$

Also, it is assumed by all authors that $\hbar\omega_f \simeq E_f(\vec{k})$ in what follows:

$$\hat{D}_y = \sqrt{N} \sum_{f\alpha} \{\langle 0|d_{\alpha y}|f\rangle [u_{\alpha\vec{k}f} + v_{\alpha\vec{k}f}]\}(B_{\vec{k}f} + B^{+}_{\vec{k}f}) \tag{109}$$

$$\hat{P}_x = \frac{i\sqrt{N}}{\hbar} \sum_{f} E_f(\vec{k})\{\sum_{\alpha}\langle 0|d_{\alpha y}|f\rangle [u_{\alpha\vec{k}f} + v_{\alpha\vec{k}f}]\} (B_{\vec{k}f} - B^{+}_{\vec{k}f}) \tag{110}$$

Combining equations (107), (109) and (110) gives a sum rule relation

$$2 \sum_f E_f(\vec{k})\{\sum_\alpha <0|d_{\alpha x}|f>[u_{\alpha\vec{k}f} + v_{\alpha\vec{k}f}]\}\{\sum_\beta <0|d_{\beta y}|f> [u_{\beta\vec{k}f} + v_{\beta\vec{k}f}]\} = \hbar^2 \frac{e^2}{m} S\, \delta_{xy} \qquad (111)$$

Introducing

$$\underset{\sim}{d}_{o,f}(\vec{k}) = \sum_\alpha <0|d_\alpha|f>[u_{\alpha\vec{k}f} + v_{\alpha\vec{k}f}] \qquad (112)$$

equation (106) becomes

$$2 \sum_f E_f(\vec{k})|P_{of}(\vec{k})|^2 \cos\psi_y(f\vec{k}) \cos\psi_x(f\vec{k}) = \hbar^2 \frac{e^2}{m} S\delta xy \qquad (113)$$

where ψ_j is the angle between the vector $\hat{d}_{of}(\vec{k})$ and $\vec{U}_{\vec{k}j}$, $j = 1,2,3$, the unit polarization vector of the photon. Equation (113) may now be rewritten as

$$\varepsilon(\omega,\vec{k}) = 1 - \frac{1}{2}\sum_f \frac{\omega_p{}^2 F_{f\leftarrow o}(\vec{k}) \sin^2\psi_3(f\vec{k})}{\omega^2 - (E_f(\vec{k})/\hbar)^2} \pm \frac{1}{2}\left\{\left[\sum_f \frac{\omega_p{}^2 F_{f\leftarrow o}(\vec{k}) \cos^2\psi_1(f\vec{k}) - \cos^2\psi_2(f\vec{k})}{\omega^2 - (E_f(k)/\hbar)^2}\right]^2 + 4\left[\sum_f \left[\frac{\omega_p{}^2 F_{f\leftarrow o}(\vec{k}) \cos\psi_1(f\vec{k}) \cos\psi_2(f\vec{k})}{\omega^2 - (E_f(\vec{k})/\hbar)^2}\right]^2\right]^{\frac{1}{2}}\right\} \qquad (114)$$

where $F_{f\leftarrow o}$ is the oscillator strength of the quantum transition f←o

$$F_{f\leftarrow o} = \frac{2m}{e^2} E_f(\vec{k}) |\underset{\sim}{d}_{of}(\vec{k})|^2 \tag{115}$$

Thus equation (114) has a built in dependence on crystal anisotropy due to the microscopic approach used. It reduces to the classical case for an isotropic medium, where there exist two degenerate transverse modes $|\underset{\sim}{d}_{of}| \perp \vec{k}$ and one longitudinal mode $|\underset{\sim}{d}_{of}| \parallel \vec{k}$. In this case $E_f(\vec{k})$ depends only on the absolute value of $\vec{k}$ and one obtains

$$\varepsilon(\omega\vec{k}) = 1 - \frac{1}{2} \sum_f \left[\frac{\omega_p^2 F_{f\leftarrow o}}{\omega^2 - (E_f(\vec{k})/\hbar)^2}\right] \tag{116}$$

For the case of an isolated transition the f sum is dropped giving the classical result

$$\varepsilon(\omega\vec{k}) = \varepsilon_o + \left[\frac{\omega_p^2 F_{1\leftarrow o}}{\omega^2 - (E_f(\vec{k})/\hbar)^2}\right] \tag{117}$$

where

$$\varepsilon_o = 1 + \sum_{f>1} \left[\frac{\omega_p^2 F_{f\leftarrow o}}{\omega^2 - (E_f(\vec{k})/\hbar)^2}\right] \tag{118}$$

It is interesting to note the laborious route to the classical result <u>via</u> a microscopic approach as compared to the simple manner in which equation (117) is obtained in the macroscopic treatment.

Exciton-Phonon and Polariton-Phonon Interactions

Exciton-phonon coupling in crystals with two molecules per unit cell

The treatment presented here is due to Sethuraman (274) and is similar to that given by Davydov (270) for the one molecule per unit cell case and by Craig and Dissado (275) for a two molecule case. Since we are most interested in low temperature behavior ($\sim$2-20°K) we shall assume that translational and librational motions are sufficiently decoupled and consider the translational motions only in constructing the lattice modes. Any general translational distortion, $\vec{R}_{m\alpha}$, may be expanded in terms of the six translational modes (three optic, three acoustic) as

$$\vec{R}_{m\alpha} = \frac{1}{\sqrt{Nm}} \sum_{q} \vec{e}_{\vec{q}s,\alpha} \, \psi_{\vec{q}s} \, e^{i\vec{q}\cdot\vec{m}} \tag{119}$$

where $\vec{q}$ is the phonon wave vector in the first Brillouin zone $\vec{m} = (m_a, m_b, m_c) \equiv \vec{R}_{mo}$ is a vector locating the unit cell $\psi_{\vec{q}s} = \left(\frac{\hbar}{2\omega_{\vec{q}s}}\right)^{\frac{1}{2}} (b_{\vec{q}s} + b^{+}_{-\vec{q}s})$, $b_{\vec{q}s}$ is the second quantization operator for phonons of wave vector $\vec{q}$ and normal mode index s = 1,2...6. $\omega_{\vec{q}s}$ is the frequency of a normal mode, $\vec{e}_{\vec{q}s,\alpha}$ is a normal coordinate vector corresponding to the s^{th} mode and wave vector $\vec{q}$, α is the site index α=1,2, and m is the mass of the molecule. For conciseness of

description, only a two-level system (ground state o, excited state f) will be considered. The starting point in the Heitler-London approximation is the same H_{coul} as that given in equation (78) except now the site indices α are included

$$H_{coul} = \sum_{n\alpha} [\Delta\varepsilon^f + D^f] B^{+f}_{n\alpha} B^f_{n\alpha} + \sum_{n\alpha,m\beta} M^f_{n\alpha,m\beta} B^{+f}_{n\alpha} B^f_{m\beta} \qquad (120)$$

where $\Delta\varepsilon^f$ is the free molecule excitation energy, D^f is defined in equation (13) and $M^f_{n\alpha,m\beta}$ is defined in equation (80). In order to introduce an H_{int}-type term, H_{coul} will be assumed to have a dependence on lattice motion. Davydov has formulated the exciton-lattice interaction by a procedure identical to that for an isolated molecule. The following is an appropriate modification of his results for the case of two molecules per unit cell. In the linear approximation

$$D^f(\vec{R}) \simeq D^{(o)}_{n\alpha,m\beta} + (\vec{R}_{n\alpha}\cdot\vec{\nabla}_{n\alpha} + \vec{R}_{m\beta}\cdot\vec{\nabla}_{m\beta}) D_{n\alpha,m\beta}(\vec{R}) \Big|_{\vec{R}=0} \qquad (121)$$

$$L_{n\alpha,m\beta}(\vec{R}) \simeq L^{(o)}_{n\alpha,m\beta} + (\vec{R}_{n\alpha}\cdot\vec{\nabla}_{n\alpha} + \vec{R}_{m\beta}\cdot\vec{\nabla}_{m\beta}) D_{n\alpha,m\beta}(\vec{R}) \Big|_{\vec{R}=0} \qquad (122)$$

where $\vec{R}_{n\alpha}$ is the deviation of the $n\alpha^{th}$ molecule from its equilibrium position. Making use of equations (119), (121) and (122), equation (120) may be rewritten in terms of the $\vec{k}$ dependent creation and annihilation operators defined in equations (76a) and (76b) as

$$H = \sum_{\alpha} [\Delta\epsilon^{f} + \sum_{m\beta} D_{o\alpha,m\beta}(0)] \sum_{\vec{k}} B^{+}_{\alpha}(\vec{k})B_{\alpha}(\vec{k})$$

$$+ \sum_{m,\alpha\beta} L_{o\alpha,m\beta}(0)\, B^{+}_{\alpha}(\vec{k})B_{\beta}(\vec{k})$$

$$+ \sum_{\vec{k}\alpha,\vec{q}s} \chi^{\alpha}_{\vec{q}s}\psi_{\vec{q}s}\, B^{+}(\vec{K})_{\alpha}B(\vec{k})_{\alpha}$$

$$+ \sum_{\vec{k}\alpha\beta,\vec{q}s} F^{\alpha\beta}_{k\vec{q}s}B^{+}_{\alpha}(\vec{K})B_{\beta}(\vec{k})\psi_{\vec{q}s} \qquad (123)$$

in equation (123)

$$\chi^{\alpha}_{\vec{q}s} = \left(\frac{\hbar}{2N_m\omega_{\vec{q}s}}\right)^{\frac{1}{2}} \sum_{m\beta} (\vec{e}_{\vec{q}s\alpha}\cdot\vec{\nabla}_{o\alpha} + e^{i\vec{q}\cdot\vec{n}}\,\vec{e}_{\vec{q}s\beta}\cdot\vec{\nabla}_{m\beta})$$

$$D^{\alpha\beta}_{om}\Big|\vec{R}=0 \qquad (124)$$

and

$$F^{\alpha\beta}_{\vec{k}\vec{q}s} = \left(\frac{\hbar}{2N_m\omega_{\vec{q}s\alpha}}\right)^{\frac{1}{2}} \sum_{n} e^{i\vec{k}\cdot\vec{n}}\,(\vec{e}_{\vec{q}s\alpha}\cdot\vec{\nabla}_{o\alpha}$$

$$+ e^{i\vec{q}\cdot\vec{n}}\,\vec{e}_{\vec{q}s\beta}\cdot\vec{\nabla}_{m\beta})M_{o\alpha,m\beta}\Big|R=0 \qquad (125)$$

where $\vec{K} = \vec{k} + \vec{q}$

The rigid lattice form of equation (123) (obtained when $\chi^{\alpha}_{\vec{q}s}$ and $F^{\alpha\beta}_{\vec{k}\vec{q}s} = 0$) may be diagonalized by the transformation

$$B_{\vec{k}1} = cB_{\vec{k}+} + sB_{\vec{k}-} \tag{126}$$

$$B_{\vec{k}2} = sB_{\vec{k}+} - cB_{\vec{k}-} \tag{127}$$

where $c \equiv \cos(\theta(\vec{k}))$ and $s \equiv \sin(\theta(\vec{k}))$ as follows

$$\begin{aligned} H = &\sum_{k} (\Delta_{\vec{k}+} B^{+}_{\vec{k}+} B_{\vec{k}+} + \Delta_{\vec{k}-} B^{+}_{\vec{k}-} B_{\vec{k}-}) \\ &+ \sum_{\vec{k}\vec{q}s} \psi_{\vec{q}s} [F^{++}_{\vec{k}\vec{q}s} B^{+}_{+}(\vec{K}) B^{+}_{+}(\vec{k}) \\ &+ F^{--}_{\vec{k}\vec{q}s} B^{+}_{-}(\vec{K}) B_{-}(\vec{k}) + F^{+-}_{\vec{k}\vec{q}s} B^{+}_{+}(\vec{K}) B_{-}(\vec{k}) \\ &+ F^{-+}_{\vec{k}\vec{q}s} B^{+}_{-}(\vec{K}) B_{+}(\vec{k})] \end{aligned} \tag{128}$$

$\Delta k\pm$ are the roots of the determinant

$$\begin{vmatrix} \Delta\varepsilon^{f} + \sum_{n\alpha} D^{1\beta}_{on}(0) + \sum_{n} L^{11}_{on}(0) - \lambda & \sum_{n} L^{12}_{on}(0) \\ \sum_{n} L^{21}_{on}(0) & \Delta\varepsilon^{f} + \sum_{m\beta} D^{2\beta}_{on}(0) + \sum_{n} L^{22}_{on}(0) - \lambda \end{vmatrix} = 0 \tag{129}$$

The solutions of equation (129) are the same energies obtained in equation (14), i.e., they are the solutions of H_{coul} in the absence of phonons. The F terms in the nonrigid lattice part of H are defined by

$$F^{++}_{\vec{k}\vec{q}s} = c^{2} f^{11}_{\vec{k}\vec{q}s} + s^{2} f^{22}_{\vec{k}\vec{q}s} + cs(F^{12}_{\vec{k}\vec{q}s} + F^{21}_{\vec{k}\vec{q}s}) \tag{130}$$

$$F^{--}_{\vec{k}\vec{q}s} = s^2 f^{11}_{\vec{k}\vec{q}s} + c^2 f^{22}_{\vec{k}\vec{q}s} + cs(F^{12}_{\vec{k}\vec{q}s} + F^{21}_{\vec{k}\vec{q}s}) \qquad (131)$$

$$F^{+-}_{\vec{k}\vec{q}s} = cs(f^{11}_{\vec{k}\vec{q}s} - f^{22}_{\vec{k}\vec{q}s}) + s^2 F^{21}_{\vec{k}\vec{q}s}\ c^2 F^{12}_{\vec{k}\vec{q}s} \qquad (132)$$

$$F^{-+}_{\vec{k}\vec{q}s} = cs(f^{11}_{\vec{k}\vec{q}s} - f^{22}_{\vec{k}\vec{q}s}) + s^2 F^{12}_{\vec{k}\vec{q}s} - c^2 F^{21}_{\vec{k}\vec{q}s} \qquad (133)$$

where $f^{\alpha\alpha}_{\vec{k}\vec{q}s} = F^{\alpha\alpha}_{\vec{k}\vec{q}s} + \chi^{\alpha\alpha}_{\vec{q}s}$. In a monoclinic crystal such as naphthalene for k derivations || or $\perp$ to the $\underline{b}$ crystalographic axis the choice of $\theta=45°$, i.e., $c=s=1\sqrt{2}$ will diagonalize the rigid lattice Hamiltonian. In equation (128) terms involving F^{++}, F^{--}, F^{+-} and F^{-+} which describe exciton-phonon scattering events cannot be easily diagonalized. The nondiagonal form suffices to describe the physics associated with the exciton picture; F^{++} and F^{--} coefficients lead to intraband scattering, while F^{+-} and F^{-+} lead to interband scattering (i.e., that between different Davydov components). These two types of scattering processes are depicted in Figure 3a.

Thermal broadening and exciton-phonon interaction

In the one-phonon scattering approximation it is possible to derive a simple expression for the temperature-dependent line width for absorption of broad-band incident light. The $\vec{k}$ dependent line width is

$$\Gamma_{\vec{k}} = \sum_{\vec{q}s} \delta(\varepsilon_{\vec{k}} + \omega_{\vec{q}s} - \varepsilon_{\vec{K}}) \left| V^{\text{ex-phonon}}_{\vec{K}+\vec{q},\vec{k}} \right|^2 \qquad (134)$$

where $V^{ex\text{-}phonon}$ is given by the terms linear in $\psi_{\vec{q}s}$ in equation (128). For absorption to a final state $|(\vec{k})_-, n_{\vec{q}s}>$

$$V^{ex\text{-}phonon}_{\vec{k}+\vec{q},\vec{k}} = <(\vec{k}+\vec{q})_\pm, \bar{n}_{\vec{q}s}-1 | \sum_s (F^{\pm}_{\vec{k}\vec{q}s} B^{+}_{\vec{K}\pm} B_{\vec{k}-} \psi_{\vec{q}s} |$$

$$(\vec{k})_-, \bar{n}_{qs}> \qquad (135)$$

$\bar{n}_{qs}$ is the phonon thermal occupation number

$$\bar{n}_{\vec{q}s} = \frac{1}{(e^{\beta\omega_{\vec{q}s}}-1)} \qquad (136)$$

$\beta = \frac{1}{kT}$, k = Boltzman's constant, T = temperature in °Kelvin, ω_{qs} = the active phonon mode. For the case when the + and - components are well-separated, i.e., the density of thermal phonons of frequency ≈ band gap is <<1, $\Gamma_{\vec{k}}$ can be estimated for a situation such as the lower energy Davydov component in naphthalene. Assuming that the lower factor group component has a positive effective mass, m* (taken to be direction-independent) and that the factor group splitting is $>kT$ for the temperatures of interest, the range of values of $\vec{k}+\vec{q}$ of the upper factor group component which can be reached by absorption of a phonon limits possible scattering events to the intraband type. We consider only the acoustic modes and since they obey a nearly linear dispersion relation away from the zone boundaries the isotropic dependence of

phonon frequency on $\vec{q}$ may be written

$$\omega_{\vec{q}s} = v_s q \quad . \tag{137}$$

Thus $\bar{n}_{\vec{q}s} \to 0$ as $T \to 0$ for acoustic modes, as required. With the above approximations

$$V^{\text{ex-phonon}}_{\vec{k}+\vec{q},\vec{k}} = \langle (\vec{k}+\vec{q})_-, \bar{n}_{\vec{q}s} - 1 | \sum_{s=123} F^{--}_{\vec{k}\vec{q}s} B^{+}_{\vec{k}-} B_{\vec{k}-} \psi_{\vec{q}s}$$

$$| (\vec{k})_-, \bar{n}_{\vec{q}s} \rangle$$

$$= \sum_s (\bar{n}_{\vec{q}s})^{\frac{1}{2}} F^{--}_{\vec{k}\vec{q}s} \tag{138}$$

Therefore

$$\Gamma_{\vec{k}} = \sum_{\vec{q}s} \delta(\varepsilon_{\vec{k}} + \omega_{\vec{q}s} - \varepsilon_{\vec{K}}) \bar{n}_{\vec{q}s} | F^{--}_{\vec{k}\vec{q}s} |^2 \tag{139}$$

This result is similar to that obtained by Dissado (123, 124). In the limit of a continuous distribution of $\vec{q}$, we may convert the $\vec{q}$ sum into an integral

$$\sum_{\vec{q}} = \frac{V}{(2\pi)^3} \int d^3\vec{q} = \frac{V}{(2\pi)^3} \int d\Omega_{\vec{q}} \int_0^{\vec{q}_{max}} d\vec{q} \cdot q^2 \tag{140}$$

where $\vec{q}_{max}$ is determined by the condition that a Debye sphere of radius $\vec{q}_{max}$ contain the same number of allowed $\vec{q}$ values as the first Brillouin zone. Evaluation of the $\vec{q}$ sum requires knowledge of the exciton-dispersion relations for each direction in the crystal (!). To assume an isotropic

dependence is highly unphysical since the exciton dispersion relations are known to be very direction dependent. Realizing that the end result will be less than satisfactory let

$$\varepsilon_{\vec{k}} = \frac{\hbar^2 k^2}{2m^*}$$

for all $\vec{k}$ directions. Further $F_{\vec{k}\vec{q}s}$ will be approximated by a $\vec{k},\vec{q}$ and s independent constant, F. With these drastic approximations

$$\Gamma_k = 3|F|^2 \frac{V}{(2\pi)^3} \int d\Omega_{\vec{q}} \int d\vec{q}\cdot q^2 \frac{1}{e^{\hbar\beta\omega_{\vec{q}}}-1} \cdot \delta\left(\frac{\hbar^2 q^2}{2m^*} - \hbar\nu_{\vec{q}}\right) \tag{141}$$

where now $\omega_{\vec{q}s} = \omega_{\vec{q}} = \nu_{\vec{q}}$, and

$$\varepsilon_{\vec{K}} - \varepsilon_{\vec{k}} = \varepsilon_{\vec{k}+\vec{q}} - \varepsilon_{\vec{k}} \approx \frac{\hbar^2 q^2}{2m^*} \tag{142}$$

Thus, assuming that only one phonon mode is active, the band broadening should go roughly as $\frac{1}{e^{\hbar\beta\omega_{\vec{q}}}-1}$. A similar type of temperature dependence involving optical (librational) modes has been suggested by Dissado (123,124) to explain band broadening data for anthracene and phenanthrene. The validity of such an approach will be considered in chapter four.

Urbach rule behavior

There is another procedure of extracting exciton-phonon coupling data from experimental band profiles which has also received much attention and again seems to be founded on very shaky experimental evidence. This is the Urbach rule behavior explanation for the lowest energy band edge in molecular crystals (80,85,86). Originally developed for ionic systems, approximate Urbach rule behavior has been claimed for a large number of systems. Urbach rule behavior gives a straight line fit for log K vs $\hbar\omega$ where K and $\hbar\omega$ are defined by

$$K = K_o \exp\left[- \frac{\sigma(\hbar\omega_o - \hbar\omega)}{kT} \right] \tag{143}$$

K is the absorption coefficient (in cm^{-1}), $\hbar\omega_o$ is the resonance frequency (usually taken as the band maxima), k is Boltzman's constant, T is the temperature (T remains constant for each plot of $\hbar\omega$ vs log K), lastly σ/kT is a constant giving the slope of the absorption curve for a given temperature. The small correction factor σ is taken to be a measure of the strength of exciton-phonon coupling.

$$\sigma = \sigma_o \frac{2kT}{\hbar\omega_{ph}} \tanh \frac{\hbar\omega_{ph}}{2kT} \tag{144}$$

Concurrently, an equally large number of theoretical explanations of the effect have appeared (83,84). At present it still remains an unsolved mystery. It seems reasonably certain that for systems of large oscillator strength one is not measuring the absorption band edge with transmission data. Since it appears from the calculated band profiles of Philpott and those given here, that true absorption may be far different than transmission, it is difficult to know what value to place on the results that have been reported (80-86).

Polariton-phonon coupling

Polariton-phonon coupling has been discussed mostly as it affects spectroscopic processes in semiconductor systems (247-249). Agranovich and Konobeev (236) have extended the second quantization treatment presented earlier to include the case of weak polariton coupling to acoustic lattice vibrations for the case of one molecule per unit cell. In the rigid lattice approximation the polariton Hamiltonian in terms of the Tyablikov operators of equations (91) and (92) is simply

$$H_{pol} = \sum_{\vec{k},\mu} E_{\mu} \xi^{+}_{\vec{k}}(\mu) \xi_{\vec{k}}(\mu) \qquad (145)$$

The operator of the lattice is

$$H_{lat} = V_o + \sum_s \frac{M_n \dot{r}_n^2}{2}$$

$$+ \sum_{\substack{n,m \\ x_1 x_2}} A_{n,mx_1x_2} r_{nx_1} r_{mx_2} \qquad (146)$$

where r_{nx} is the x-projection of the displacement vector of the n^{th} molecule, moved from its equilibrium position, M_n is the mass of the n^{th} molecule and A_{n,m,x_1x_2} is the force constant.

An additional H_{int} term is required to describe the interactions of the polaritons and lattice vibrations which is

$$H_{pol\text{-}phonon} = \frac{1}{N} \sum_{\substack{n,x \\ \vec{k}\mu,\vec{k}'\mu'}} u^*_{\vec{k}\mu} u_{\vec{k}'\mu'} e^{i\vec{n}(\vec{k}'-\vec{k})} [\Phi^x(\vec{k}')$$

$$- \Phi^x(\vec{k})] r_{nx} \xi^+_{\vec{k}}(\mu) \xi_{\vec{k}'}(\mu') \qquad (147)$$

where

$$\Phi^x(\vec{k}) = \sum_m \Phi^x_{n,m} e^{i\vec{k}(\vec{n}-\vec{m})} \qquad (148)$$

$\Phi_{n\alpha,m\beta}$ is the gradient of the matrix elements $L^f(\vec{k})$ and $M_{n,m}$ defined in equations (79) and (80). The total Hamiltonian for the polariton-phonon system is

$$H_{total} = V_o + \sum_{\vec{k}\mu} E(\mu)\ \varepsilon^{+}_{\vec{k}}(\mu)\ \varepsilon_{\vec{k}}(\mu)$$

$$+ \sum_{\substack{n,m \\ x_1 x_2}} A^{x_1 x_2}_{n,m}\ r_{nx_1}\ r_{mx_2} + \frac{1}{2}\sum_{n} \frac{M_n\ \dot{r}_n^{\,2}}{2}$$

$$+ \sum_{\substack{k\mu,k'\mu' \\ nx}} B(\vec{k}\mu,\vec{k}'\mu';nx)$$

$$\xi^{+}_{n}(\mu)\ \xi_{n'}(\mu')\ r_{nx} \qquad (149)$$

where $$B(\vec{k}\mu,\vec{k}'\mu',nx) = \frac{u^{*}_{\vec{k}\mu}\ u_{k'\mu'}}{N}\ e^{in(\vec{k}'-\vec{k})}$$

$$\cdot\ [\Phi^{x}(\vec{k}') - \Phi^{x}(\vec{k})]$$

A schematic view of polariton-phonon scattering processes is given in Figure 3b. The major difference between Figures 3a and 3b is that as mentioned for exciton-phonon interactions when the approximation that only $\vec{k}$=o exciton states are created is used then for the point at E=$\underset{\sim}{a}$, $\vec{k}$=o there are no allowed <u>downward</u> scattering events. However, for the polariton picture even at $\vec{k}$≈o downward scattering through the creation of a phonon, with an energy transition to a more photon-like portion of the dispersion curve is always available. This implies that even for temperatures sufficiently low that upward scattering is disallowed (≈0°K) a downward mechanism still exists. Hence, in the

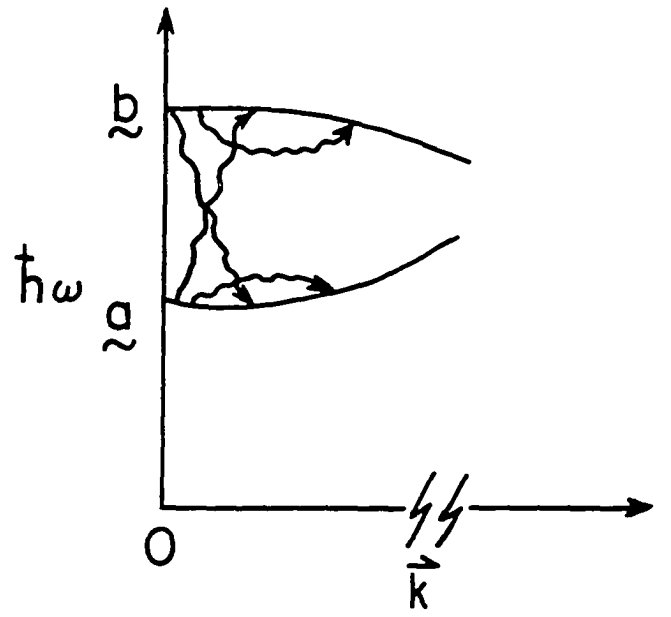

Intra- and interband scattering events between two Coulomb exciton branches with positive (a) and negative (b) effective mass

(a)

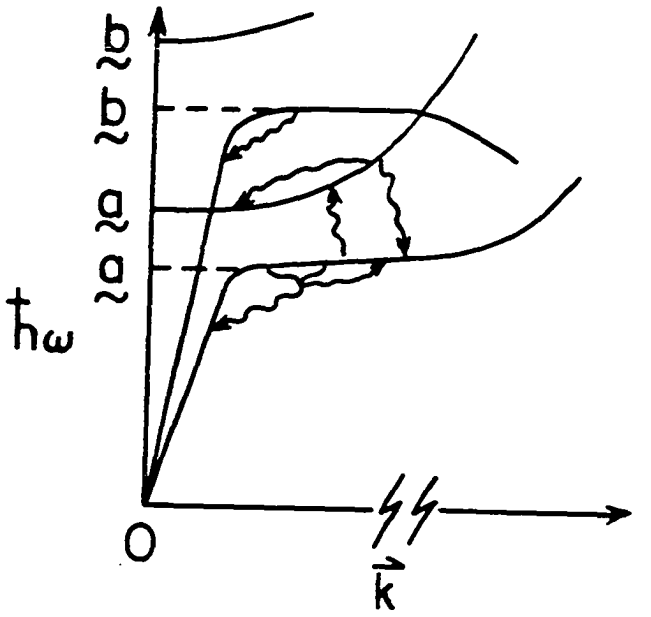

Intra- and interbranch polariton scattering events for two bands with positive (a) and negative (b) effective exciton mass

Figure 3. Exciton-phonon and polariton-phonon scattering processes

polariton picture a band such as a(0,0) will always retain a finite width, even at 0°K. Obviously, there is no experimental test of this proposition available. Whichever mechanism exists, a finite width will always be measured at low temperatures for all real crystals due to inherent crystal imperfections. However, Dissado (123,124) notes that in fitting the temperature dependent bandwidth data on phenanthrene and anthracene significant improvement was achieved with the inclusion of downward scattering. (Note that downward scattering was not expected to contribute in the exciton-phonon coupling picture Dissado used.)

EXPERIMENTAL

Liquid Helium Cryostats and Spectrometers

All spectra presented in this thesis were recorded photoelectrically. The cryostats used were an Andonian metal dewar, model MHD-3L-30N, with a 0-7 MH throttling system, and a metal Janis dewar, model 10 DT. In both dewars the samples are cooled by the boil off of liquid helium. To obtain temperatures above 6°K, a 5W heater at the bottom of the sample chamber was used to warm the helium gas before it passed over the crystal. Temperatures between 1.6° and 2.2°K, the helium λ-point, were obtained by pumping on the liquid helium covering the sample with a large capacity Stokes pump.

Temperatures from 1.6° to 100°K were measured with Cryo-Cal germanium resistance thermometers (precision ∿0.1°K) which were attached by paper tape to the outside of the sample holder at the level of the crystal. Their accuracy was monitored periodically by checking their readings when submerged in liquid helium or nitrogen. Unwanted infrared radiation from the light sources (vide infra) was removed prior to sample irradiation by use of a water filter. The estimated discrepancy between measured and sample temperatures is ≲ 1°K.

Two spectrometers were used in the course of the experiments. Preliminary data were taken on a 1-meter Jarrell-Ash Czerny-Turner spectrometer with a resolving power of ca. 50,000 corresponding to a resolution of 0.07 Å in the region of interest, 3200 Å. Instrumental broadening of sharp bands was suspected. Subsequent spectra run on a 1.5 meter Jobin-Yvon HR 1500 spectrometer with 3600 groove/mm holographically ruled grating and resolution of 0.001 Å (resolving power 261,000) proved this to be the case. Crystal limited half-widths as narrow as 0.3 cm^{-1} were recorded on the J-Y instrument. An EMI 9558 QB photomultiplier tube was used in conjunction with both spectrometers. The output of the photomultiplier tube was fed into a picoammeter (Keithley Instruments model 414S) and displayed on a strip chart recorder (Omniscribe model 5121-5 or Texas Instruments model FS01 W6d).

Light Sources, Filters and Polarizers

For transmission measurements a Hanovia 750W Xenon lamp powered by an Oriel C-72-50 power supply was employed. Emission spectra were run using a 500W PEK mercury excitation lamp in conjunction with an Illumination Industries Inc. model 200 power supply and a Sorenson Voltage Regulator model 1750. Naphthalene fluorescence was excited from the back at normal incidence using a

2537 Å interference filter (Oriel G-521-2537) to block unwanted mercury lines in the naphthalene emission region. Polarized spectra were obtained using either one or two Glan-Thompson polarizers. Optimal polarization was achieved by slight adjustments of polarizers after the crystals were aligned in the optical path at liquid helium temperature.

Calibration and Intensity Measurements

Naphthalene bands were calibrated in wavelength by superimposing the lines of a 20 mA Fe-Ne lamp (Jarrell-Ash hollow cathode, type 45455) over the spectrum. The full width-half maxima reported were measured by hand using disperions derived from the known calibration lines. The relative areas under the transmission curves were obtained by cutting out the bands and weighing them on a four-place analytical balance. An error of no more than 10% is introduced by this method, as judged by the scatter in data points. Other sources of error, such as base-line drift and polarization leakage, should be negligible for temperatures below 35°K, but may be a source of error at higher temperatures ($\sim$50-70°K).

Sample Handling

The strain-free mounting of naphthalene crystals on the order of a micron in thickness presented special

difficulties. First, the high vapor pressure of naphthalene results in complete sublimation of thin flakes in a few minutes in air at room temperature. Therefore, all mounting and alignment procedures were carried out in a cold room at ∿30°F. Second, crystals tend to adhere to a glass or metal surface; therefore, Teflon-coated utensils were used for transfer and positioning procedures.

Naphthalene crystals grown by sublimation produce only $\underset{\sim}{ab}$ faces. Crystals were aligned coniscopically with respect to the $\underset{\sim}{a}$ and $\underset{\sim}{b}$ crystallographic axes using a Leitz polarizing microscope equipped with a Bertrand lens. The $\underset{\sim}{a}$ and $\underset{\sim}{b}$ directions in very thin high quality crystals are easily characterized by complete extenction under the crossed polars. Thicknesses were determined using a Leitz Tilting Compensator, model M, in conjunction with the polarizing microscope. The most uniform crystals display only one color in polarized light, allowing a determination of thickness accurate to ∿0.2μ using the tilting compensator. However, for nonuniform crystals (wedge-shaped), only an average thickness can be assigned. In such cases, the smallness of the pinhole relative to the sublimation flake insures that the spectral manifestations of variation in thickness are at least minimized.

Strain-Free Mounting

The crystal mounting arrangement is shown in Figure 4. The sample holder consisted of a flat lucite plate designed to fit the sample probe of our liquid helium cryostat. The crystal flake is first positioned between two pieces of Kleenex. Scotch tape is then applied in approximately 2mm wide strips around the outer edge of the top piece of tissue to form a "frame" which sandwiches (lightly) the crystal between the two pieces of tissue. In this way the crystal is not directly affixed to a solid support. A quartz cover disk of the same dimensions as the bottom disk and set in a Lucite holder is then placed over the enclosed crystal. The outer edges of the two Lucite pieces are joined with paper tape to prevent sublimation of the crystal during transfer to the cryostat and to prevent mechanical damage to the crystal by helium gas flow or boiling once inside the cryostat. The sample holder contains a small recess which can be filled with crushed solid naphthalene to provide an atmosphere rich in naphthalene vapor surrounding the crystal. The design of the sample holder owes much to a paper by Prikhot'ko and Soskin (276).

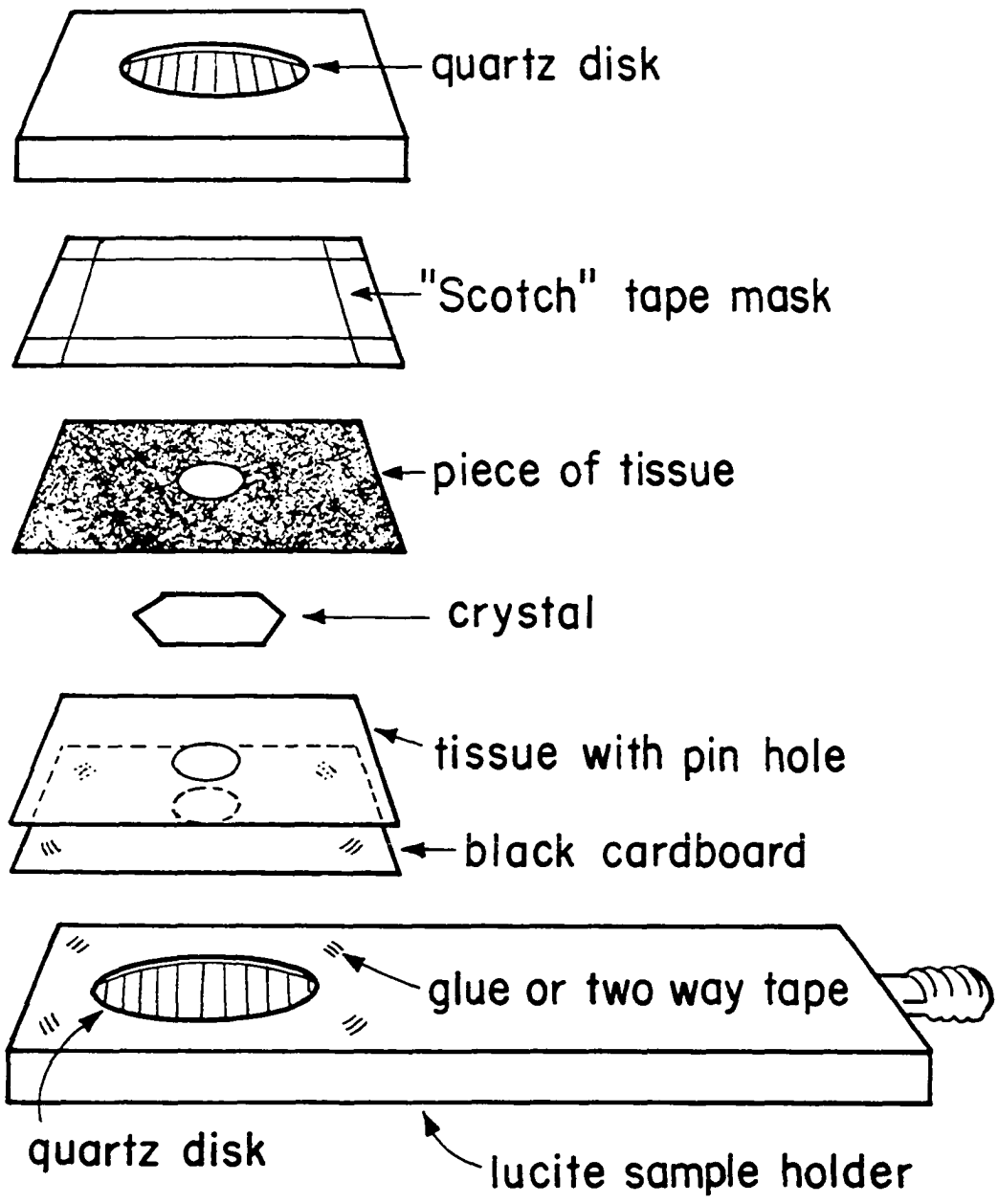

Figure 4. Strain-free sample holder

Sample Preparation

Purification

Aldrich Chemical naphthalene (98% purity) was subjected to fusion with potassium metal for 20-30 minutes to remove β-methylnaphthalene and subsequently zone refined 80-150 passes. The Pyrex apparatus used for the potassium fusion allowed transfer of the molten naphthalene into a zone tube while keeping the material under an inert atmosphere of 300-370 mm of dry nitrogen gas. For the mixed crystal studies, anthracene (Aldrich Chemicals, 98% purity) was also zone refined 80-100 passes. β-methylnaphthalene (MCB Gold Label grade, +99% purity) was used without further purification.

Crystal growth

The thinnest (0.5 to 10μ) most uniform single crystal flakes were grown by a simple sublimation method in an air atmosphere. About five grams of crushed naphthalene were placed in the bottom of a 6 in. evaporating dish. The dish is then covered with a cardboard ring (o.d. ∿155 mm, i.d. ∿50 mm) and a piece of filter paper with pinholes. A 150 ml beaker nested in a 400 ml beaker is placed over the pinholes. The evaporating dish was set in an oil bath kept at 74°-75°C and the entire arrangement loosely covered with aluminum foil. The apparatus is shown in Figures 5 and 6.

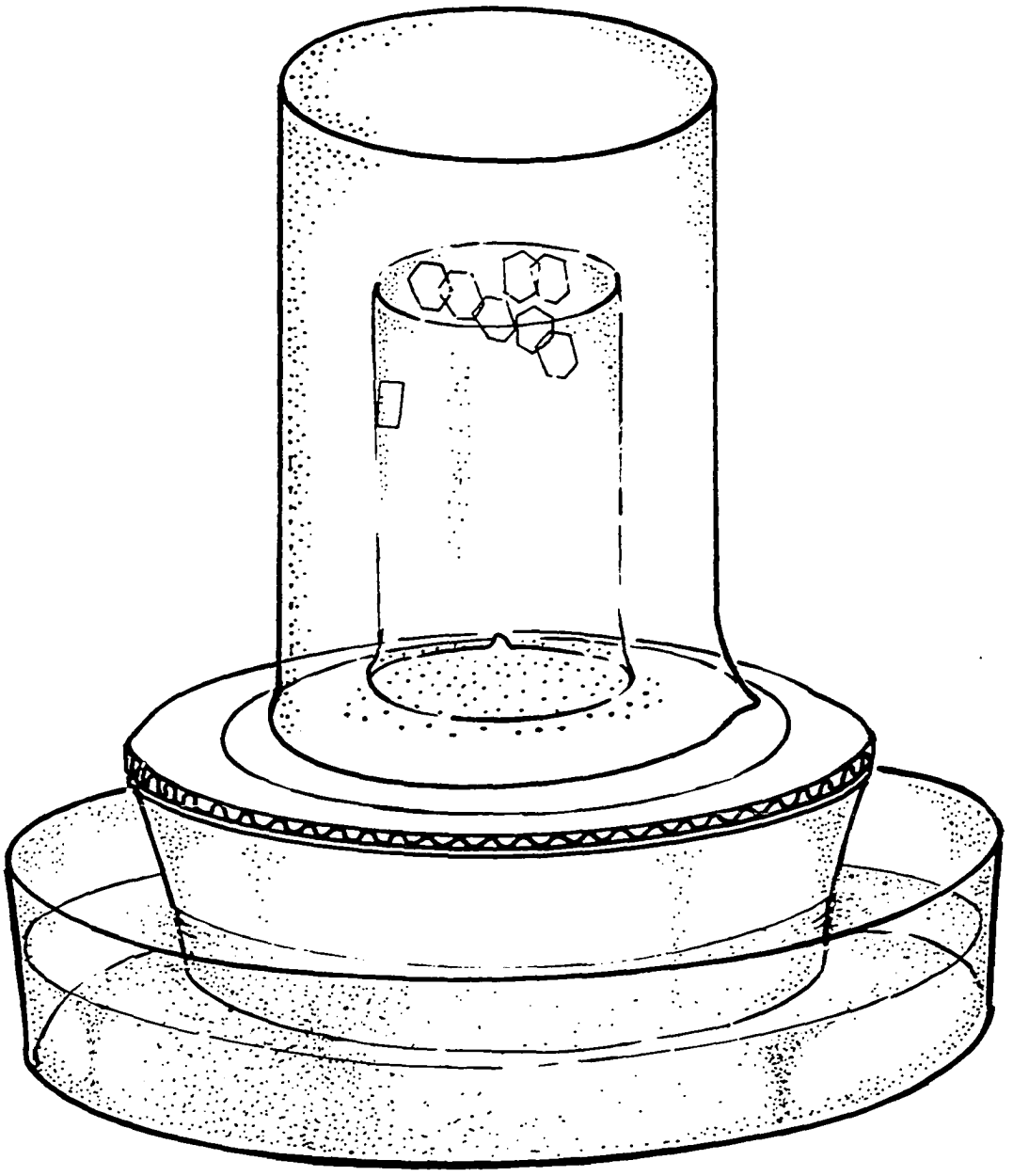

Figure 5. Covered beaker sublimation apparatus

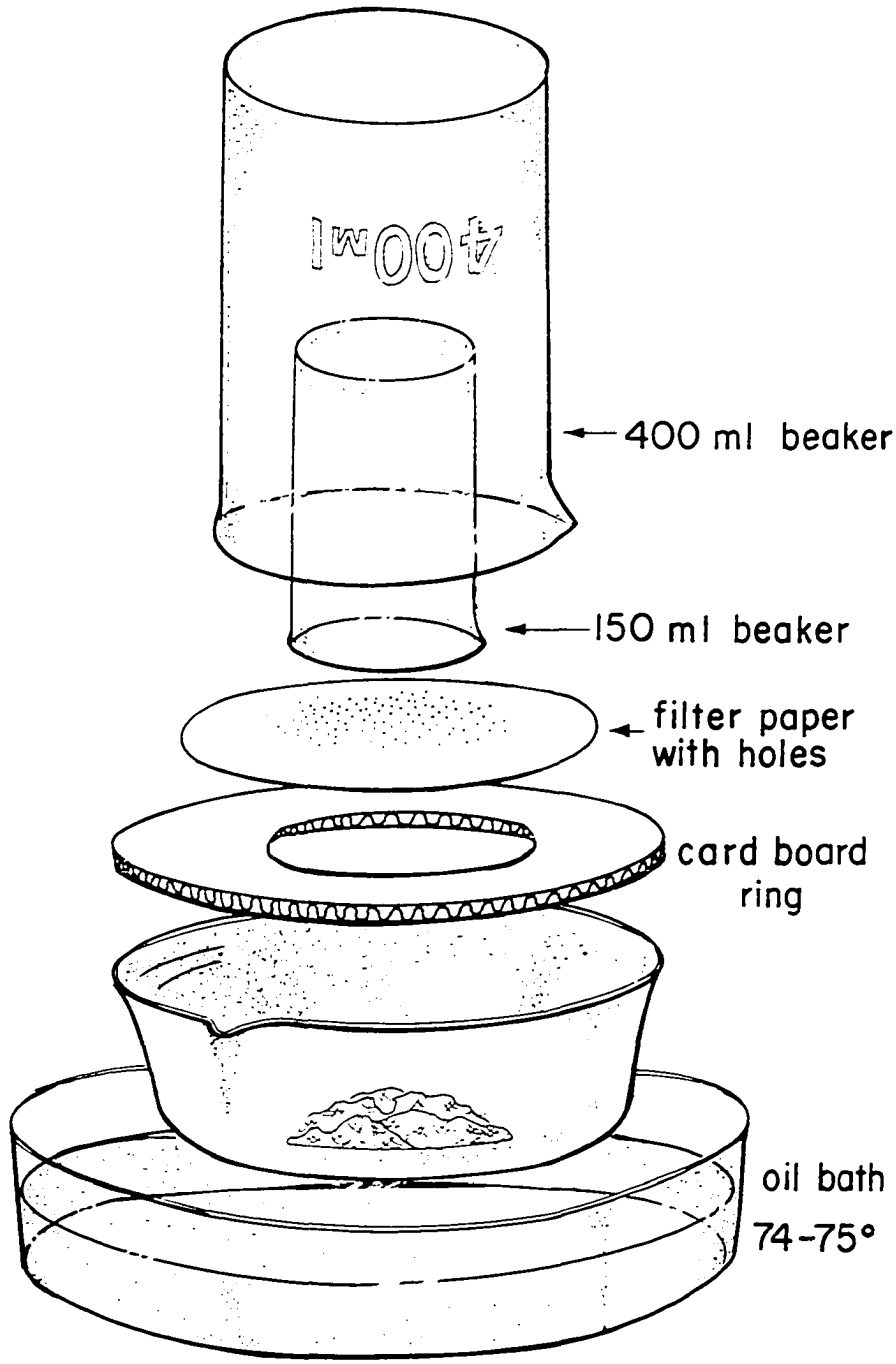

Figure 6. Covered beaker sublimation apparatus

The crucial requirement for the growth of high quality crystals by sublimation appears to be the establishment of a temperature gradient of 15-20°C between the nearly molten naphthalene in the evaporating dish and the surface of the beakers where crystals form.

A second method satisfying the temperature gradient requirement allowed crystal growth under an inert gas atmosphere using a vacuum-tight Pyrex container such as shown in Figure 7. Crushed naphthalene (1-2 g) is placed in the bottom; the container evacuated and then approximately an atmosphere of N_2 gas introduced. The bottom of the container was submerged ($\sim$1 cm) in an oil bath with the copper rod heated slightly to produce the desired 15-20° temperature gradient between the oil bath and the copper collection cup. Crystals grown in this apparatus tended to be thicker ($\gtrsim$10μ) than those grown in the inverted beaker arrangement.

Like several other aromatic systems, the naphthalene growth habit from sublimation afforded flakes in which the surface area increased far more rapidly than the thickness. As a result, it is possible to grow naphthalene crystals 5 to 10 mm across but only 0.5 to 10μ in thickness. Very pure naphthalene sublimation crystals grow in the shape of elongated hexagons with smooth parallel surfaces, while small amounts of an impurity such as anthracene ($\sim 10^{-4}$ m/m)

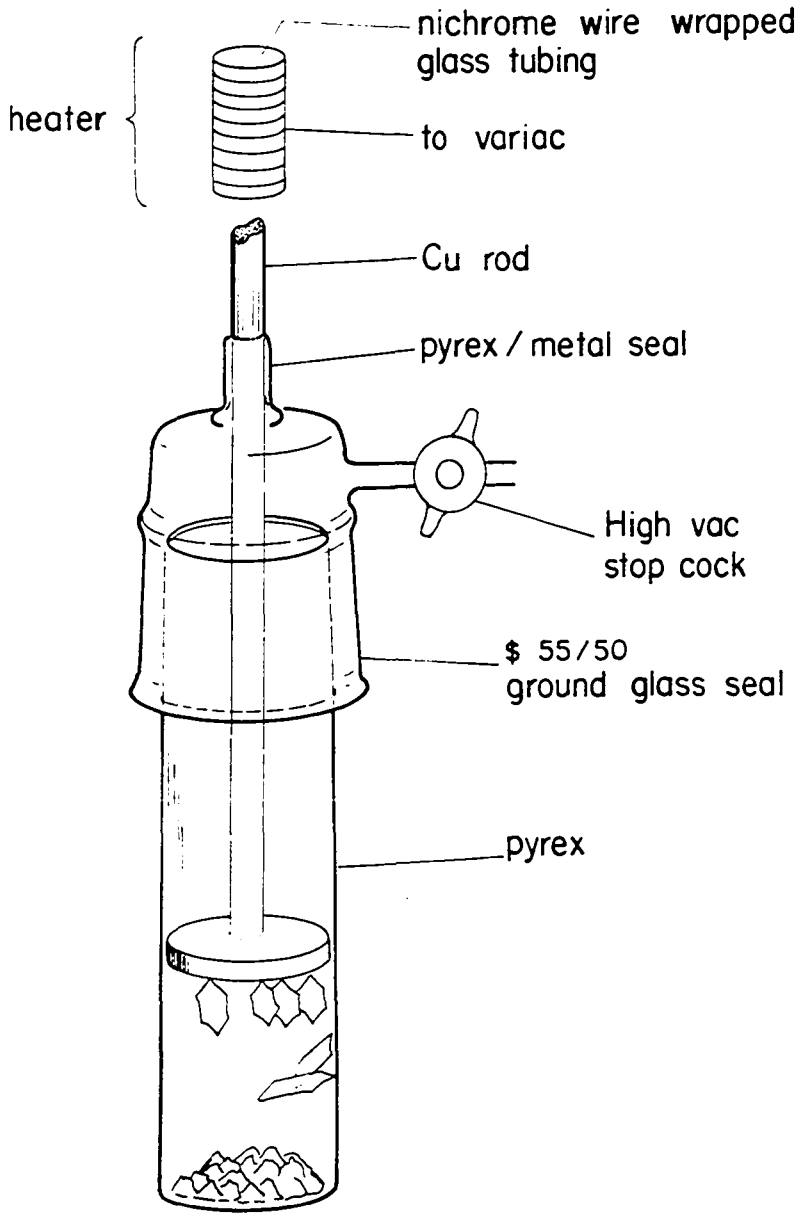

Figure 7. Vacuum sublimation apparatus

destroy the hexagonal growth habit and result in crystals with jagged edges and irregular surfaces. Apparently very pure naphthalene under either an air or nitrogen atmosphere is reluctant to form crystals of the hexagonal type. Slight misadjustments in temperature yield feather-shaped crystals or needles and/or granules. When small amounts of impurities such as anthracene are present large yields of inferior quality sublimation flakes are obtained.

Mixed crystals

When anthracene or β-methylnaphthalene were used as dopants, known amounts were first mixed with molten naphthalene under a nitrogen atmosphere to form solid solutions. The solid solutions were then opened to the air, transferred to evaporating dishes where doped crystal growth proceeded by the first method outlined.

The actual concentration of anthracene in the sublimation flakes was determined by dissolving a known weight of crystals in benzene and running the Cary 14 visible absorption spectrum. Using an experimentally derived ε value (7670) for the 3800 Å anthracene absorption, one can measure ∿ nanomole quantities when several crystal flakes are employed. Unfortunately, this method only provides average concentrations and not the impurity level of the individual flake used in a given experiment.

No satisfactory method was found to measure low ($\lesssim 10^{-4}$ m/m) β-methylnaphthalene concentrations, although higher concentrations ($\gtrsim$ .02%) can be determined by gas chromatography-mass spectroscopy.

A possible alternative method which may prove useful for quantitation of β-methylnaphthalene concentration is based on detection of its fluorescence. At liquid helium temperatures β-methylnaphthalene is simple to detect qualitatively, its emission lines are extremely sharp ($\sim$0.5 cm^{-1}) and readily identified. The difficulty with using this method to assign concentrations is that the fluorescence intensity for β-methylnaphthalene emission may not vary linearly with its concentration.

RESULTS AND DISCUSSION

Computer Spectra

It should be stated explicitly that all experimental spectra shown in this dissertation are transmission data, not absorption. Recall that A = 1-R-T. Ideally, one would like to record the reflection, transmission and photoexcitation spectrum simultaneously for a given crystal over a large temperature range (e.g., 2°-77°K). We note that Ferguson (228,229) has succeeded in measuring the photoexcitation (A) and transmission spectra for anthracene using a somewhat different experimental set-up. He obtains the reflection spectrum indirectly. Due to light intensity difficulties in the 300 nm region we were forced to employ computer generated power spectra (Figures 8-15) to estimate the magnitude of the reflection correction for the a (0,0) 31475 cm^{-1} band of naphthalene. Calculations were also done for the b (0,0) origin, 31625 cm^{-1} (Figures 16-19).

Although input parameters for naphthalene were used the spectra generated must be regarded as only approximations to real crystal data since the model assumes an isotropic slab without spatial dispersion, i.e., the model is nearly identical to that of Lorentz.[1] Philpott has performed very

---

[1]The program used for these calculations was borrowed from Dr. K. L. Kliewer of the I.S.U. Physics Department.

Figure 8. Computer generated reflection, transmission and absorption for a 0.3 μ crystal

Explanation of Figures 8-19

A is the oscillator strength of the transition

γ is a damping parameter. (Increasing values of γ for a fixed crystal thickness are meant to simulate an experimental increase in temperature)

θ is the angle of incident light, i.e., the angle of $\vec{k}_{inc}$ with $\vec{z}$

Ω is the resonance frequency of the exciton absorption. Here $\hbar\Omega$ corresponds to the naphthalene $\underset{\sim}{a}(0,0)$ resonance, 31475 cm^{-1}

P is polarization → $\vec{E}$ in xz plane, $E_y = H_x = H_z = 0$

In Figures 8-15 the oscillator strength used, $\sim 10^{-6}$, is appropriate for the $\underset{\sim}{a}(0,0)$ band of naphthalene

In Figures 16-19 a larger value of the oscillator strength, $\sim 10^{-4}$, reasonable for the $\underset{\sim}{b}(0,0)$ band was used

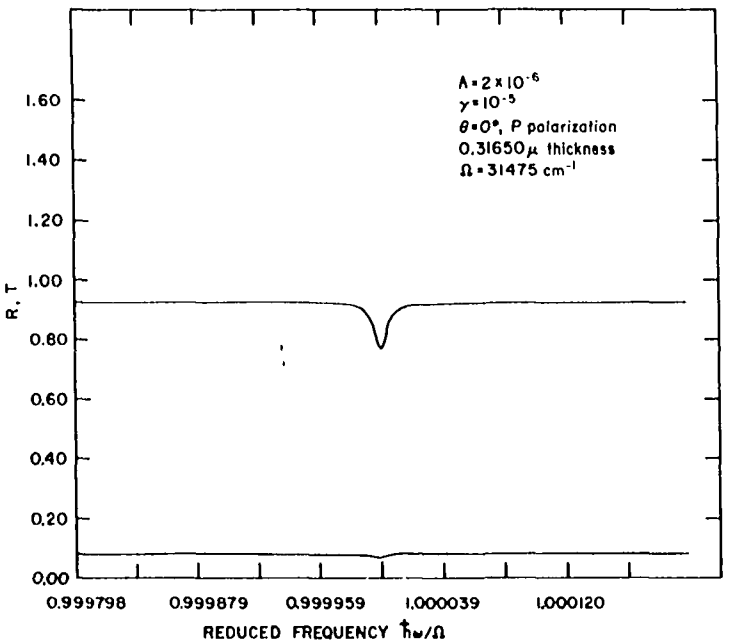
A = 2 x 10⁻⁶
γ = 10⁻⁵
θ = 0°, P polarization
0.31650 μ thickness
Ω = 31475 cm⁻¹
R, T
1.60
1.40
1.20
1.00
0.80
0.60
0.40
0.20
0.00
0.999798
0.999879
0.999959
1.000039
1.000120
REDUCED FREQUENCY ħω/Ω

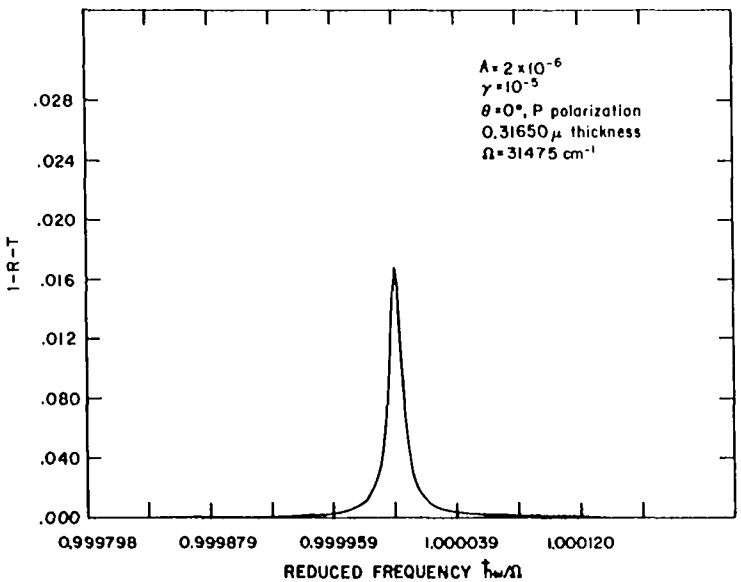
A = 2 x 10⁻⁶
γ = 10⁻⁵
θ = 0°, P polarization
0.31650 μ thickness
Ω = 31475 cm⁻¹
1-R-T
.028
.024
.020
.016
.012
.080
.040
.000
0.999798
0.999879
0.999959
1.000039
1.000120
REDUCED FREQUENCY ħω/Ω

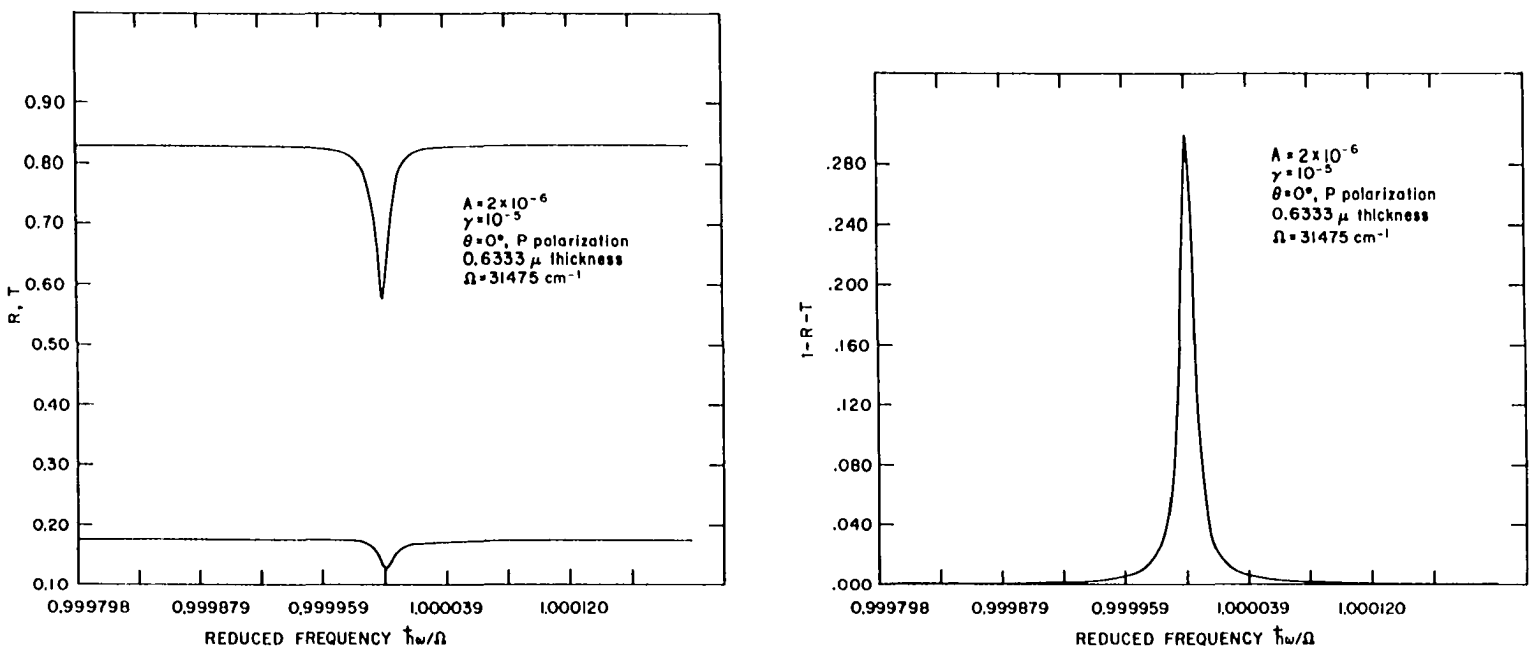

Figure 9. Computer generated reflection, transmission and absorption for a 0.6 μ crystal

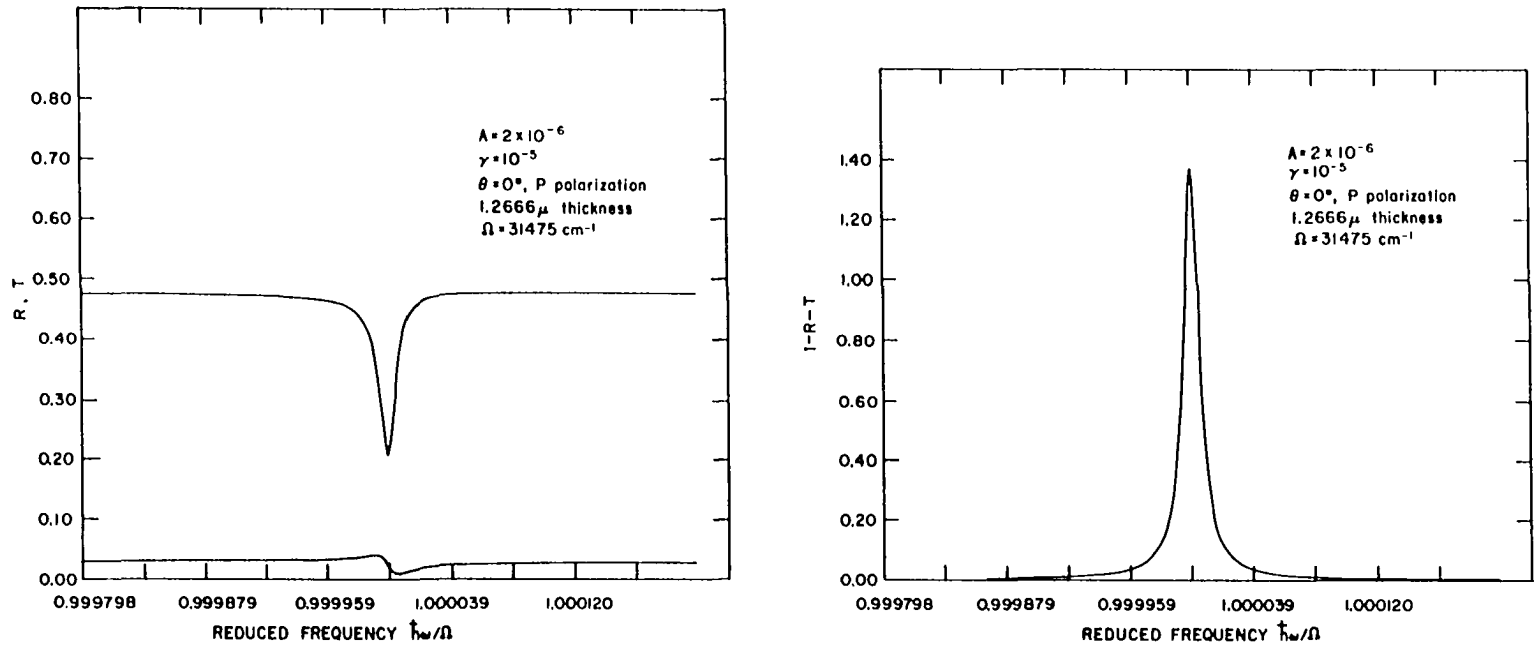

Figure 10. Computer generated reflection, transmission and absorption for a 1.3 μ crystal

Figure 11. Computer generated reflection, transmission and absorption for a 3.2 μ crystal

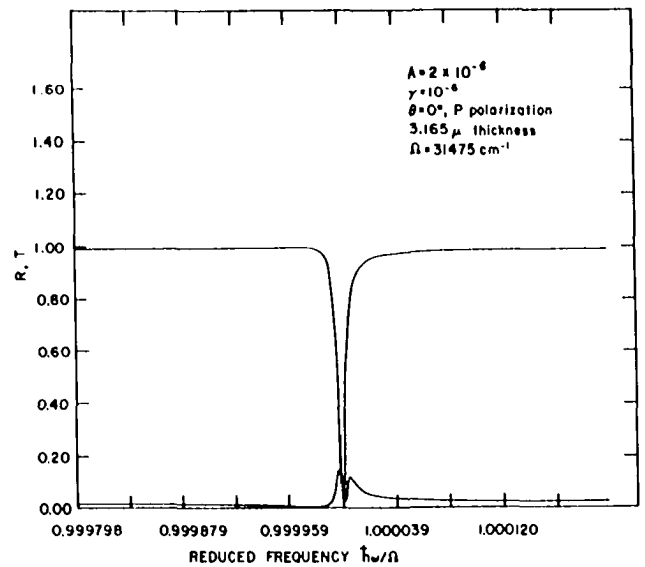
A=2 x 10⁻⁶
γ=10⁻⁶
θ=0°, P polarization
3.165 μ thickness
Ω=31475 cm⁻¹
R, T
1.60
1.40
1.20
1.00
0.80
0.60
0.40
0.20
0.00
0.999798
0.999879
0.999959
1.000039
1.000120
REDUCED FREQUENCY ħω/Ω

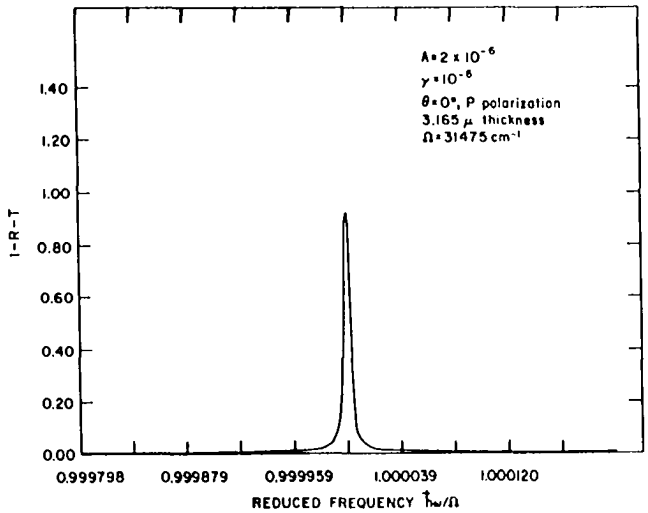
A=2 x 10⁻⁶
γ=10⁻⁶
θ=0°, P polarization
3.165 μ thickness
Ω=31475 cm⁻¹
1-R-T
1.40
1.20
1.00
0.80
0.60
0.40
0.20
0.00
0.999798
0.999879
0.999959
1.000039
1.000120
REDUCED FREQUENCY ħω/Ω

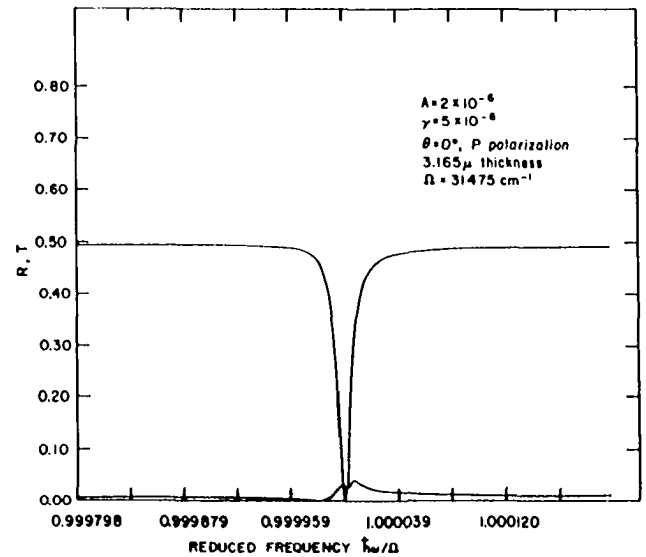
A=2 x 10⁻⁶
γ=5 x 10⁻⁶
θ=0°, P polarization
3.165 μ thickness
Ω=31475 cm⁻¹
R, T
0.80
0.70
0.60
0.50
0.40
0.30
0.20
0.10
0.00
0.999798
0.999879
0.999959
1.000039
1.000120
REDUCED FREQUENCY ħω/Ω

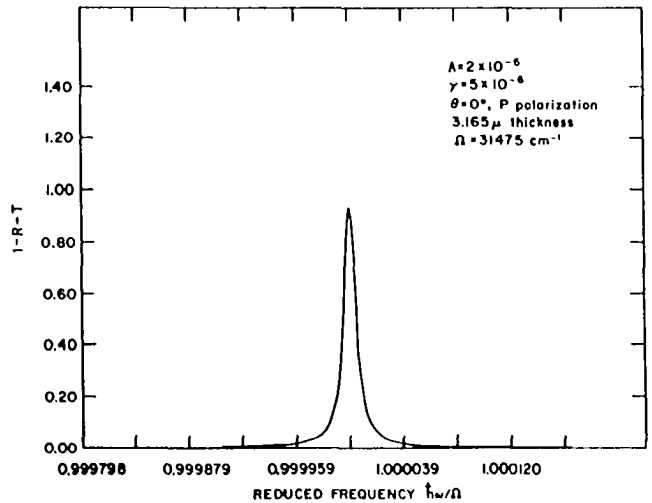
A=2 x 10⁻⁶
γ=5 x 10⁻⁶
θ=0°, P polarization
3.165 μ thickness
Ω=31475 cm⁻¹
1-R-T
1.40
1.20
1.00
0.80
0.60
0.40
0.20
0.00
0.999798
0.999879
0.999959
1.000039
1.000120
REDUCED FREQUENCY ħω/Ω

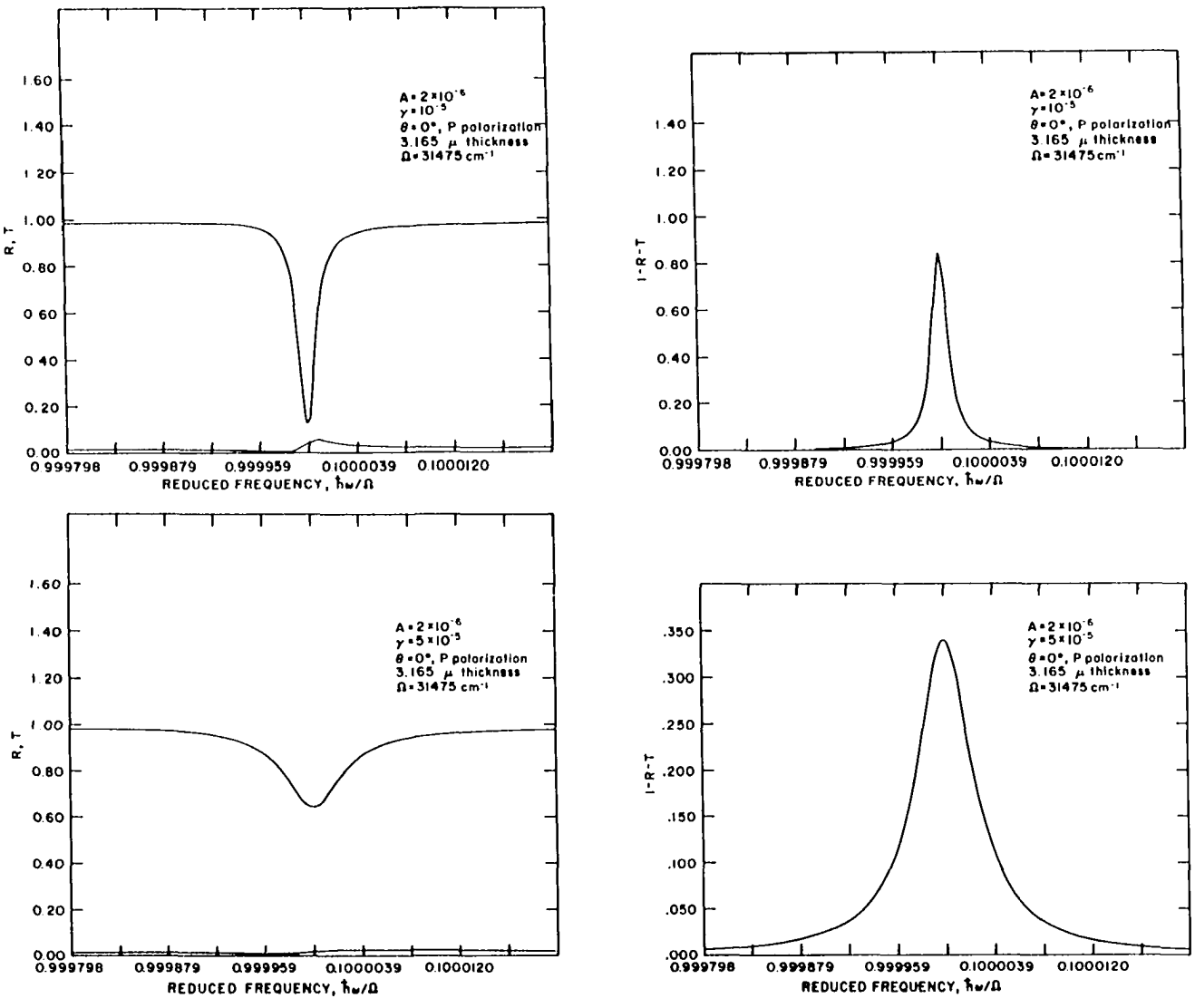

Figure 11. (Continued)

Figure 12. Computer generated reflection, transmission and absorption for a 5 μ crystal

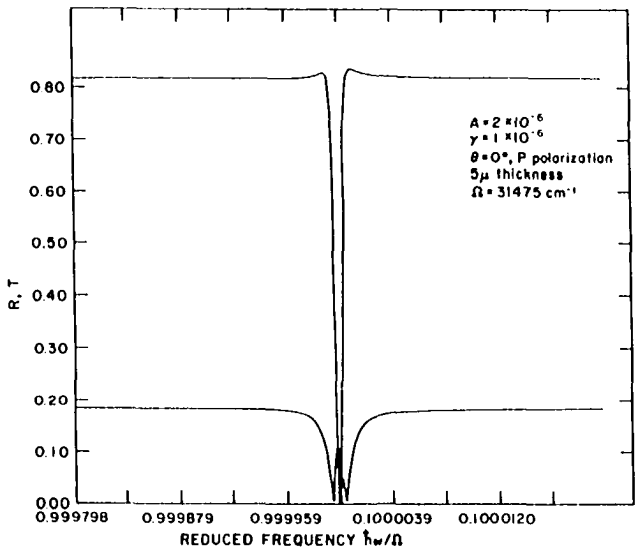
A = 2 × 10⁻⁶
γ = 1 × 10⁻⁶
θ = 0°, P polarization
5μ thickness
Ω = 31475 cm⁻¹
R, T
0.80
0.70
0.60
0.50
0.40
0.30
0.20
0.10
0.00
0.999798
0.999879
0.999959
0.1000039
0.1000120
REDUCED FREQUENCY ħω/Ω

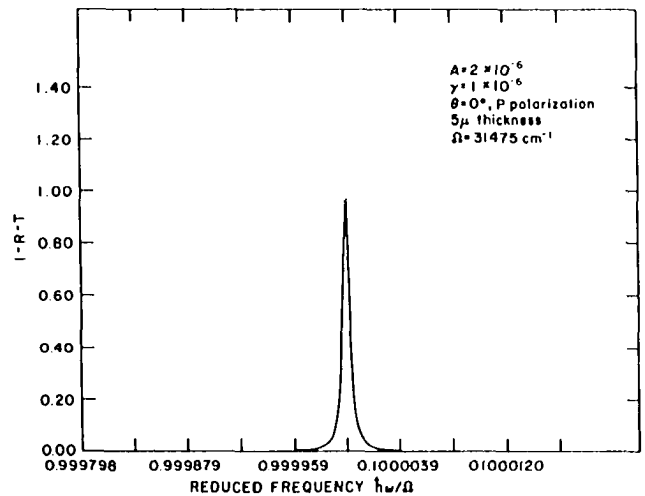
A = 2 × 10⁻⁶
γ = 1 × 10⁻⁶
θ = 0°, P polarization
5μ thickness
Ω = 31475 cm⁻¹
1-R-T
1.40
1.20
1.00
0.80
0.60
0.40
0.20
0.00
0.999798
0.999879
0.999959
0.1000039
0.1000120
REDUCED FREQUENCY ħω/Ω

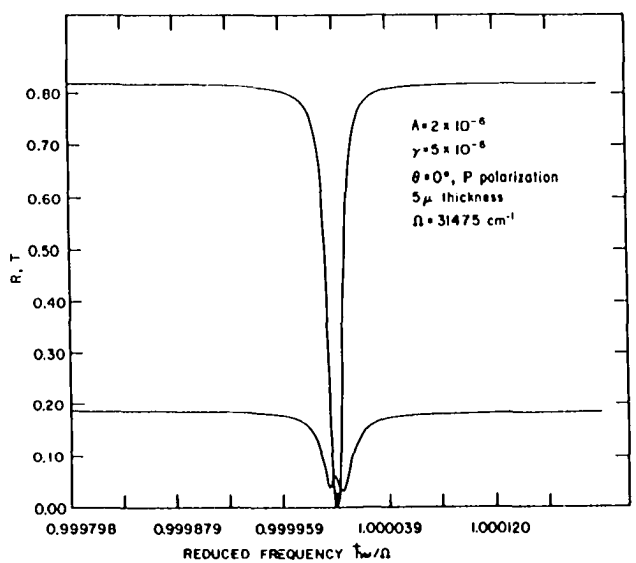
A = 2 × 10⁻⁶
γ = 5 × 10⁻⁶
θ = 0°, P polarization
5μ thickness
Ω = 31475 cm⁻¹
R, T
0.80
0.70
0.60
0.50
0.40
0.30
0.20
0.10
0.00
0.999798
0.999879
0.999959
1.000039
1.000120
REDUCED FREQUENCY ħω/Ω

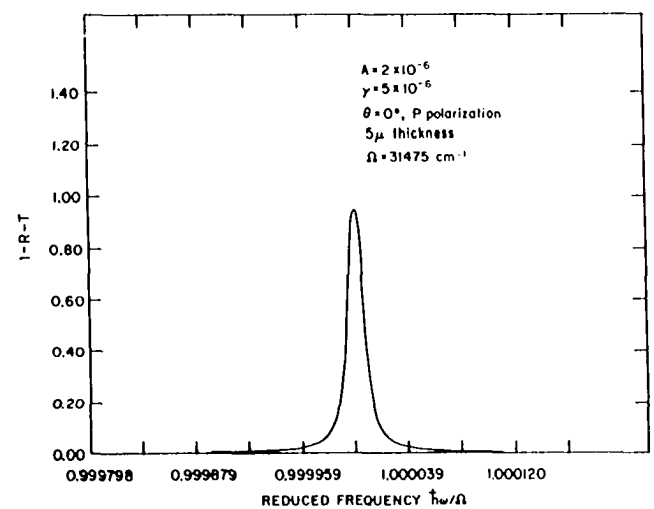
A = 2 × 10⁻⁶
γ = 5 × 10⁻⁶
θ = 0°, P polarization
5μ thickness
Ω = 31475 cm⁻¹
1-R-T
1.40
1.20
1.00
0.80
0.60
0.40
0.20
0.00
0.999798
0.999879
0.999959
1.000039
1.000120
REDUCED FREQUENCY ħω/Ω

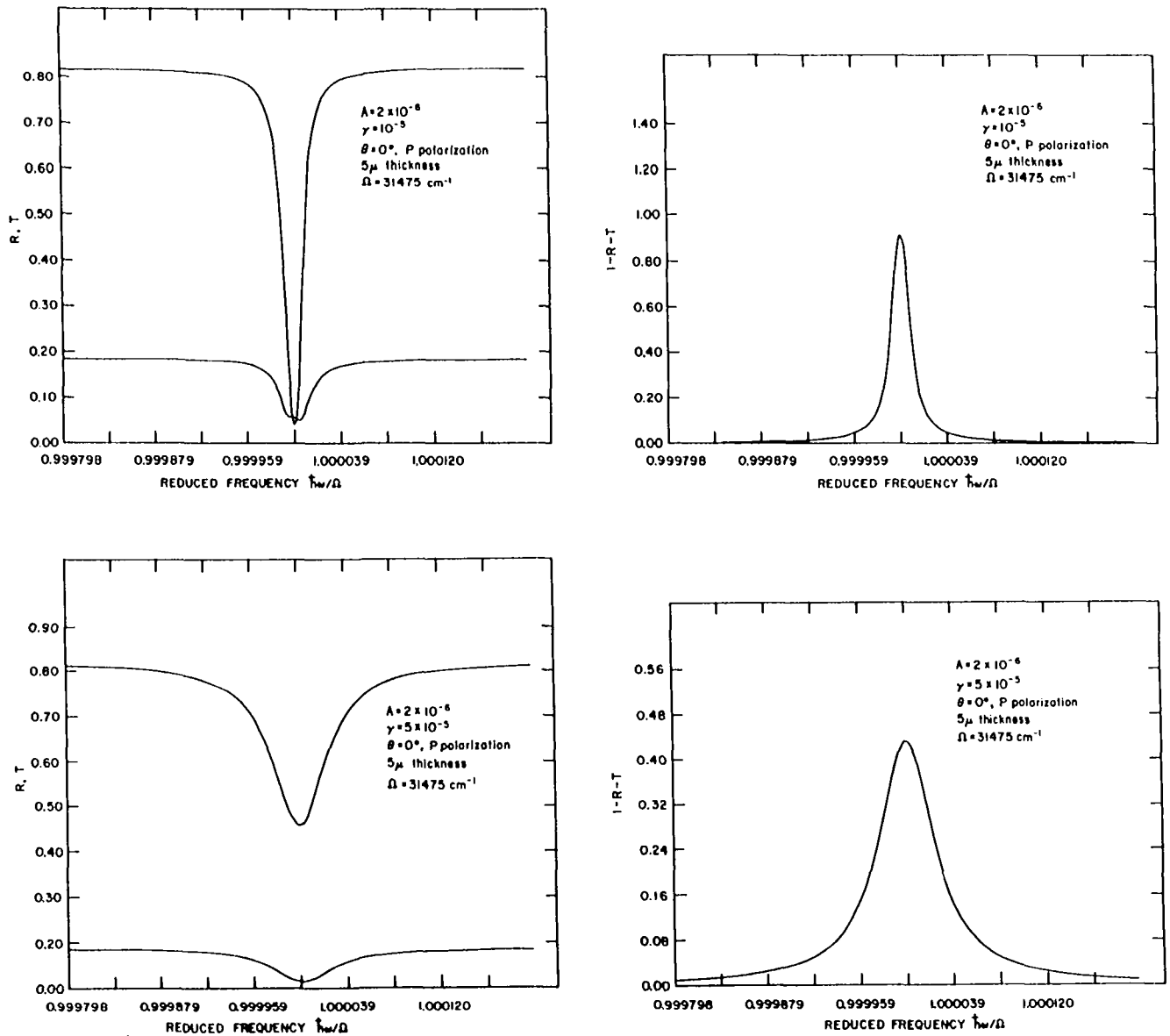

Figure 12. (Continued)

Figure 13. Computer generated reflection, transmission and absorption for a 6.3 μ crystal

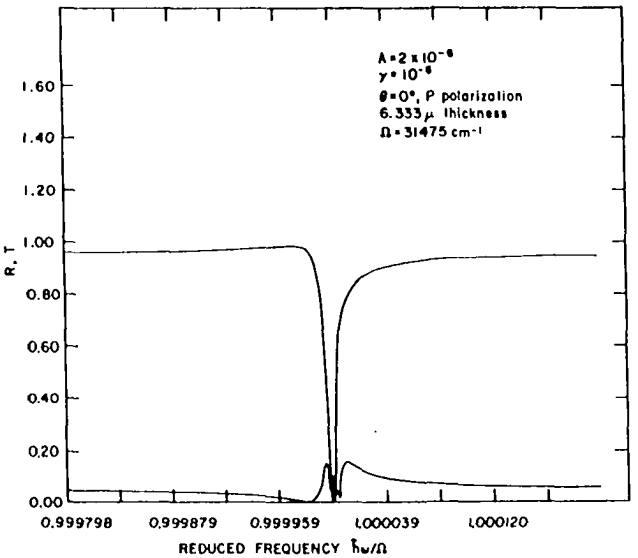
A=2×10⁻⁶
γ=10⁻⁶
θ=0°, P polarization
6.333μ thickness
Ω=31475 cm⁻¹
R, T
1.60
1.40
1.20
1.00
0.80
0.60
0.40
0.20
0.00
0.999798
0.999879
0.999959
1.000039
1.000120
REDUCED FREQUENCY ħω/Ω

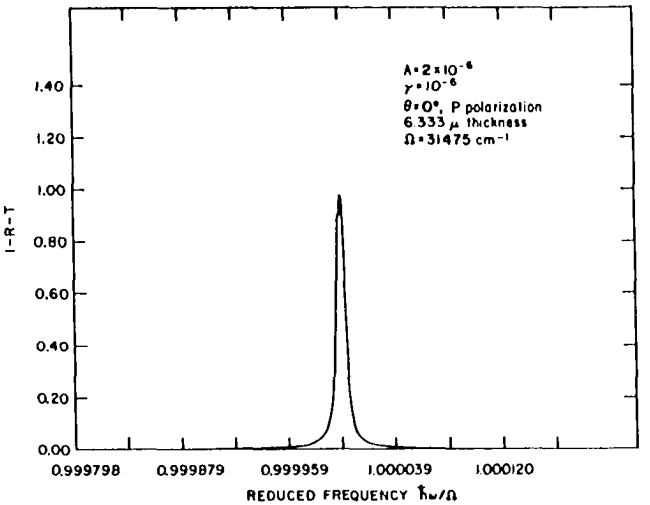
A=2×10⁻⁶
γ=10⁻⁶
θ=0°, P polarization
6.333μ thickness
Ω=31475 cm⁻¹
1-R-T
1.40
1.20
1.00
0.80
0.60
0.40
0.20
0.00
0.999798
0.999879
0.999959
1.000039
1.000120
REDUCED FREQUENCY ħω/Ω

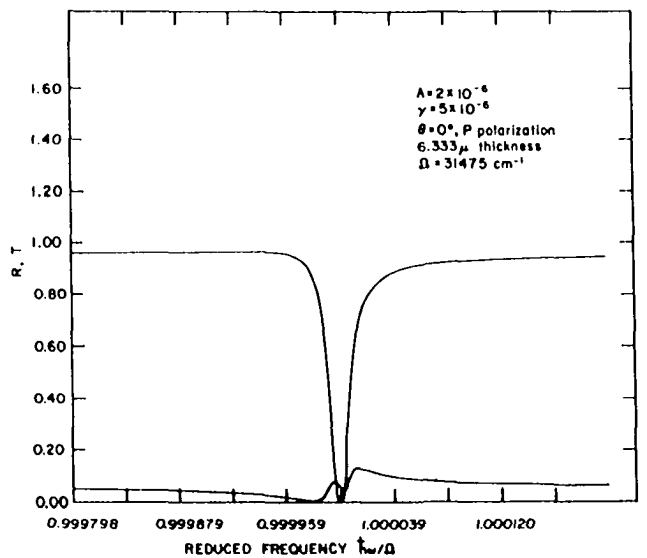
A=2×10⁻⁶
γ=5×10⁻⁶
θ=0°, P polarization
6.333μ thickness
Ω=31475 cm⁻¹
R, T
1.60
1.40
1.20
1.00
0.80
0.60
0.40
0.20
0.00
0.999798
0.999879
0.999959
1.000039
1.000120
REDUCED FREQUENCY ħω/Ω

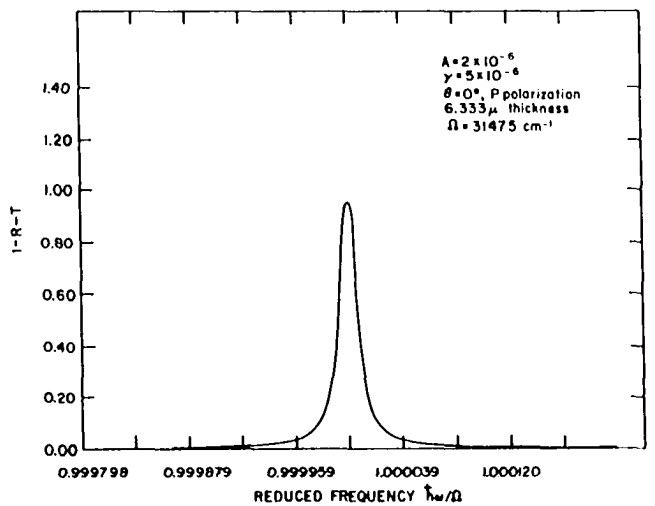
A=2×10⁻⁶
γ=5×10⁻⁶
θ=0°, P polarization
6.333μ thickness
Ω=31475 cm⁻¹
1-R-T
1.40
1.20
1.00
0.80
0.60
0.40
0.20
0.00
0.999798
0.999879
0.999959
1.000039
1.000120
REDUCED FREQUENCY ħω/Ω

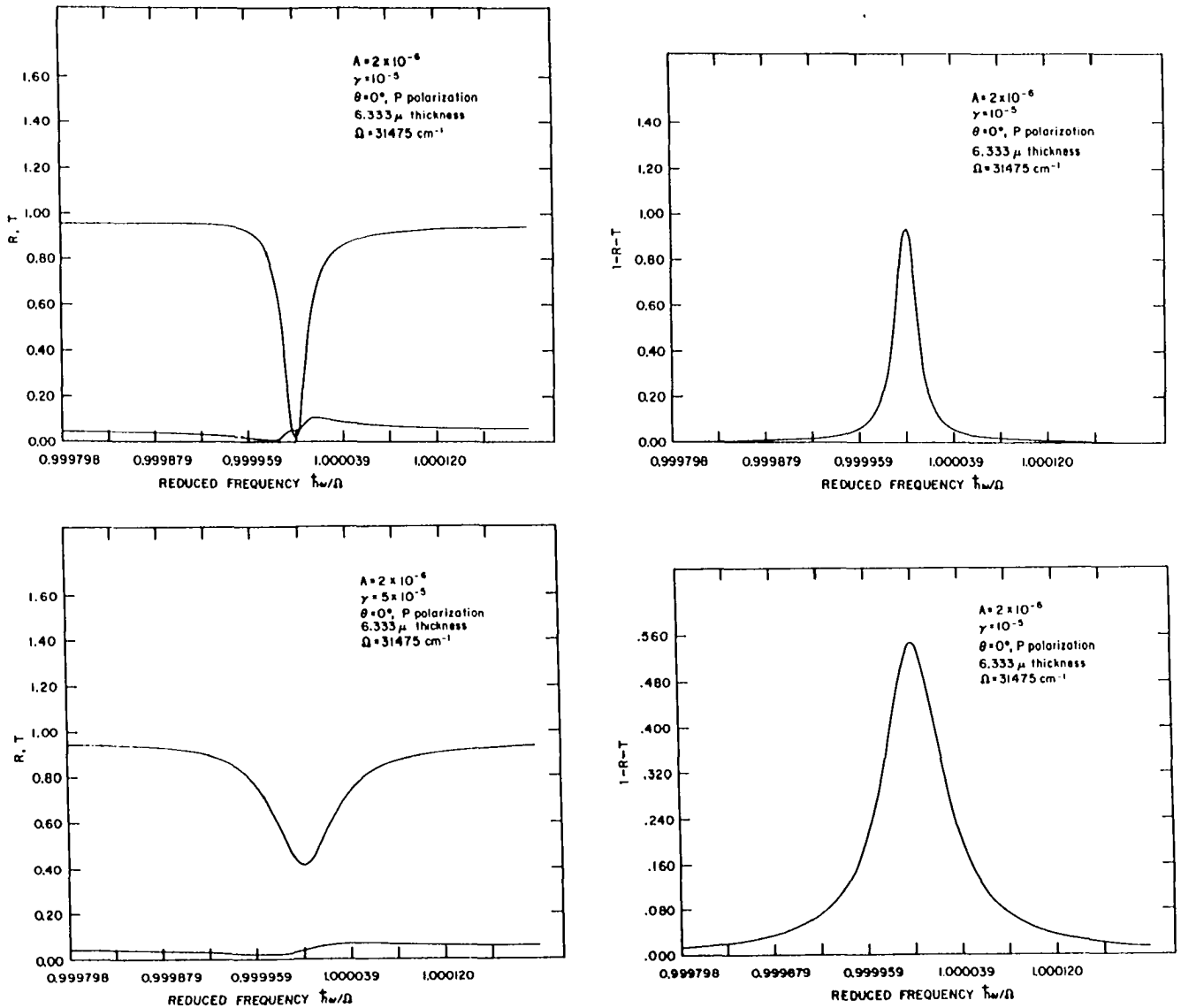

Figure 13. (Continued)

Figure 14. Computer generated reflection, transmission and absorption for a 10 μ crystal

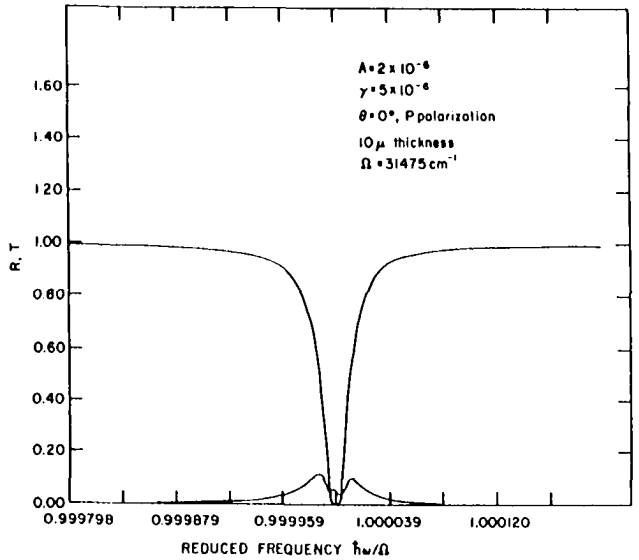
A=2×10⁻⁶
γ=5×10⁻⁶
θ=0°, P polarization
10μ thickness
Ω=31475 cm⁻¹
R, T
1.60
1.40
1.20
1.00
0.80
0.60
0.40
0.20
0.00
0.999798
0.999879
0.999959
1.000039
1.000120
REDUCED FREQUENCY ħω/Ω

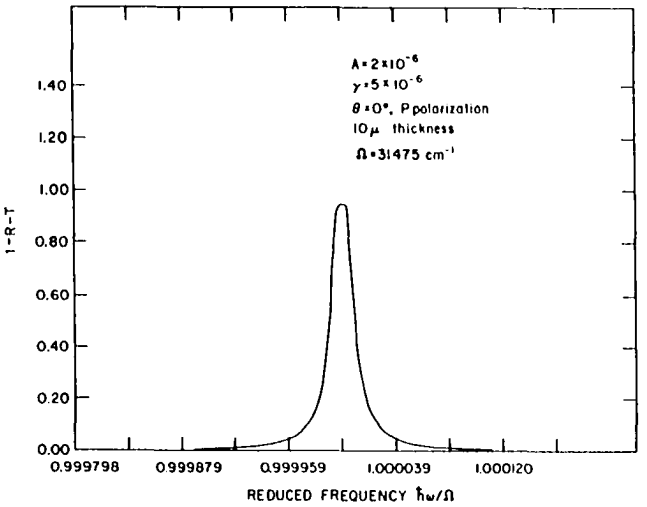
A=2×10⁻⁶
γ=5×10⁻⁶
θ=0°, P polarization
10μ thickness
Ω=31475 cm⁻¹
1-R-T
1.40
1.20
1.00
0.80
0.60
0.40
0.20
0.00
0.999798
0.999879
0.999959
1.000039
1.000120
REDUCED FREQUENCY ħω/Ω

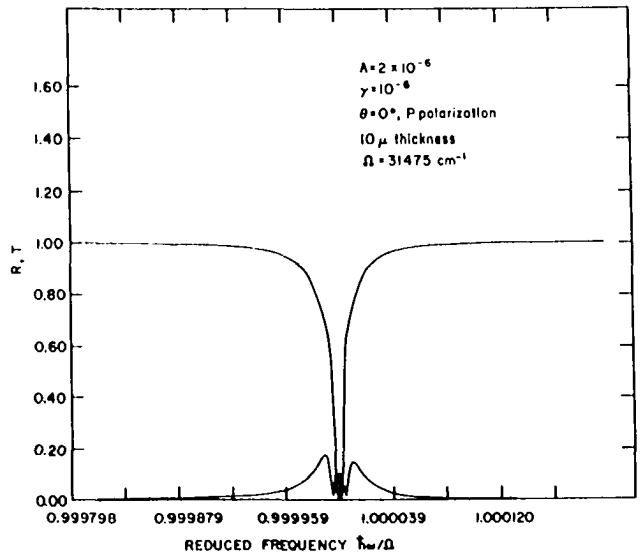
A=2×10⁻⁶
γ=10⁻⁶
θ=0°, P polarization
10μ thickness
Ω=31475 cm⁻¹
R, T
1.60
1.40
1.20
1.00
0.80
0.60
0.40
0.20
0.00
0.999798
0.999879
0.999959
1.000039
1.000120
REDUCED FREQUENCY ħω/Ω

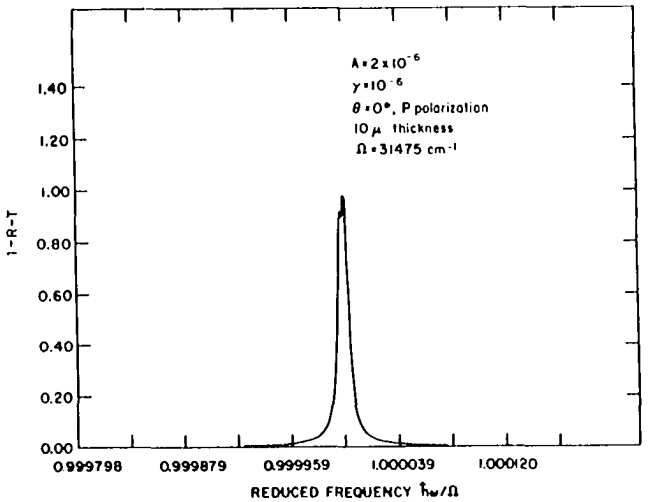
A=2×10⁻⁶
γ=10⁻⁶
θ=0°, P polarization
10μ thickness
Ω=31475 cm⁻¹
1-R-T
1.40
1.20
1.00
0.80
0.60
0.40
0.20
0.00
0.999798
0.999879
0.999959
1.000039
1.000120
REDUCED FREQUENCY ħω/Ω

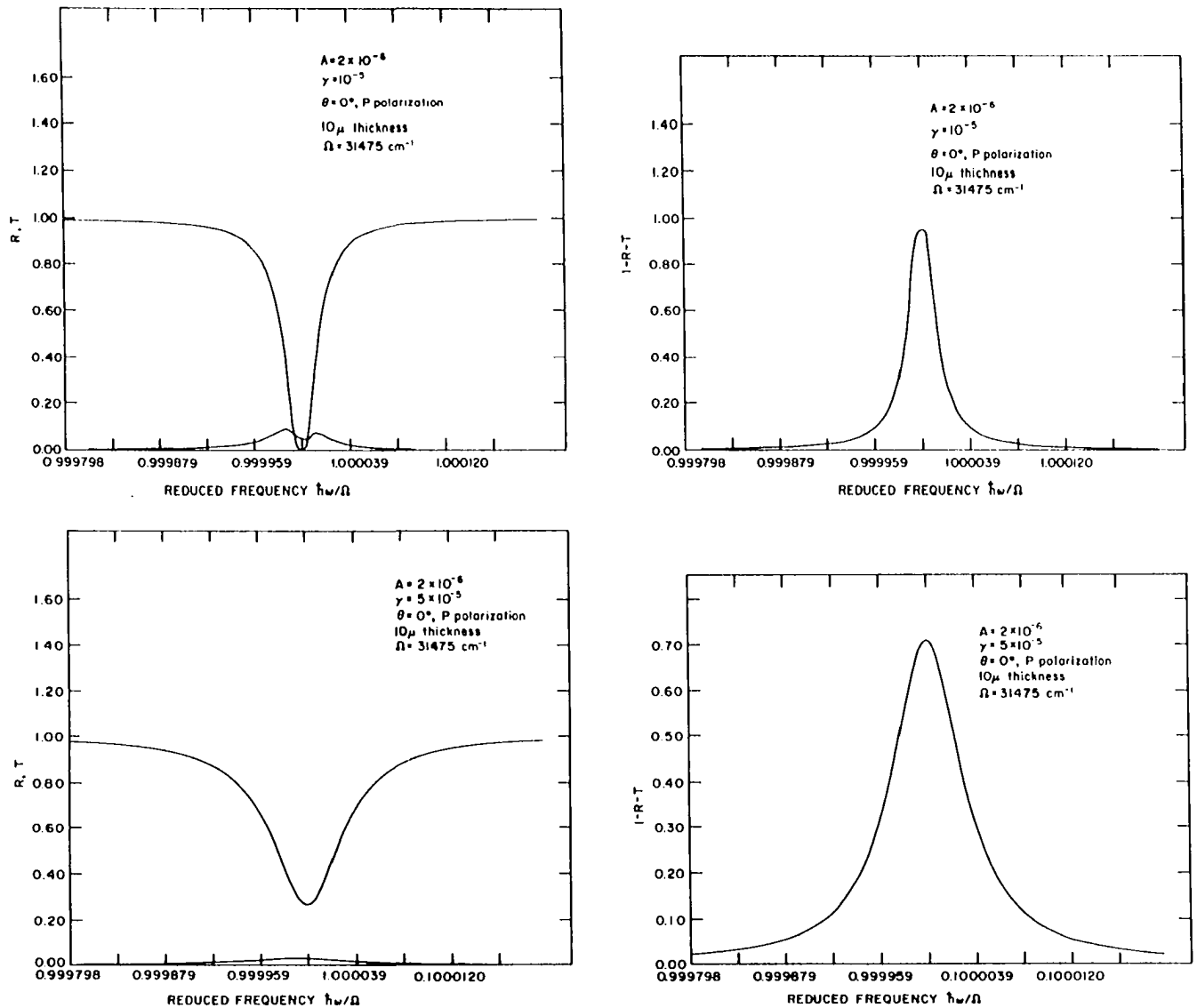

Figure 14. (Continued)

Figure 15. Computer generated reflection, transmission and absorption for a 12.7 μ crystal

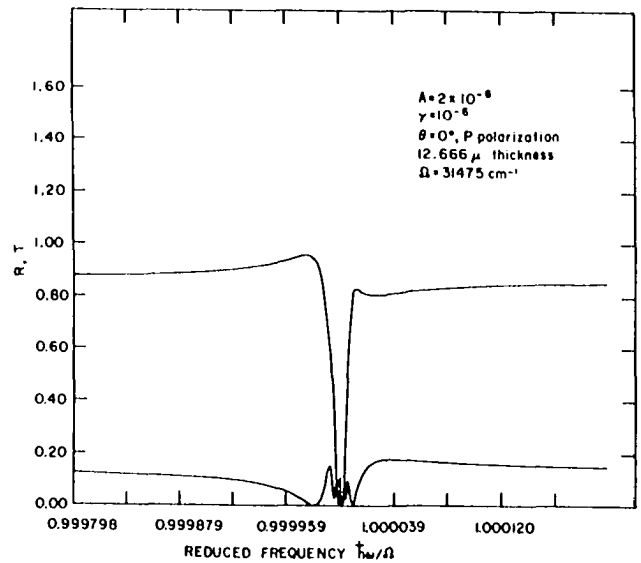
A=2x10⁻⁶
γ=10⁻⁶
θ=0°, P polarization
12.666μ thickness
Ω=31475 cm⁻¹
R, T
1.60
1.40
1.20
1.00
0.80
0.60
0.40
0.20
0.00
0.999798
0.999879
0.999959
1.000039
1.000120
REDUCED FREQUENCY ħω/Ω

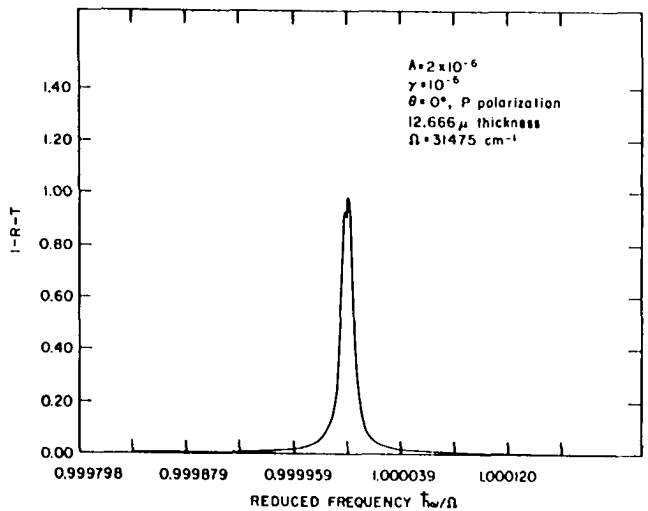
A=2x10⁻⁶
γ=10⁻⁶
θ=0°, P polarization
12.666μ thickness
Ω=31475 cm⁻¹
1-R-T
1.40
1.20
1.00
0.80
0.60
0.40
0.20
0.00
0.999798
0.999879
0.999959
1.000039
1.000120
REDUCED FREQUENCY ħω/Ω

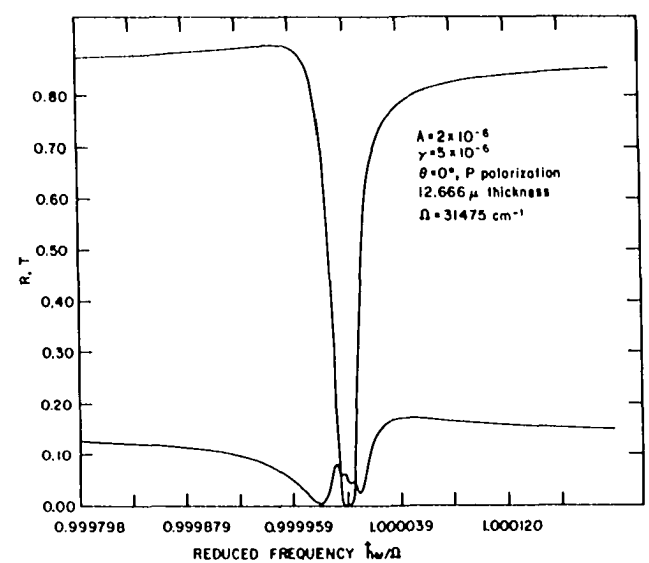
A=2x10⁻⁶
γ=5x10⁻⁶
θ=0°, P polarization
12.666μ thickness
Ω=31475 cm⁻¹
R, T
0.80
0.70
0.60
0.50
0.40
0.30
0.20
0.10
0.00
0.999798
0.999879
0.999959
1.000039
1.000120
REDUCED FREQUENCY ħω/Ω

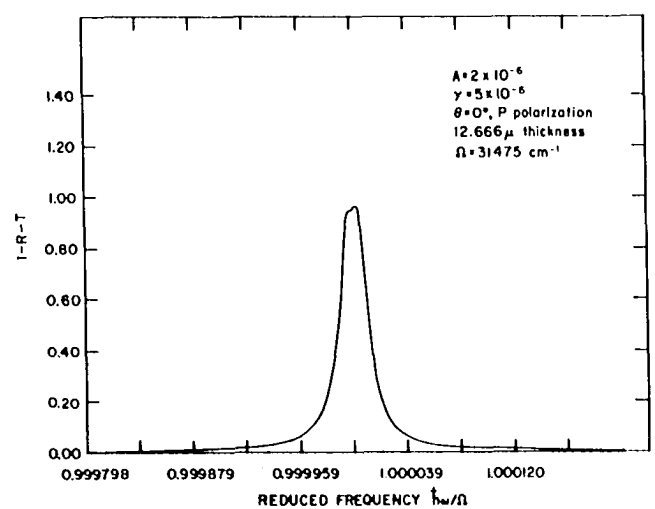
A=2x10⁻⁶
γ=5x10⁻⁶
θ=0°, P polarization
12.666μ thickness
Ω=31475 cm⁻¹
1-R-T
1.40
1.20
1.00
0.80
0.60
0.40
0.20
0.00
0.999798
0.999879
0.999959
1.000039
1.000120
REDUCED FREQUENCY ħω/Ω

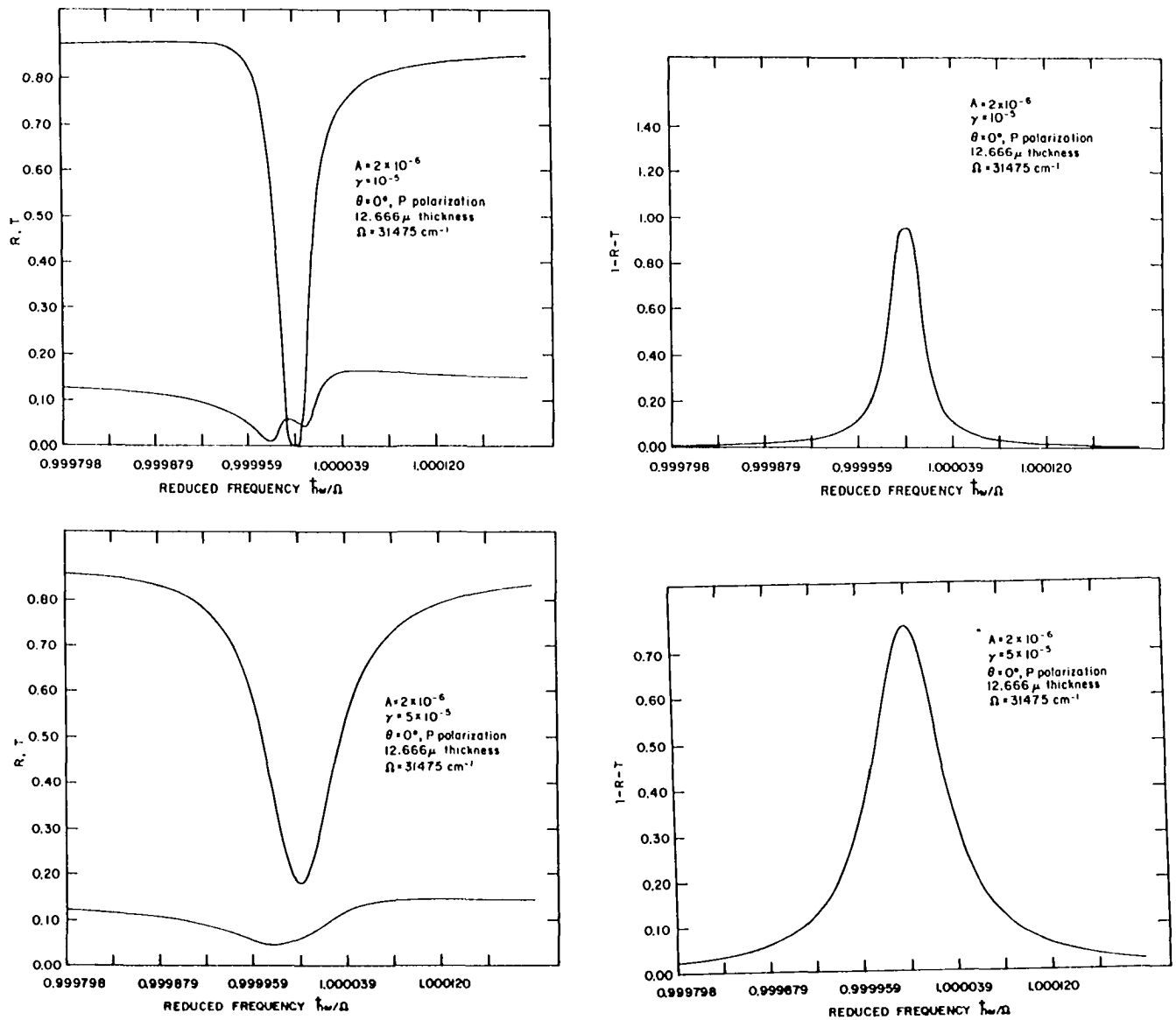

Figure 15. (Continued)

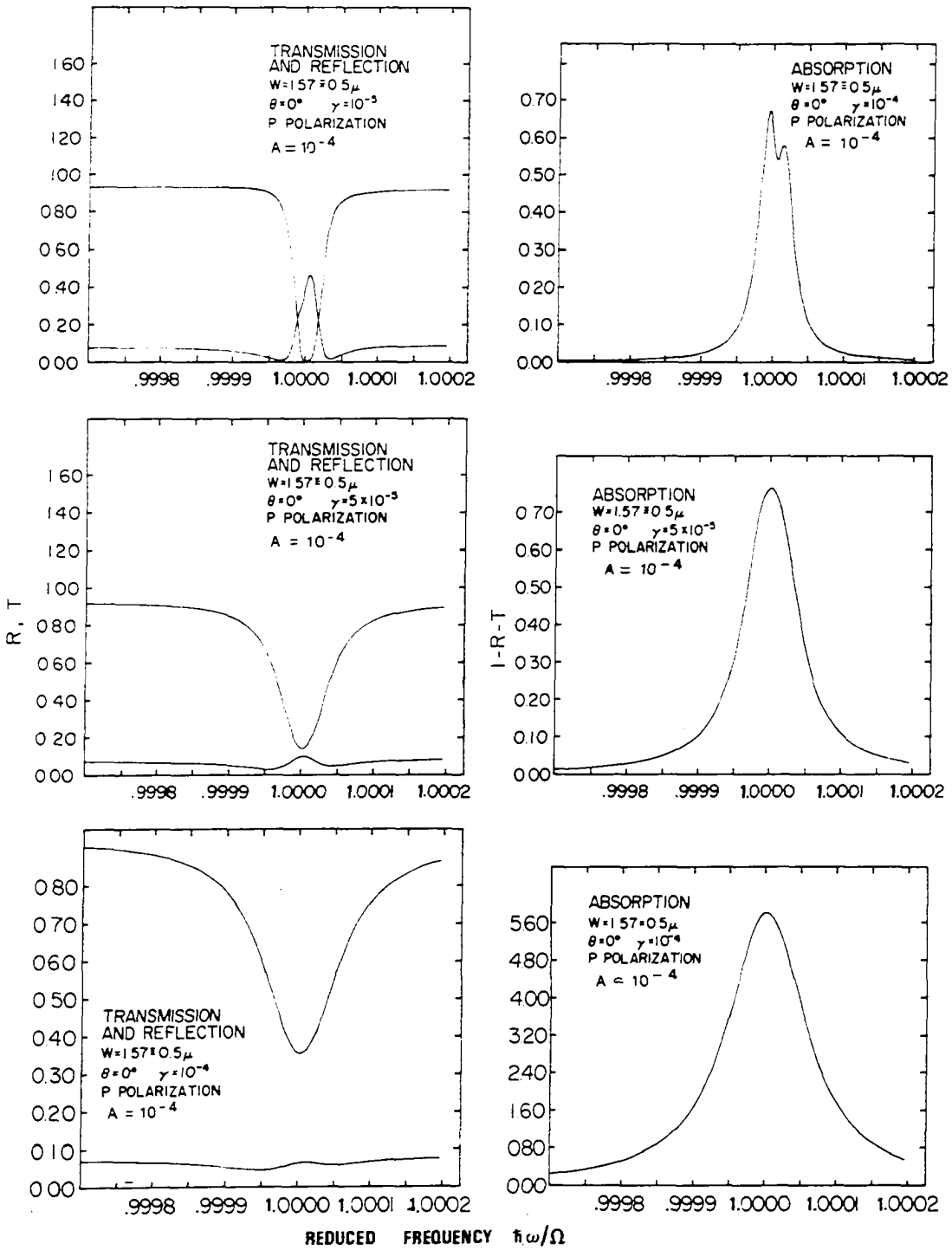

Figure 16. Computer generated reflection, transmission and absorption

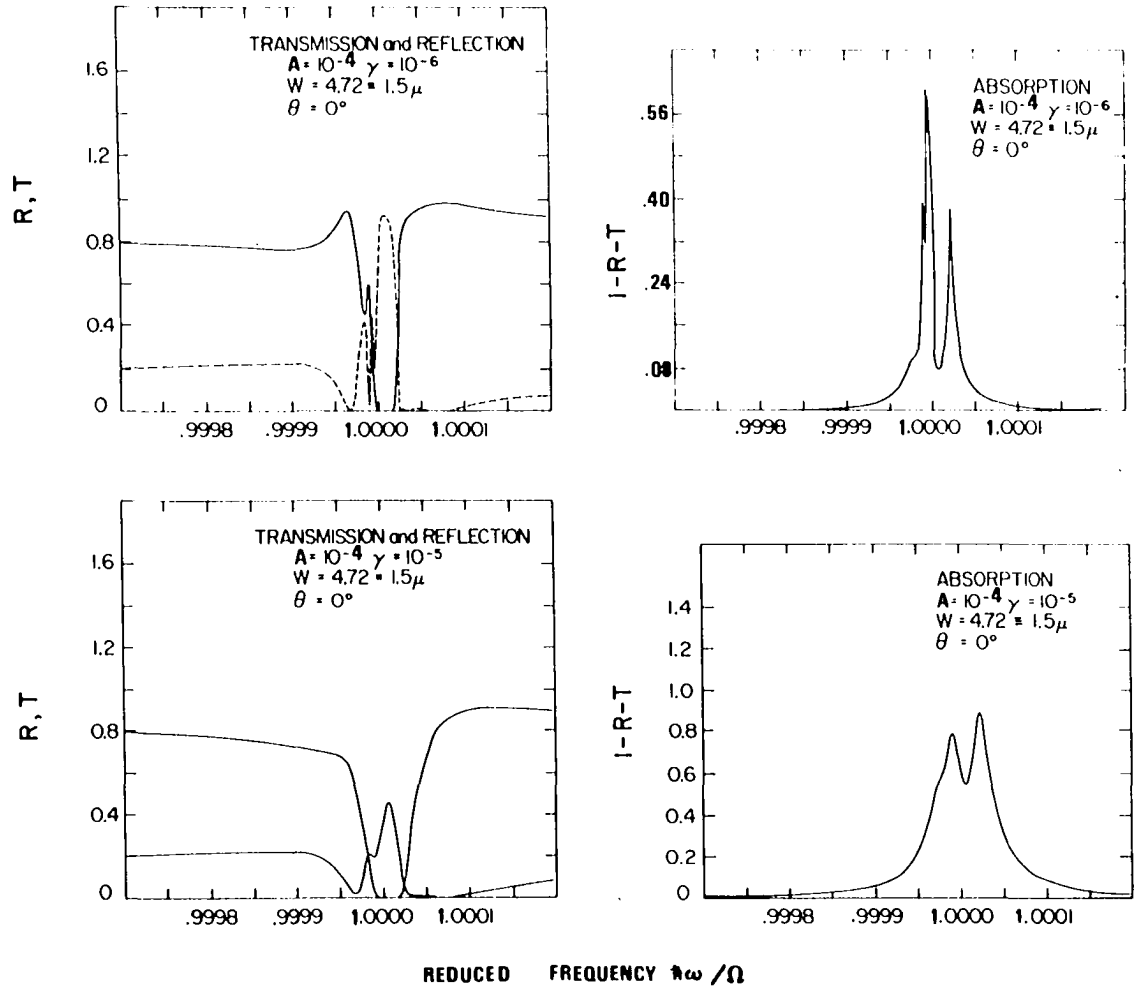

Figure 17. Computer generated reflection, transmission and absorption

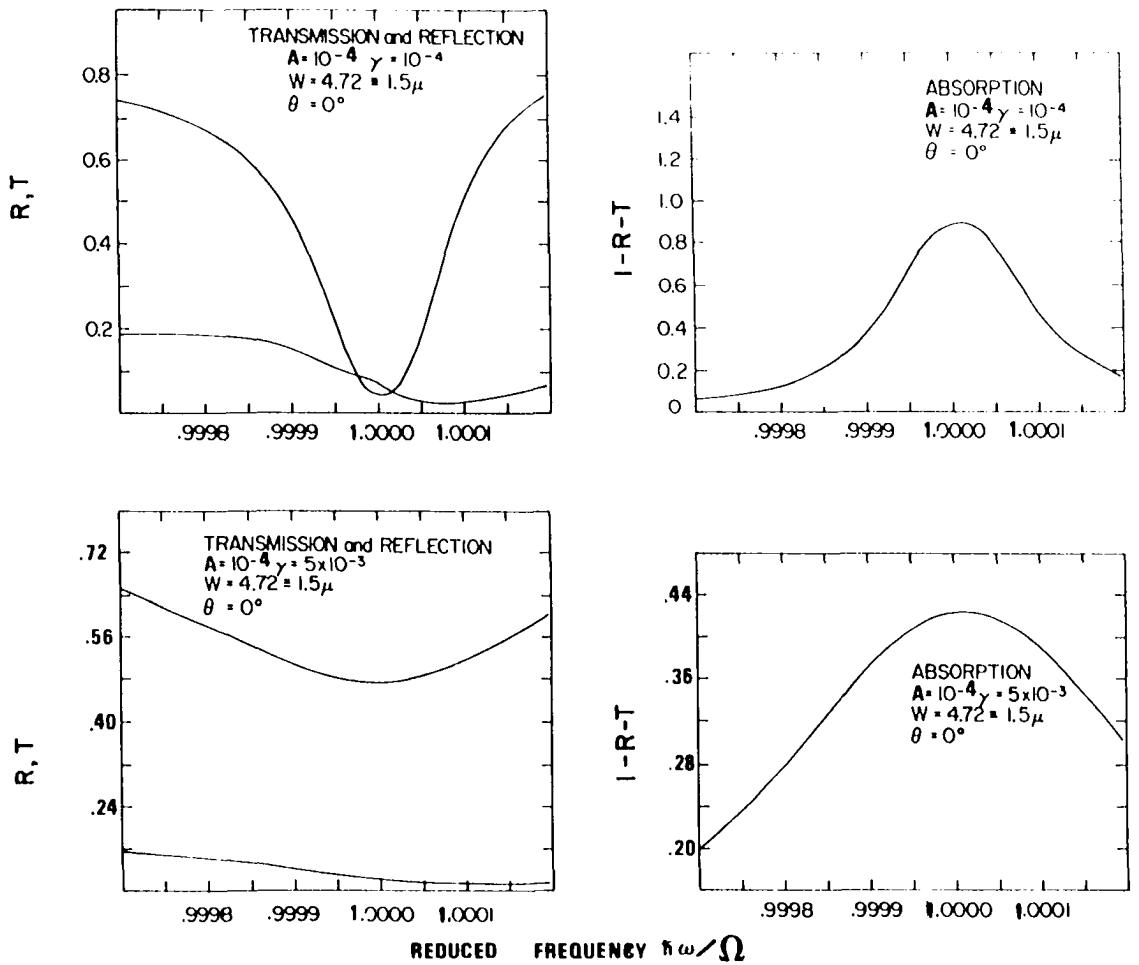

Figure 17. (Continued)

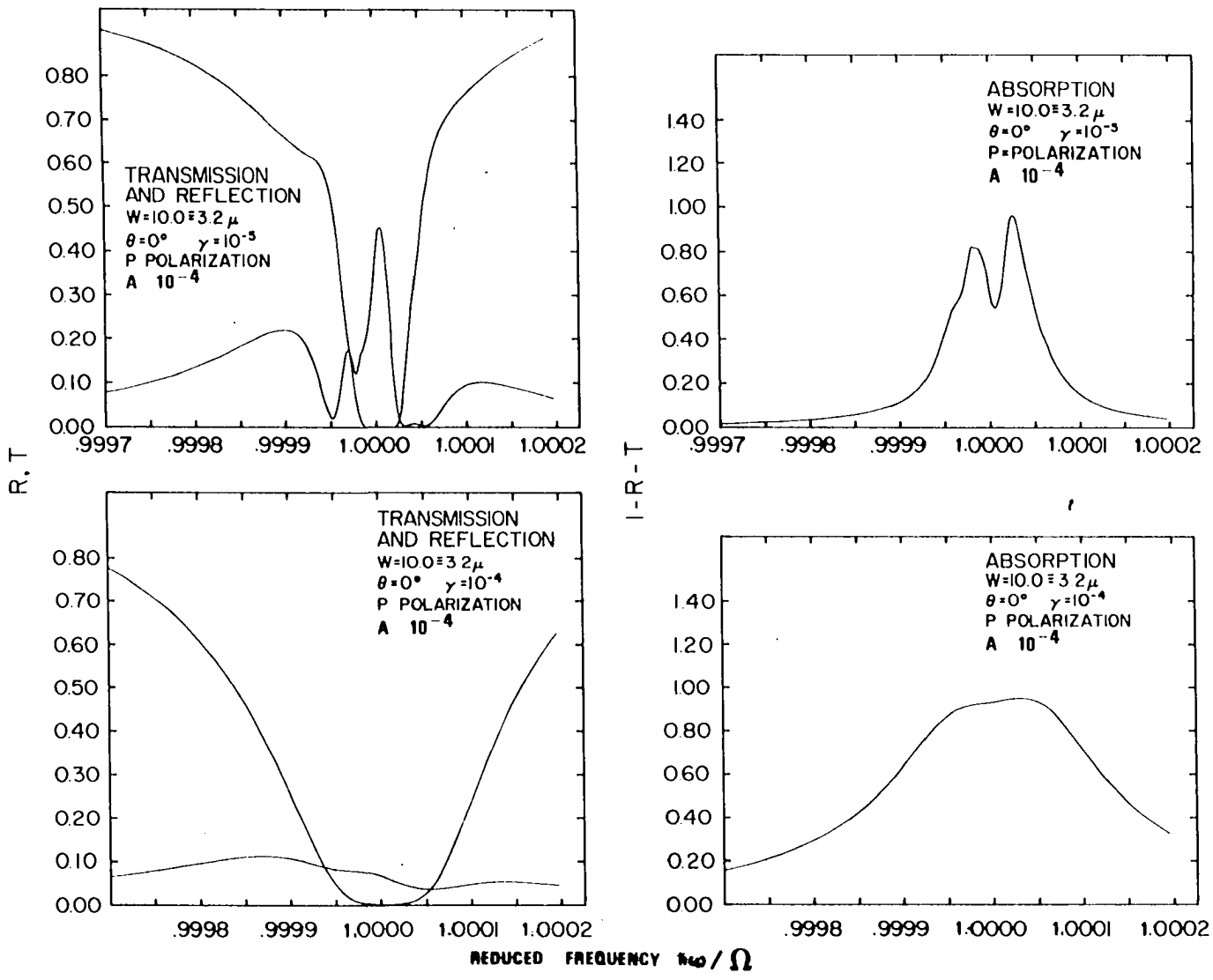

Figure 18. Computer generated reflection, transmission and absorption

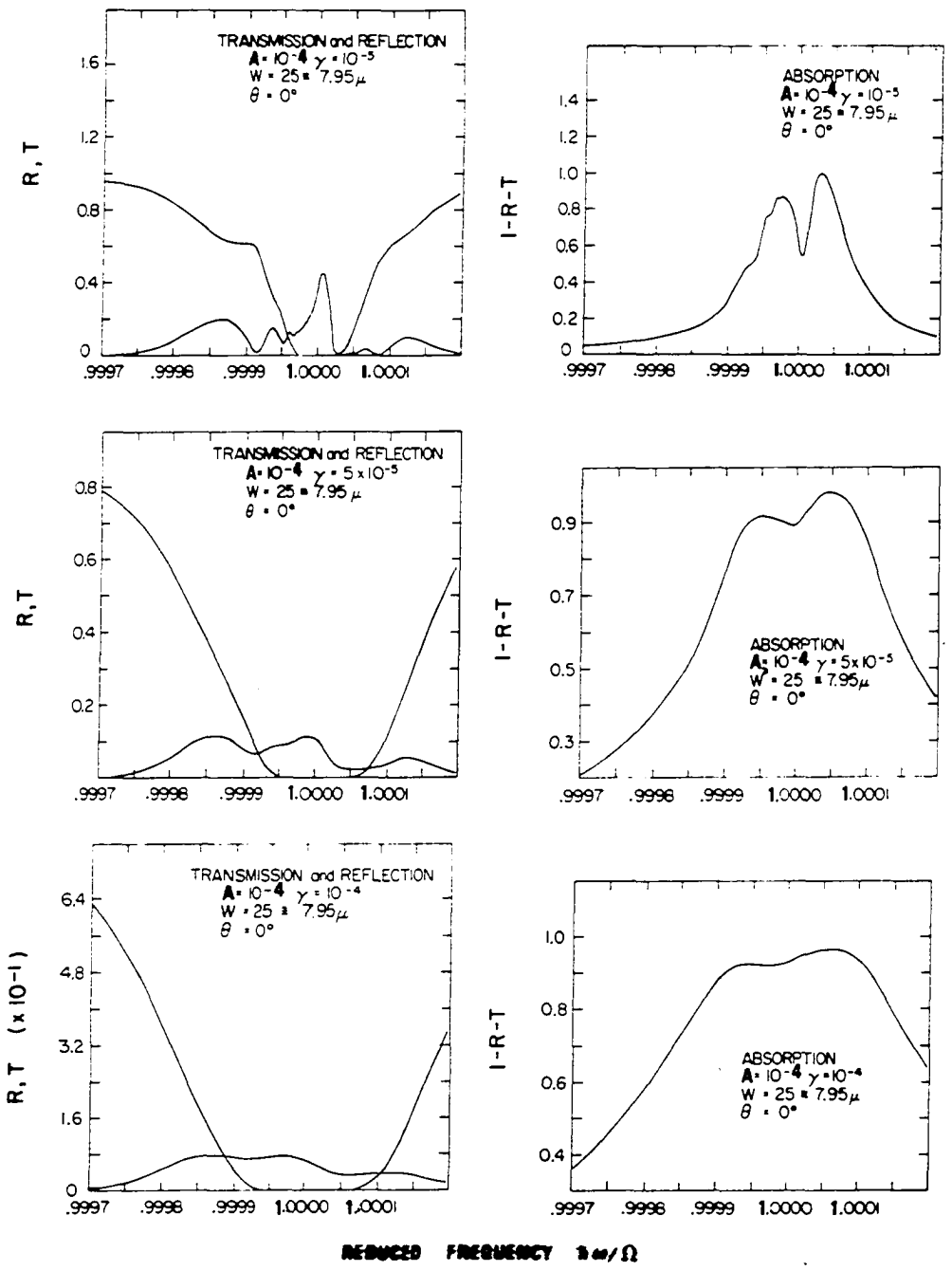

Figure 19. Computer generated reflection, transmission and absorption

similar calculations for the lowest energy band of anthracene (239) and has extended the scope of his calculations in subsequent papers to include spatial dispersion effects (242,243) and surface excitons (242). In general, calculated reflection bands are far more sensitive to spatial dispersion, choice of boundary conditions surface state effects, and angle of incidence than are simulated transmission bands. For the computer plots shown, R, T and A are defined with respect to a fixed coordinate system shown in Figure 20 for P polarization, $\vec{E}$ lies in the xz

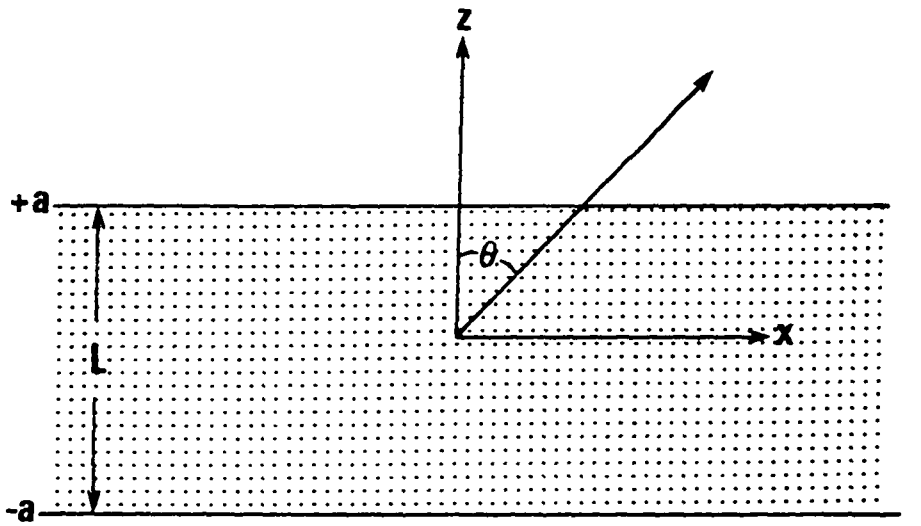

Figure 20. Idealized dielectric slab of thickness 2a

plane, $E_y = H_x = H_z = 0$. The fraction of light absorbed being given by A = 1-R-T. Kliewer and Fuchs (234,235)

and Fuchs and coworkers (233) have expressed R and T in terms of P_1 and P_2, complex numbers containing the ratios of E_x and E_z, and sufficient to completely specify all fields present. P_1 and P_2 permit an arbitrary choice of amplitude and phase for waves leaving the slab. When P_1 and P_2 are expressed as

$$P_1 = \frac{\left\{1 - \frac{\left(\frac{\omega^2\varepsilon}{c^2} - k_x^2\right)^{1/2}}{\left(\frac{\omega^2}{c^2} - k_x^2\right)^{1/2}} \tan\left[i\left(\frac{\omega^2\varepsilon}{c^2} - k_x^2\right)^{1/2} a\right]\right\}}{\left\{1 + \frac{\left(\frac{\omega^2\varepsilon}{c^2} - k_x^2\right)^{1/2}}{\left(\frac{\omega^2}{c^2} - k_x^2\right)^{1/2}} \tan\left[i\left(\frac{\omega^2\varepsilon}{c^2} - k_x^2\right)^{1/2} a\right]\right\}} \tag{150}$$

$$P_2 = \frac{\left\{1 - \frac{\left(\frac{\omega^2\varepsilon}{c^2} - k_x^2\right)^{1/2}}{\left(\frac{\omega^2}{c^2} - k_x^2\right)^{1/2}} \cot\left[i\left(\frac{\omega^2\varepsilon}{c^2} - k_x^2\right)^{1/2} a\right]\right\}}{\left\{1 + \frac{\left(\frac{\omega^2\varepsilon}{c^2} - k_x^2\right)^{1/2}}{\left(\frac{\omega^2}{c^2} - k_x^2\right)^{1/2}} \cot\left[i\left(\frac{\omega^2\varepsilon}{c^2} - k_x^2\right)^{1/2} a\right]\right\}} \tag{151}$$

for the coordinate system of Figure 20

$$T = 1/4|P_1 - P_2|^2 \tag{152}$$

$$R = 1/4|P_1 + P_2|^2 \tag{153}$$

and

$$A = 1\text{-}T\text{-}R = 1/2(1 - |P_1|^2) + 1/2(1 - |P_2|^2). \quad (154)$$

P_1 and P_2 are related to E_x and E_z by the quantities g_1 and g_2

$$g_1 = E_x^{(1)}(a)/\varepsilon E_z^{(1)}(a) \quad \text{(even parity modes)} \quad (155)$$

$$g_2 = E_x^{(1)}(a)/\varepsilon E_z^{(2)}(a) \quad \text{(odd parity modes)} \quad (156)$$

where

$$P_1 = \frac{\left[\frac{(\omega^2/c^2 - k_x 2)^{\frac{1}{2}}}{k_x} - g_1\right]}{\left[\frac{(\omega^2/c^2 - k_x 2)^{\frac{1}{2}}}{k_x} + g_1\right]} e^{-2ia(\omega^2/c^2 - k_x 2)^{\frac{1}{2}}} \quad (157)$$

Exactly the same relation as (157) exists for g_2 and P_2. The modes are taken to be of even (g_1,P_1) or odd (g_2,P_2) parity with respect to an origin at the center of the slab. Equations (152) and (153) imply that R and T involve interference between modes of opposite parity, while A, because P_1 and P_2 are squared before adding does not involve interference. Real virtual modes as noted by several authors (233-235,228) are generated by equation (154) only.

The calculated spectra show that the reflection correction for $\underset{\sim}{a}(0,0)$ is not large. In general $R \leq 0.1$ and does not change greatly with frequency for all but the

smallest γ used (10^{-6}). Since a γ of 10^{-5} corresponds to band widths in transmission of 0.31 cm^{-1} we conclude that 10^{-6} is the smallest value that is experimentally realistic. For $\gamma \geq 5 \times 10^{-6}$ R remains small and reasonably smooth around the resonance region 52.

Interference modes

The computer plots reproduce an interesting feature found in some of the experimental transmission spectra, that is the interference maxima and minima continuing in some cases to several hundred Å lower energy of the $\underset{\sim}{a}$ and $\underset{\sim}{b}$ origins (Figure 21). Because we are monitoring transmission (rather than absorption) these bands do not correspond to true virtual modes, as noted above.

Virtual modes occur in absorption as the sum of reflection and transmission curves. The interference effect in transmission is indicative of extremely flat parallel crystal faces and can be expressed by the formulae

$$n\ell = m\lambda/2 \qquad m=0,1,2 \quad \text{transmission maxima} \tag{158}$$

and

$$n\ell = (m+1)\lambda/4 \qquad m=0,1,2 \quad \text{reflection maxima} \tag{159}$$

where ℓ is the slab thickness, λ the photon wavelength and n the refractive index. Unfortunately, $n = n(\omega)$ is a rapidly changing function of frequency near an absorption

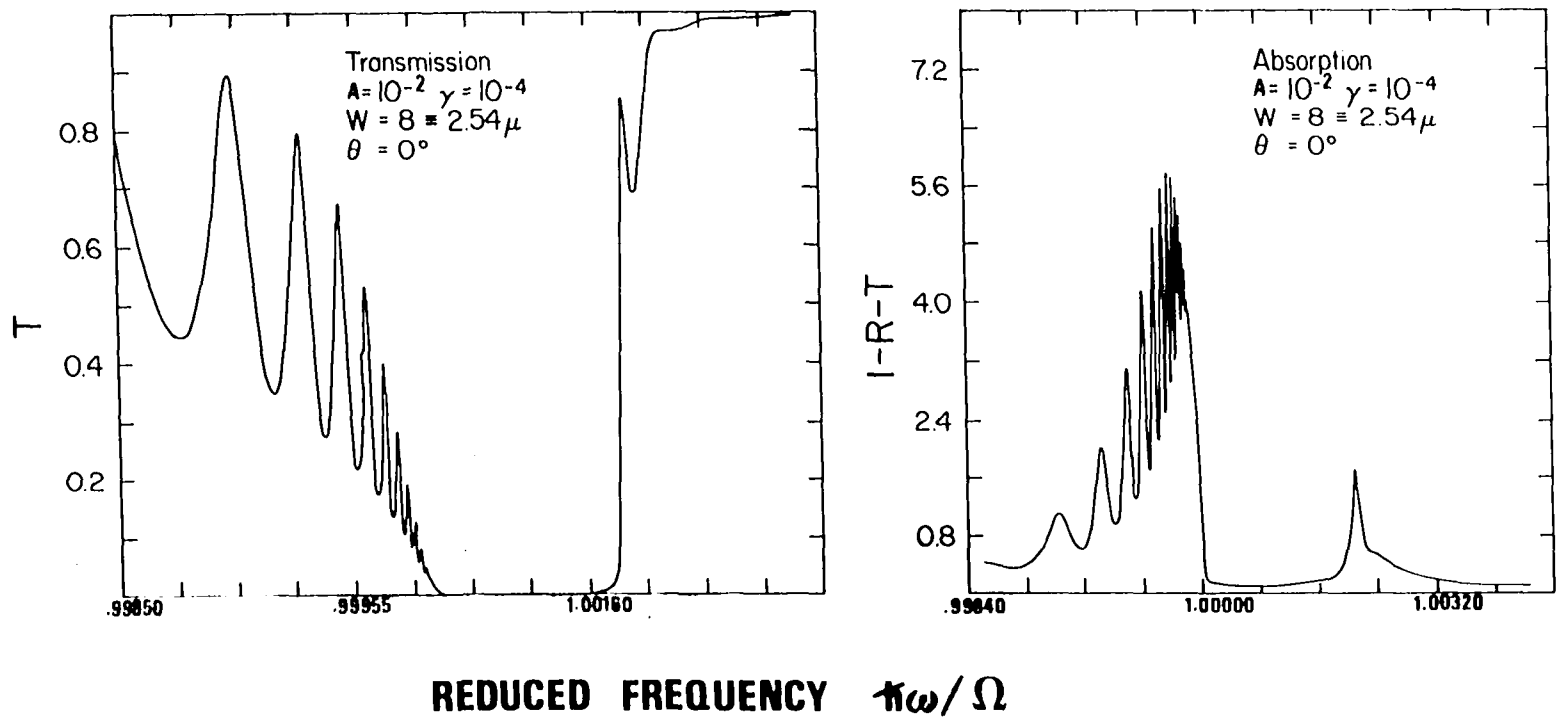

Figure 21. Computer generated interference modes

maximum. Thus, to use Equations (158) and (159) to calculate crystal thickness, one must resort to an iterative computer procedure used with very accurate experimental data. Experimental curves showing the interference modes are given in Figure 22 for $\underset{\sim}{a}$ and $\underset{\sim}{b}$ polarizations and in Figure 23 for an enlarged segment of $\underset{\sim}{b}(0,0)$ for two crystals of different thickness. The arrows mark the interference modes which are obviously thickness dependent.

The sharpest $\underset{\sim}{a}(0,0)$ band we have recorded in pure, strain-free crystals is 0.3 cm^{-1} at $\sim 2°K$, routinely line widths are $\lesssim$ 1 cm^{-1}. These are probably crystal limited widths but come close to the instrumental limit of 0.1 cm^{-1}. Even for the 2.3 μ thick crystal shown (Figure 24), $\underset{\sim}{b}(0,0)$ has "bottomed out", i.e., transmission = 0. However, to refer to the $\underset{\sim}{b}(0,0)$ band as totally "absorbing" would be misleading. In fact the true absorption for $\underset{\sim}{b}(0,0)$ in this case may be rather different from the transmission spectrum. The remainder of the spectrum shown in Figure 24 consists of vibronic bands building on the common origin (taken as 31550 cm^{-1}) - the midpoint between $\underset{\sim}{a}(0,0)$ and $\underset{\sim}{b}(0,0)$. There is even in the best $\underset{\sim}{a}$ polarized spectra a small broad band at the energy of the $\underset{\sim}{b}(0,0)$ component. While it has been claimed that this band represents a new $\underset{\sim}{a}$ polarized band, possibly a phonon building on $\underset{\sim}{a}(0,0)$ (276), it seems more likely that it is a measure of crystal imperfection.

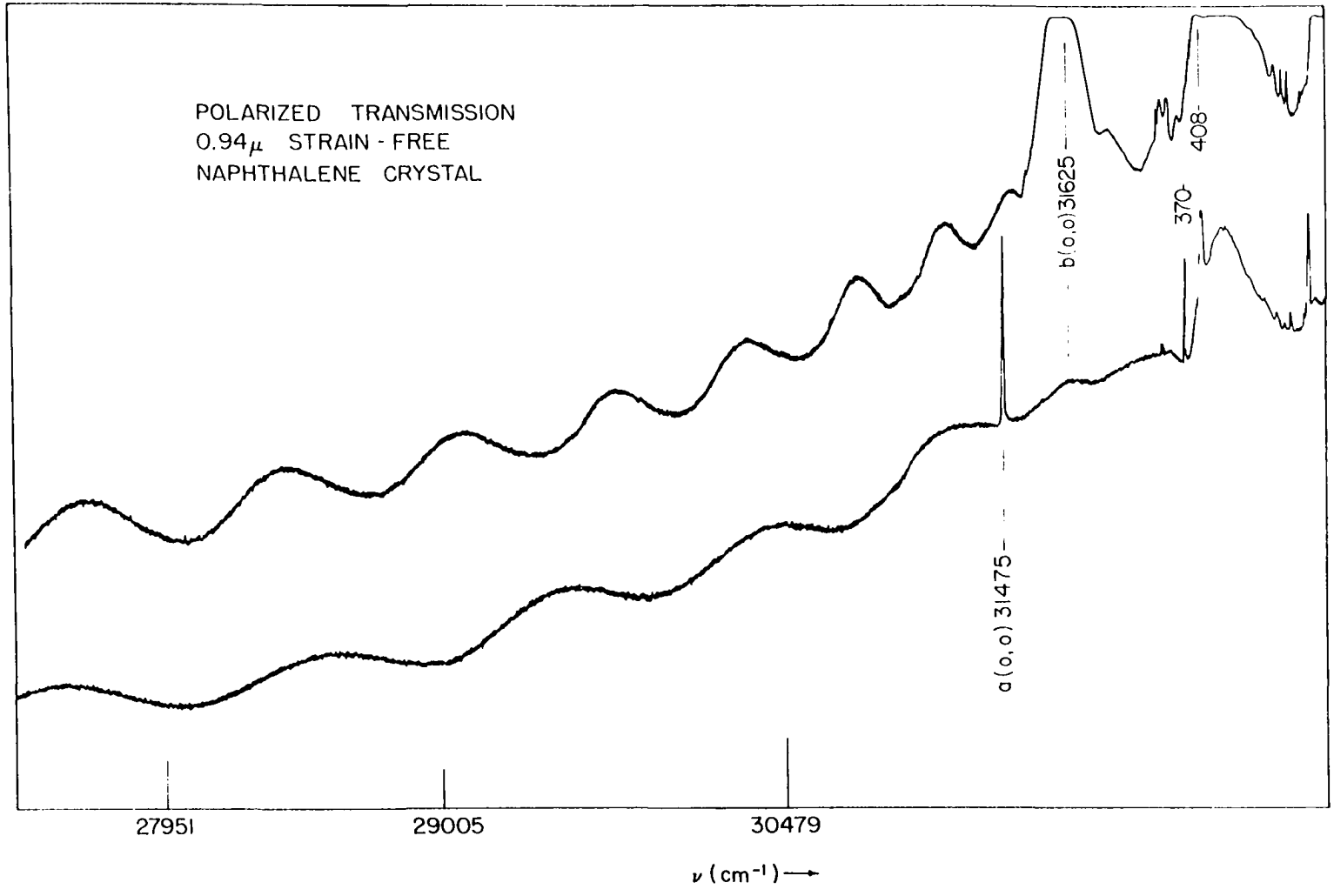

Figure 22. Polarized transmission 0.94 μ strain-free naphthalene crystal

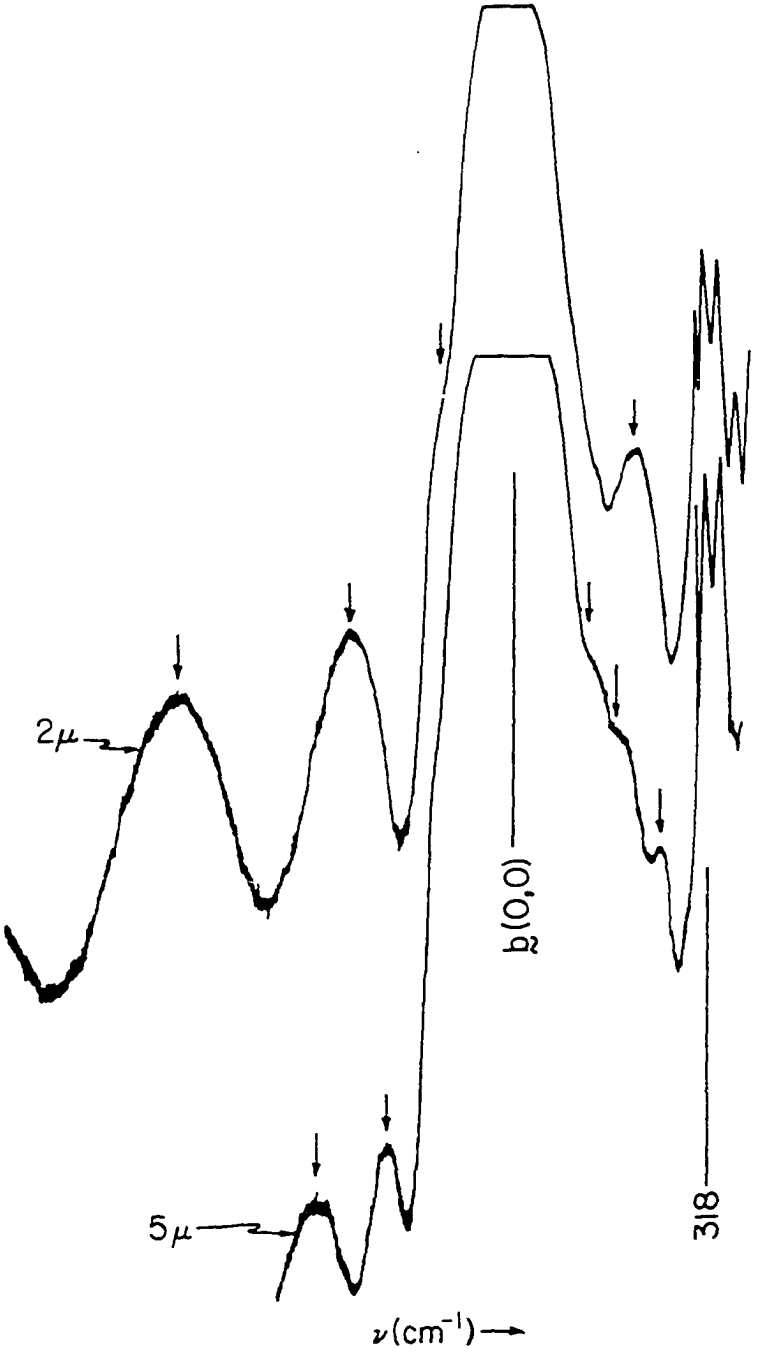

Figure 23. Thickness dependent interference modes in the $\underset{\sim}{b}(0,0)$ region

Pure Crystal Spectra

In this section frequent reference is made to "perfect" crystals. The term is defined as follows: we estimate the major chemical trap and impurity remaining in naphthalene after purification to be β-methylnaphthalene at a concentration of $\lesssim 10^{-6}$ mole/mole ($\sim$1 ppm). "Pure" will refer to this limiting impurity concentration. "Perfect" refers to well-polarized, hexagonal sublimation flakes grown from the purest naphthalene and strain-free mounted. Figure 24 shows a representative, nearly perfectly polarized spectrum of most of the first excited state (the S_2 state occurs at $\sim$35,700 cm^{-1}) of a pure, strain-free naphthalene crystal at 2°K. The two bands labeled $\underset{\sim}{a}(0,0)$ and $\underset{\sim}{b}(0,0)$ are the Davydov (factor group) components of the origin. The marked difference in width between the very sharp $\underset{\sim}{a}(0,0)$ and the broad (0,0) is obvious. A difference in width is predicted by the classical theory based only on oscillator strengths, but for both bands these widths are far narrower than those experimentally observed. The major fundamentals have been assigned previously by comparison with gas phase spectra by McClure and Schnepp (277), Craig and coworkers (278), and Broude (279). In addition to the origin, there exist two other sets of Davydov components at 694 cm^{-1} and 871 cm^{-1} which correspond to the splitting of the totally symmetric gas phase vibrations 701 cm^{-1} and 911 cm^{-1}. The 408 cm^{-1}

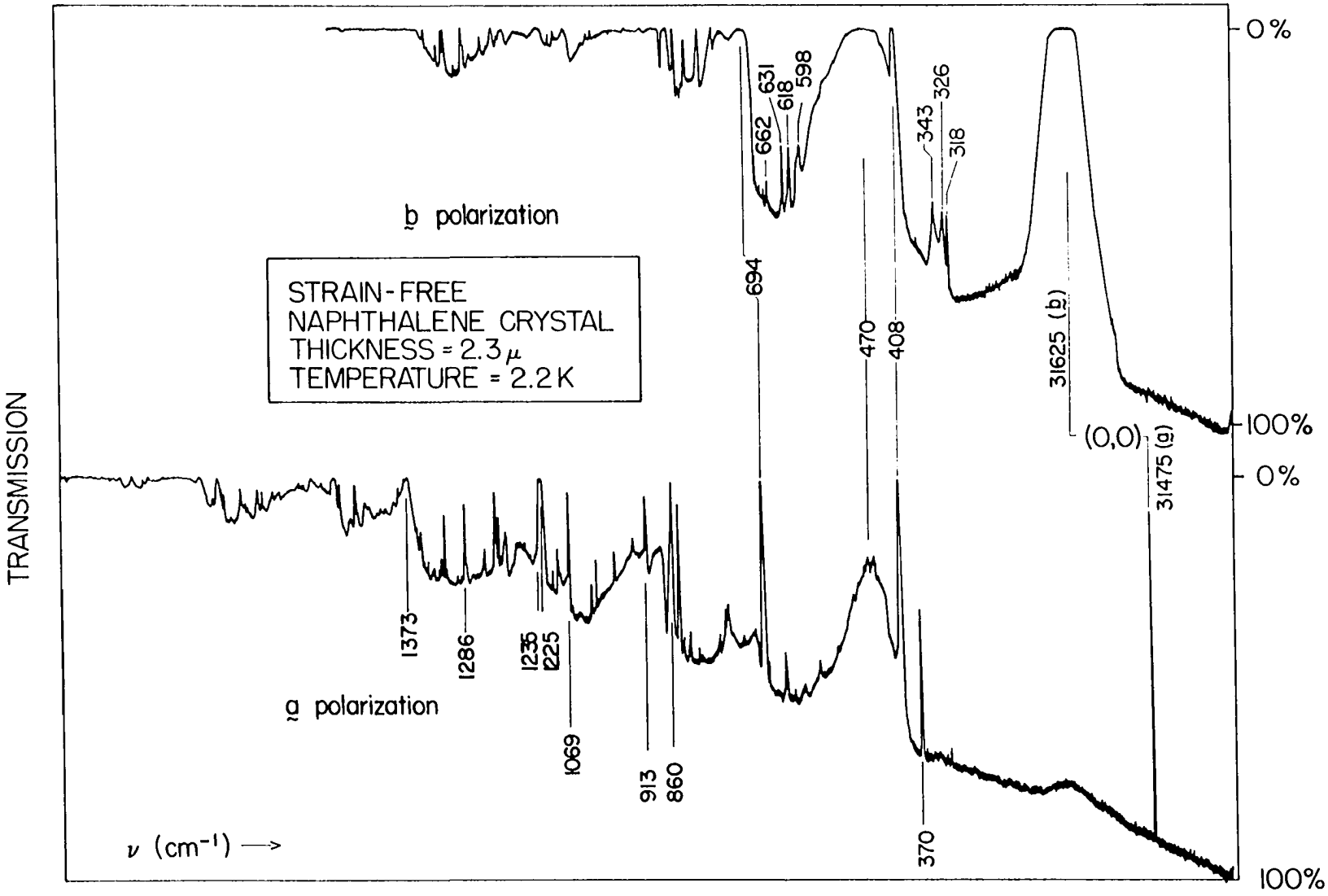

Figure 24. $S_{1\leftarrow 0}$ absorption in perfect naphthalene crystal

band, Figure 25 (vapor 438 cm^{-1}) is frequently referred to as the "M" band by Russian workers (276). A good deal of work has been done on this region since it appears to be the only area in the naphthalene spectrum where a phonon side band builds on a sharp (in this case asymmetric) fundamental. It has been argued that the broad, phonon-like region (420-560 cm^{-1}) is a replica (probably weighted) of the naphthalene phonon density of states (112). Other explanations of the "M" band region in terms of one and two particle vibronic states have also appeared (111,112,115). The sharp 408 cm^{-1} band is assigned as a one particle state, i.e., electronic and vibration excitation on the same site, while the broad side band is interpreted as belonging to two particle states where the electronic and vibrational excitation are free to migrate independently of one another and actually are found on different molecules. It appears fairly certain that the M region corresponds to a localized exciton rather than a true unit cell state by virtue of its poor polarization. A very interesting new feature is revealed in the "M" band region at higher resolution and for perfect crystals (Figure 25), that is the existence of several new sets of bands, as well-polarized as the Davydov components referred to above but not correlating with any free molecule bands.

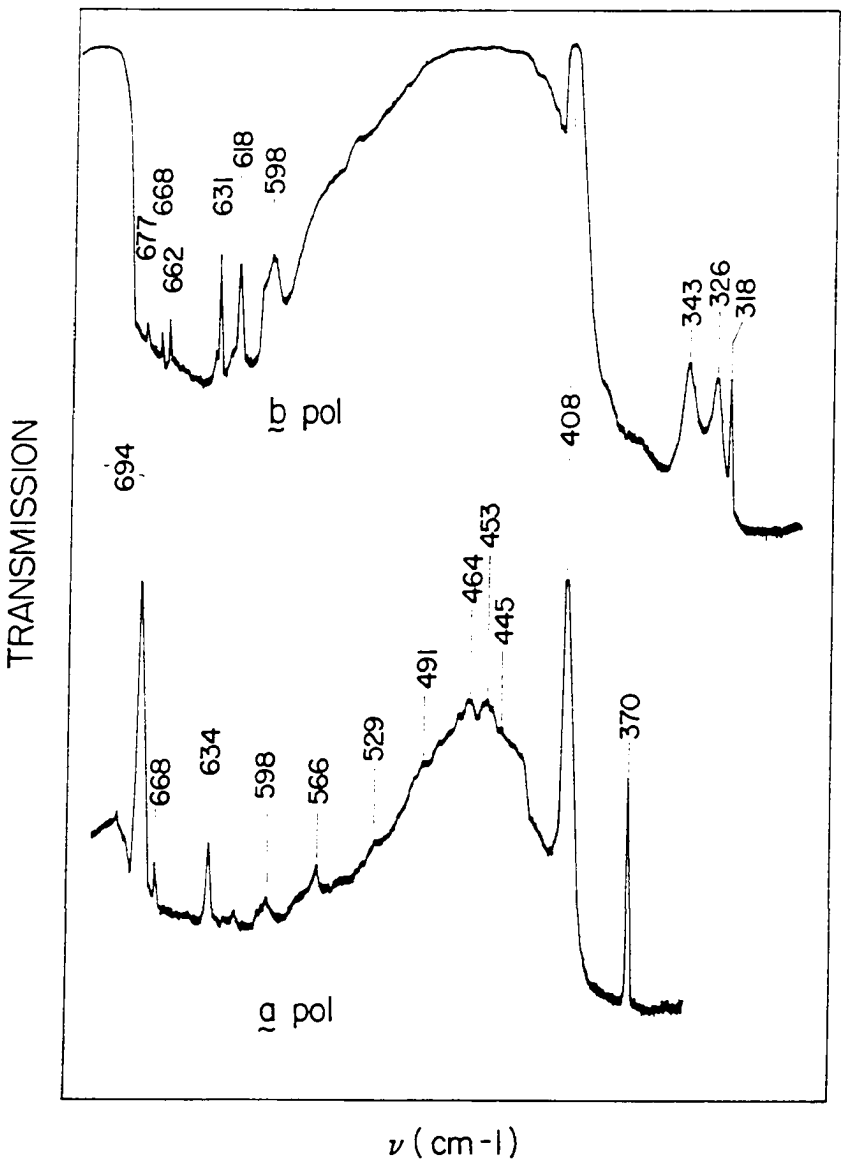

Figure 25. Enlargement of the "M" band region in perfect crystal

Temperature dependence

As discussed in section 1, when impurity concentration and defect concentration are sufficiently low, one may expect to observe a temperature dependence of absorption intensity for exciton bands. Figures 26-29 show data obtained for the a(0,0) 31475 cm^{-1} band of naphthalene for crystals of thickness >10 μ, ∿3 μ, ∿1 μ, and 0.5 μ. These bands should closely reflect true absorption behavior, i.e., R is very small. Qualitatively, one can see that the band area increase with temperature is most pronounced in the thickest crystal, and that there is no apparent increase for the 0.5 micron crystal. The $\underset{\sim}{a}(0,0)$ behavior in this thinnest crystal is obviously different - rather than increasing in area with temperature, $\underset{\sim}{a}(0,0)$ broadens very quickly, such that by 10°K the band is barely observable. At present only a tentative explanation in terms of increased surface damping (relative to bulk) can be given. Encouragingly, this behavior is predicted by the computer calculations for very thin crystals.

During runs crystals were sometimes recycled, that is allowed to warm and then recooled. In all of these cases the band broadening data remained consistent, and within experimental error the same widths were measured for recycled bands. The base line slant observed for most $\underset{\sim}{a}(0,0)$ bands is caused by a decrease in lamp intensity and at higher

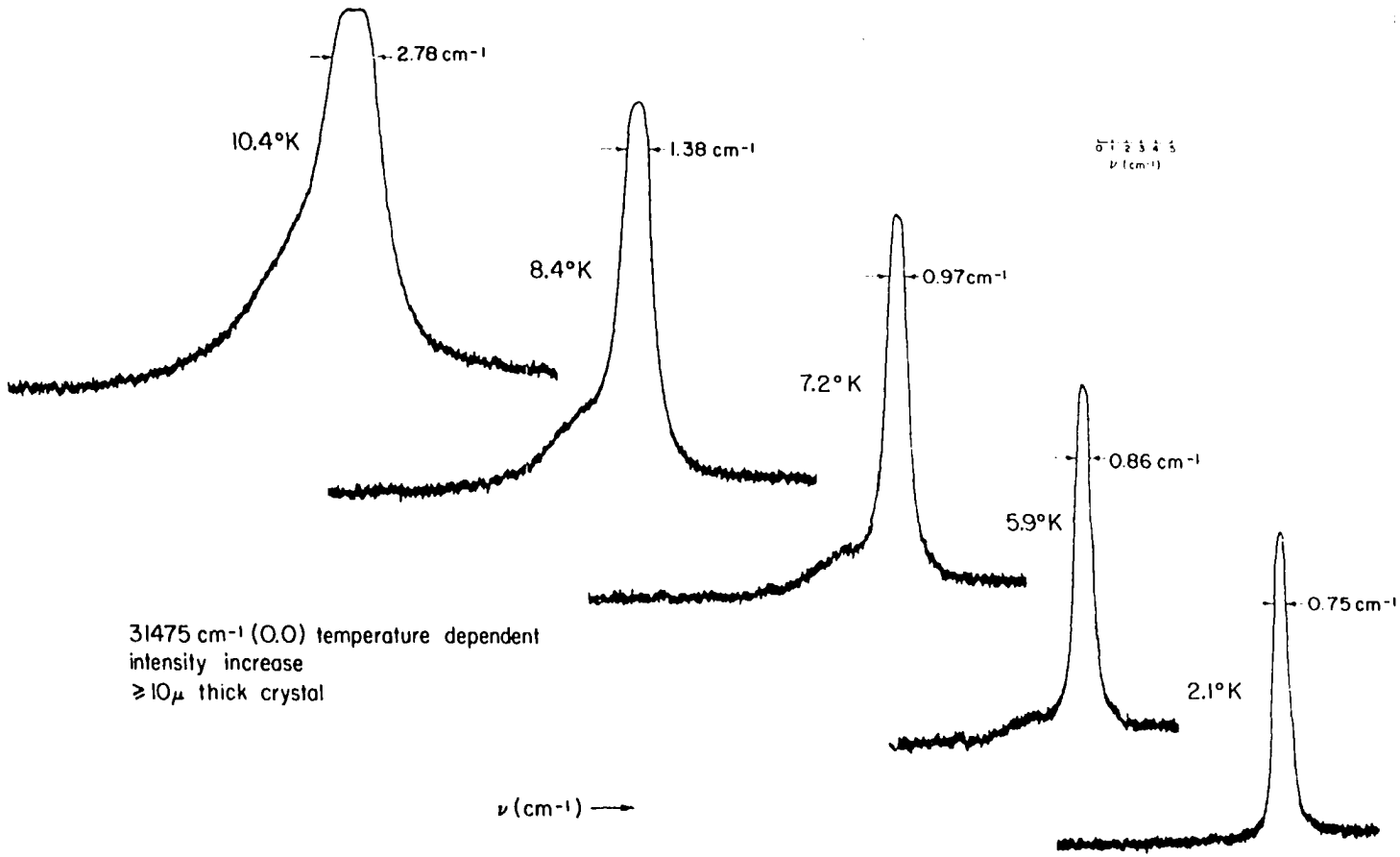

Figure 26. Spectral profile of the naphthalene a(0,0) band as a function of temperature

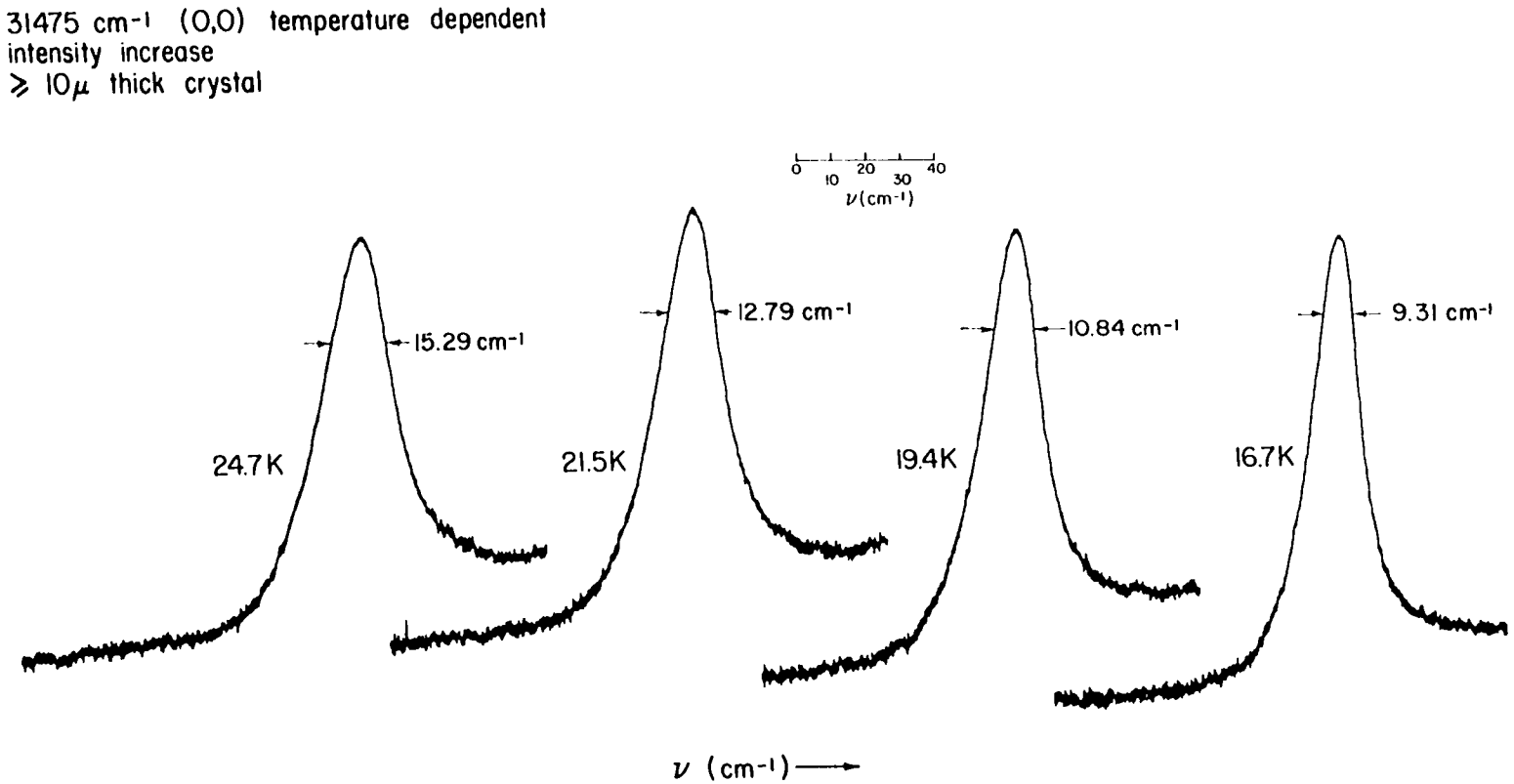

Figure 26. (Continued)

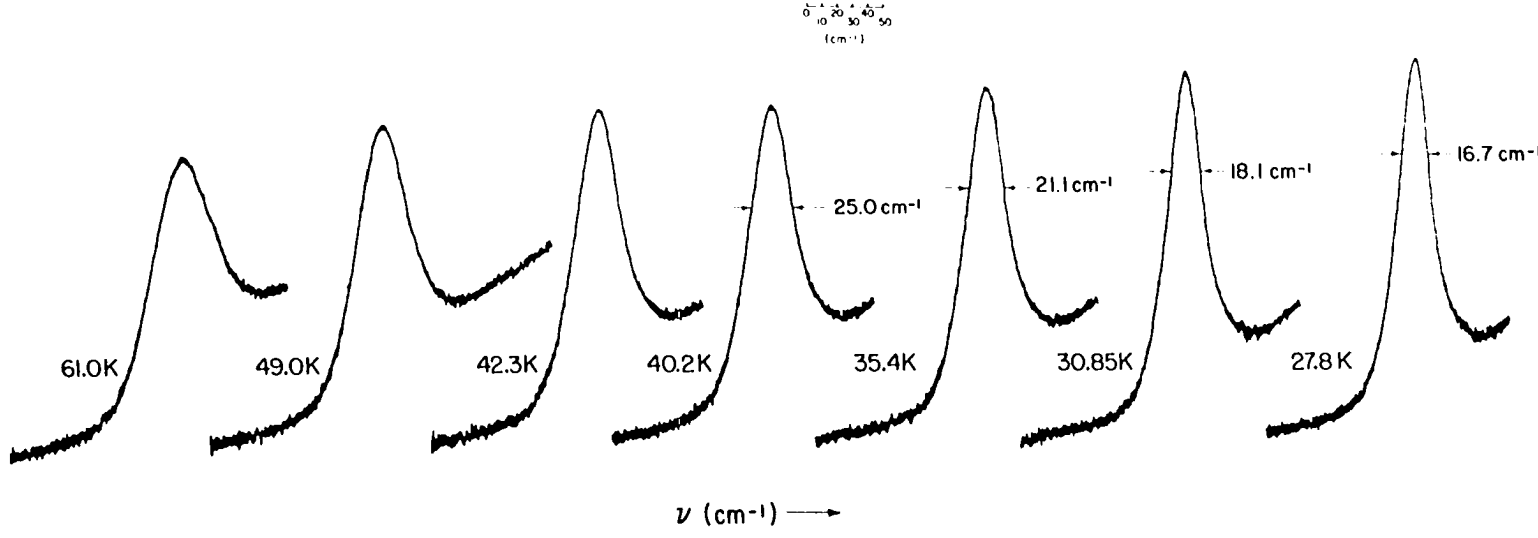

Figure 26. (Continued)

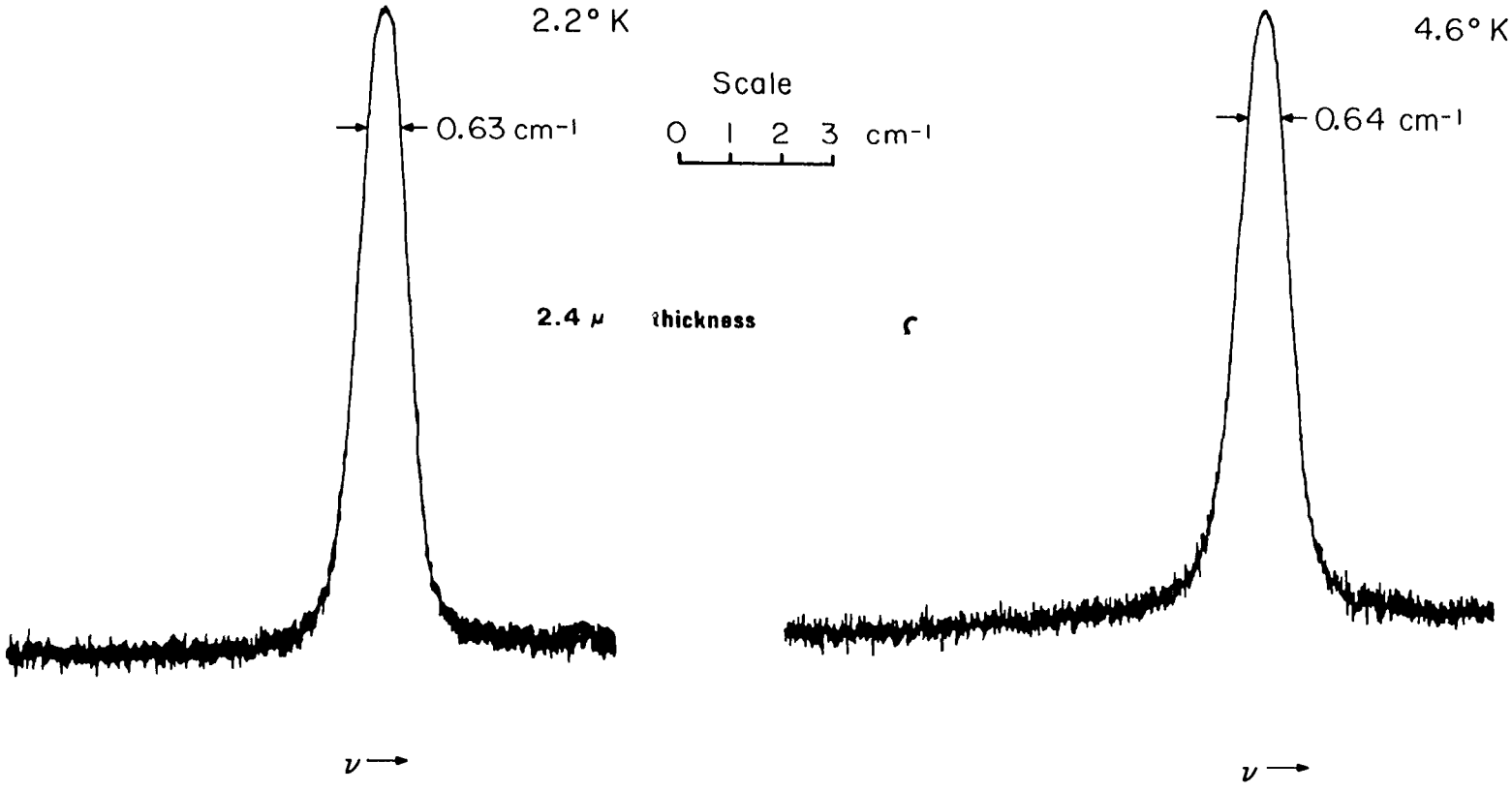

Figure 27. Spectral profile of the naphthalene a(0,0) band as a function of temperature

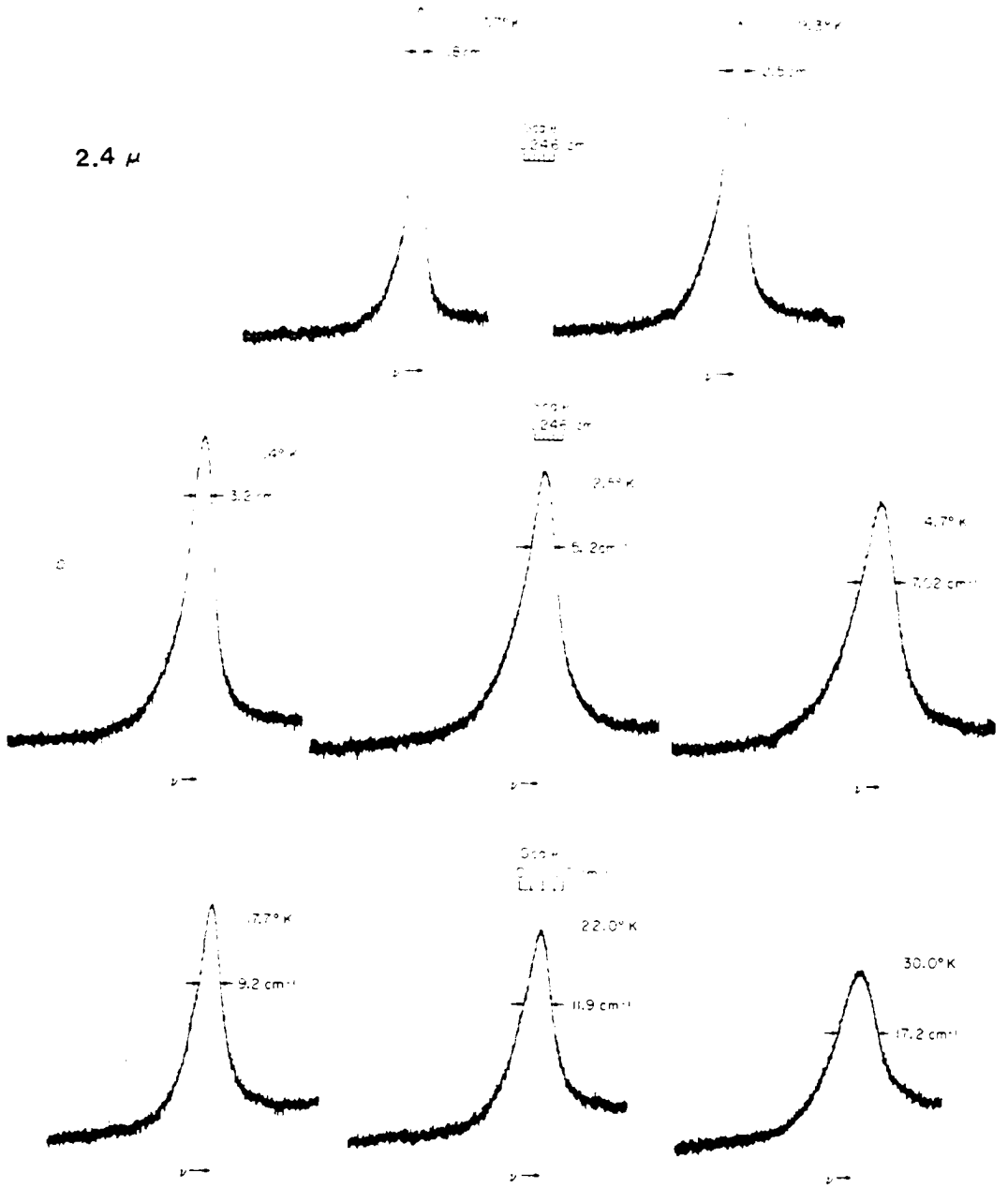

Figure 27. (Continued)

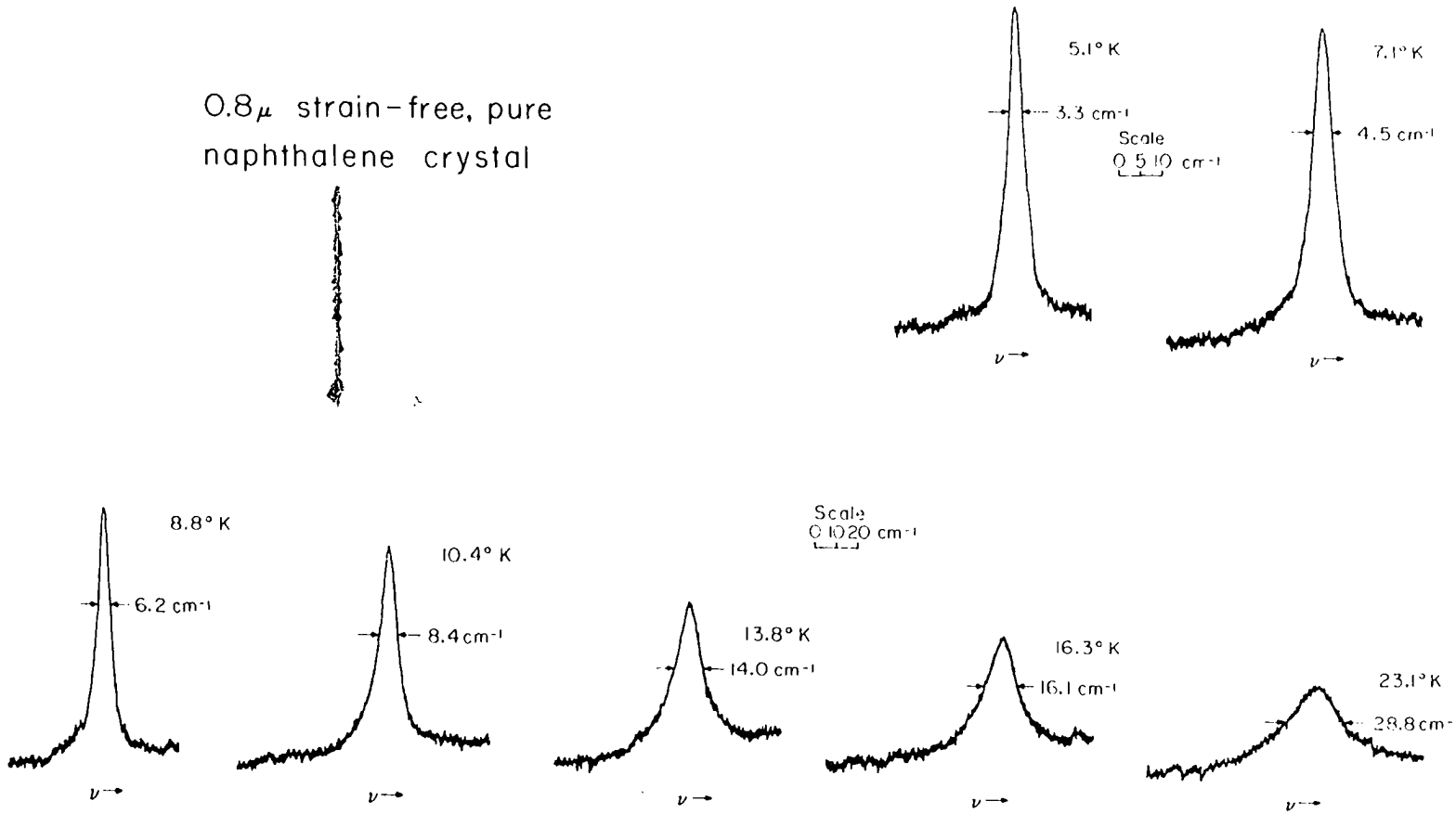

Figure 28. Spectral profile of the naphthalene a(0,0) band as a function of temperature

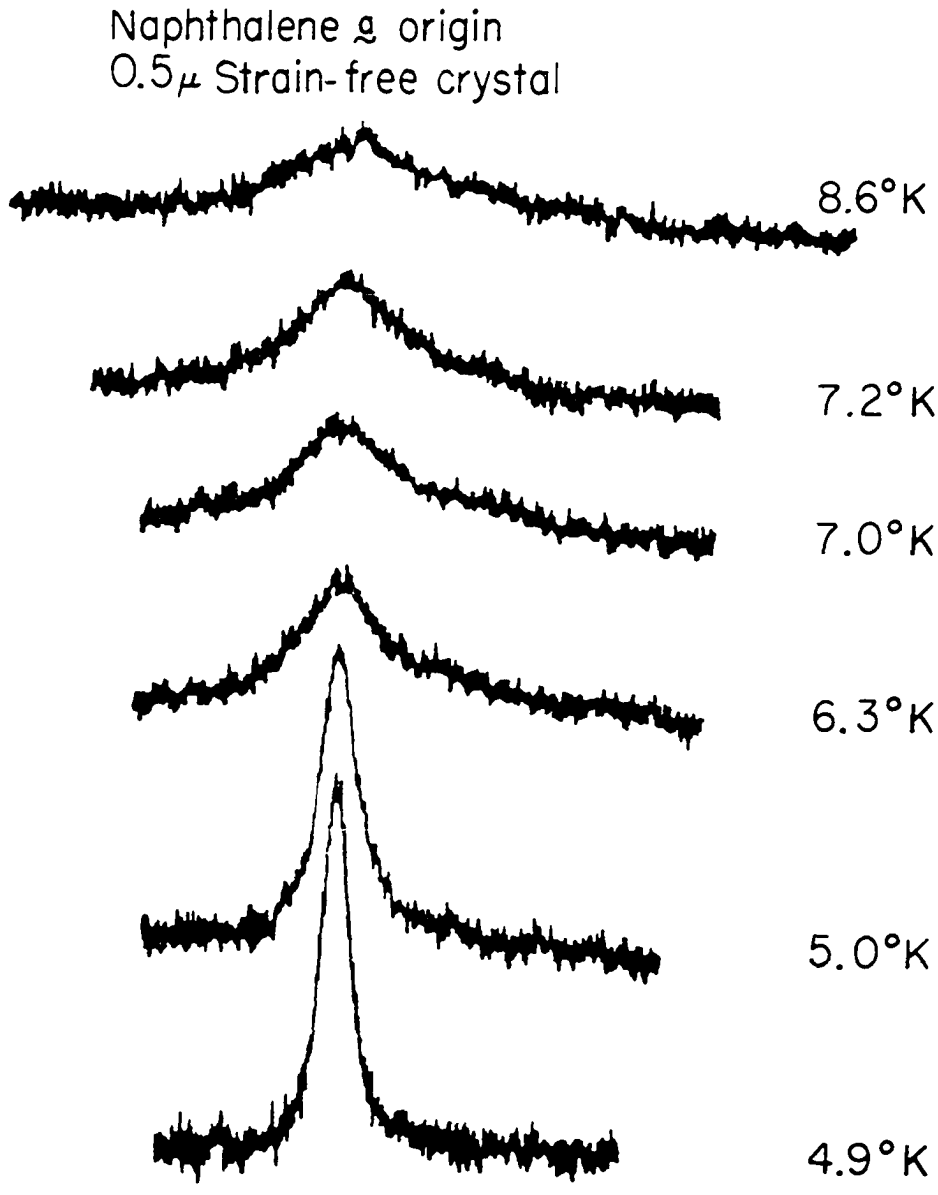

Figure 29. Spectral profile of the naphthalene $\underset{\sim}{a}(0,0)$ band as a function of temperature

temperatures, $\gtrsim$35°K, overlap of the broadening $\underset{\sim}{b}(0,0)$ band. Error introduced by the overlap of the (0,0) Davydov components is minimized for naphthalene since $\underset{\sim}{a}(0,0)$ and $\underset{\sim}{b}(0,0)$ are fairly widely separated (150 cm^{-1}) unlike many similar systems. A slight deterioration in polarization is observed with exposure to He gas. A probable interpretation of this effect is that He gas diffuses into the crystals causing a deterioration of crystal perfection.

The change in area under the $\underset{\sim}{a}(0,0)$ band with increasing temperature for a number of pure, strain-free crystals is shown in Figures 30-33. For all of these crystals the behavior is qualitatively the same. Earlier data show an $\sim$x10 increase in area, while for crystals grown and studied later in the work the increase is as large as $\sim$x25. At present we can only attribute this increase to improvement in technique in crystal growth and/or mounting procedures as the experiments progressed.

In addition to band areas, full widths-half maxima (FWHM) as a function of temperature provide useful information for exciton-phonon coupling (123,124) and polariton scattering models. Plots of FWHM's *vs* temperature for pure, strain-free crystals are shown in Figures 34-36. All curves show the same basic shape; at lower temperatures an approximately quadratic temperature dependence and at higher temperatures a linear dependence. (Other workers report

data for 300°K (123,124) which show the linear behavior continuing although it is certain that experimental uncertainty for high temperature measurements must be very large.) Initial results seemed to reveal a dependence of the broadening rate on crystal thickness, i.e., thinner crystals broadened faster. Later work, however, shows this relationship does not hold in general (Figure 35). Broadening appears to be most erratic with respect to crystal thickness in the most perfect crystals, i.e., those showing the largest band area increases with increasing temperature. An explanation may be that as purity increases the data will become very sensitive to small differences in strain and impurity concentration unique to each crystal. Further, it should be noted that for the band broadening data given here for naphthalene, the data points shown for all the crystals measured fall within the error limits shown by other workers for similar measurements on anthracene and phenanthrene.

For a few pure, strain-free crystals the broadening of the sharp $\underset{\sim}{a}$ polarized band at 370 cm^{-1} was monitored along with $\underset{\sim}{a}(0,0)$ for increasing temperature. The 370 cm^{-1} band shows only a small linear increase as compared to the quadratic increase seen for $\underset{\sim}{a}(0,0)$ (Figure 37).

Another important parameter in exciton-phonon coupling models is the shift in energy of the band center with

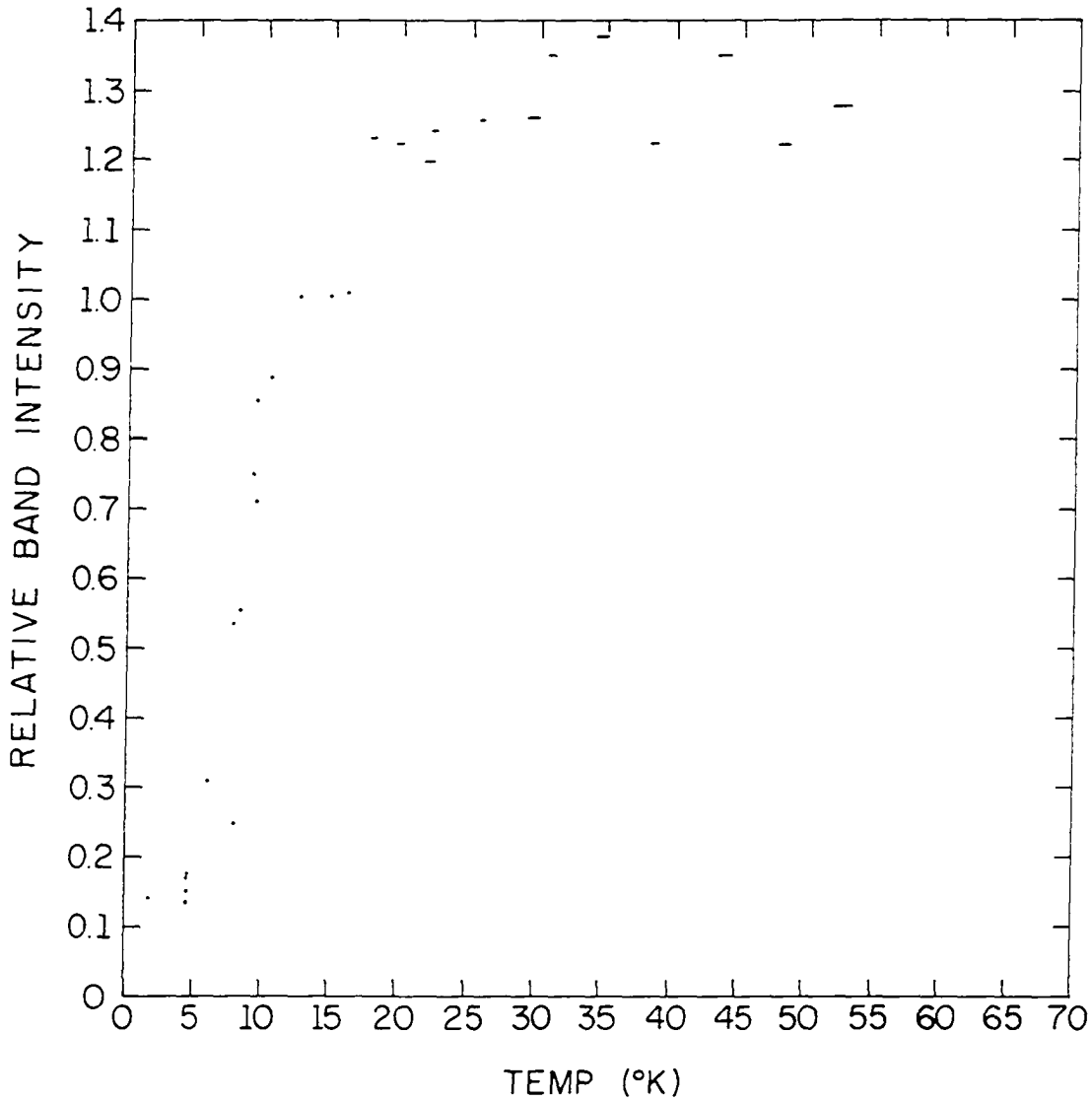

Figure 30. Area of $\underline{a}(0,0)$ in perfect, strain-free ~2.5 μ naphthalene crystal as a function of temperature

Figure 31. Area of $\underset{\sim}{a}(0,0)$ in perfect, strain-free $\geq$ 10 μ naphthalene crystal as a function of temperature

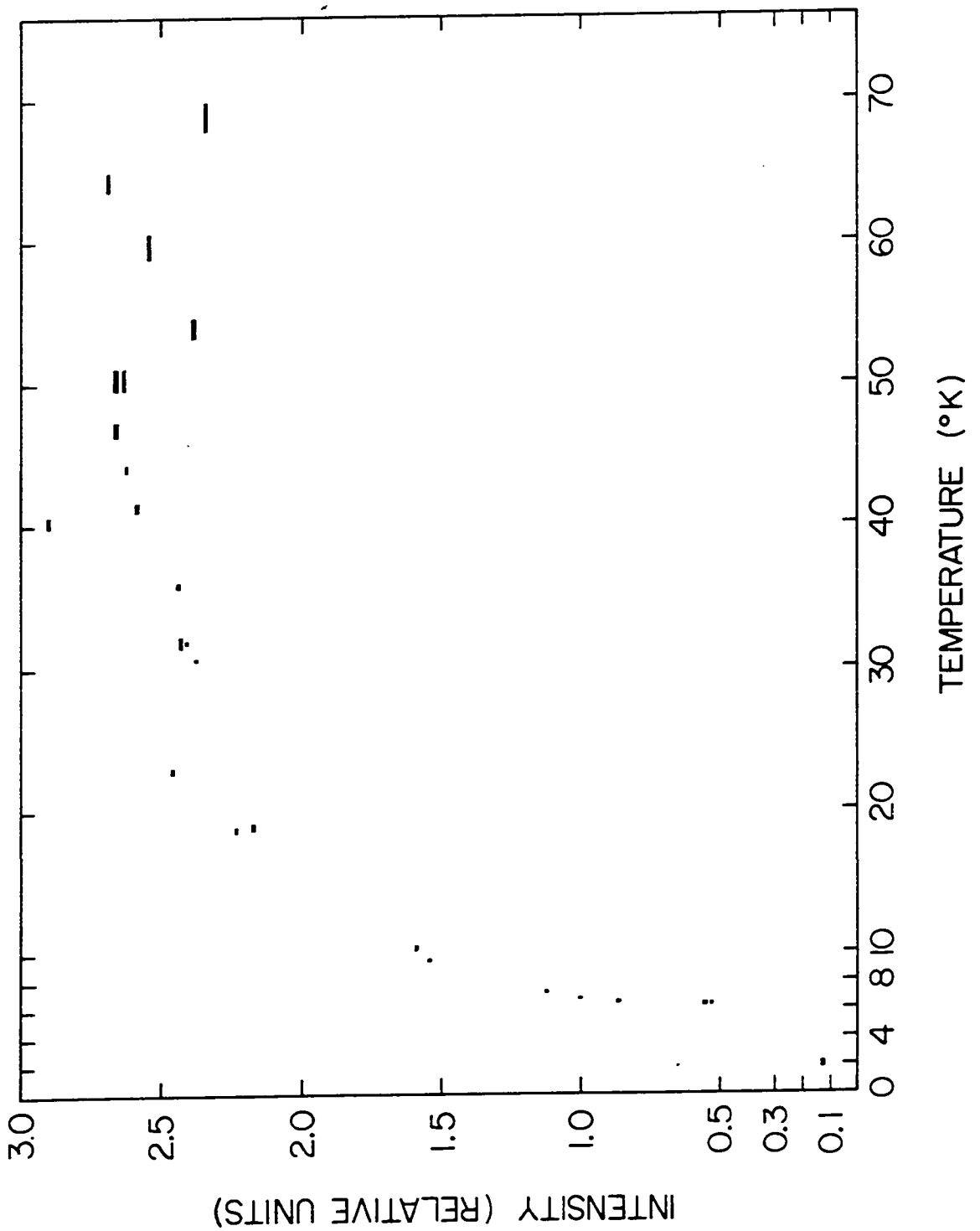
INTENSITY (RELATIVE UNITS)
3.0
2.5
2.0
1.5
1.0
0.5
0.3
0.1
0
4
8
10
20
30
40
50
60
70
TEMPERATURE (°K)

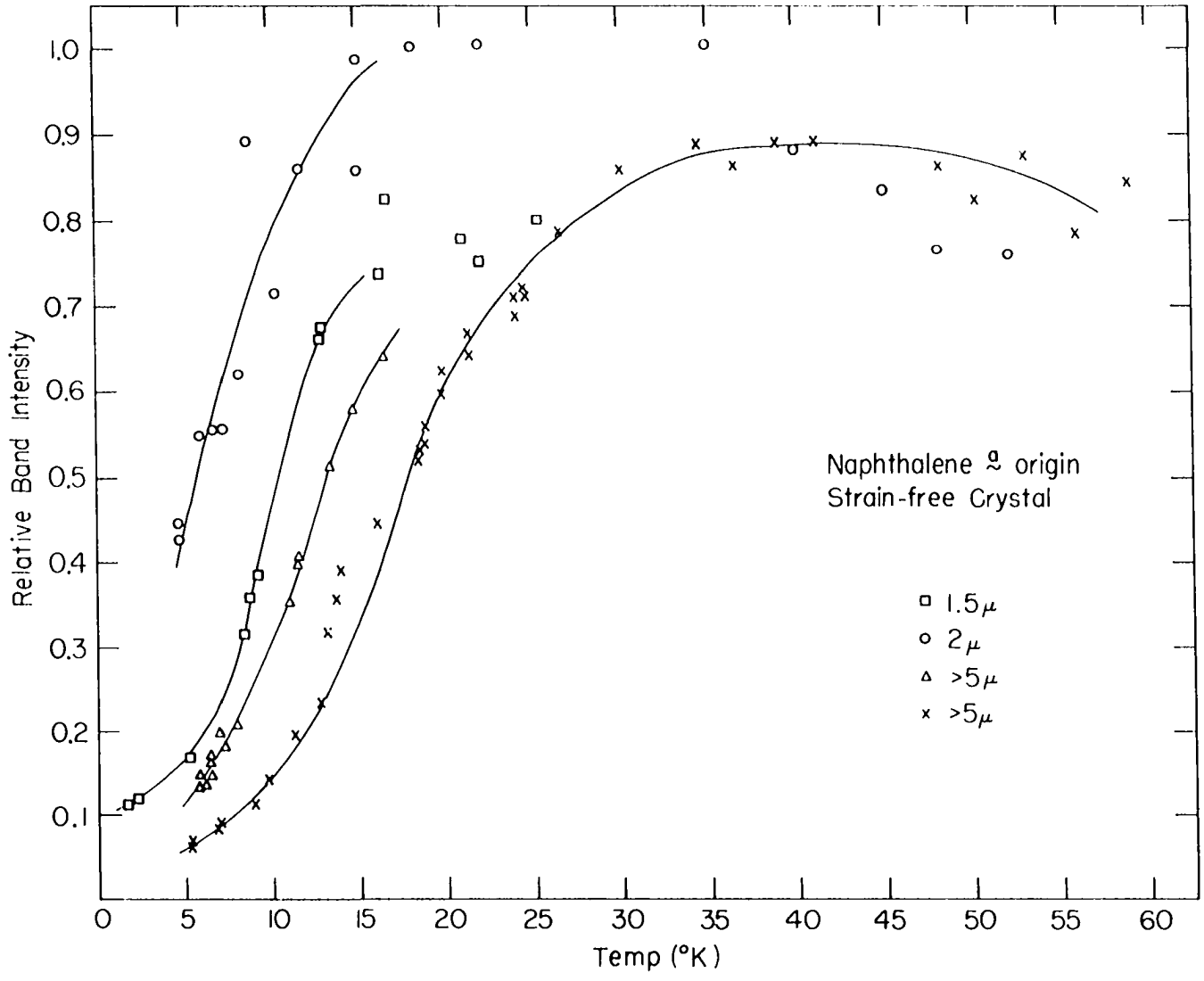

Figure 32. Area of $\underset{\sim}{a}(0,0)$ for several perfect crystals as a function of temperature

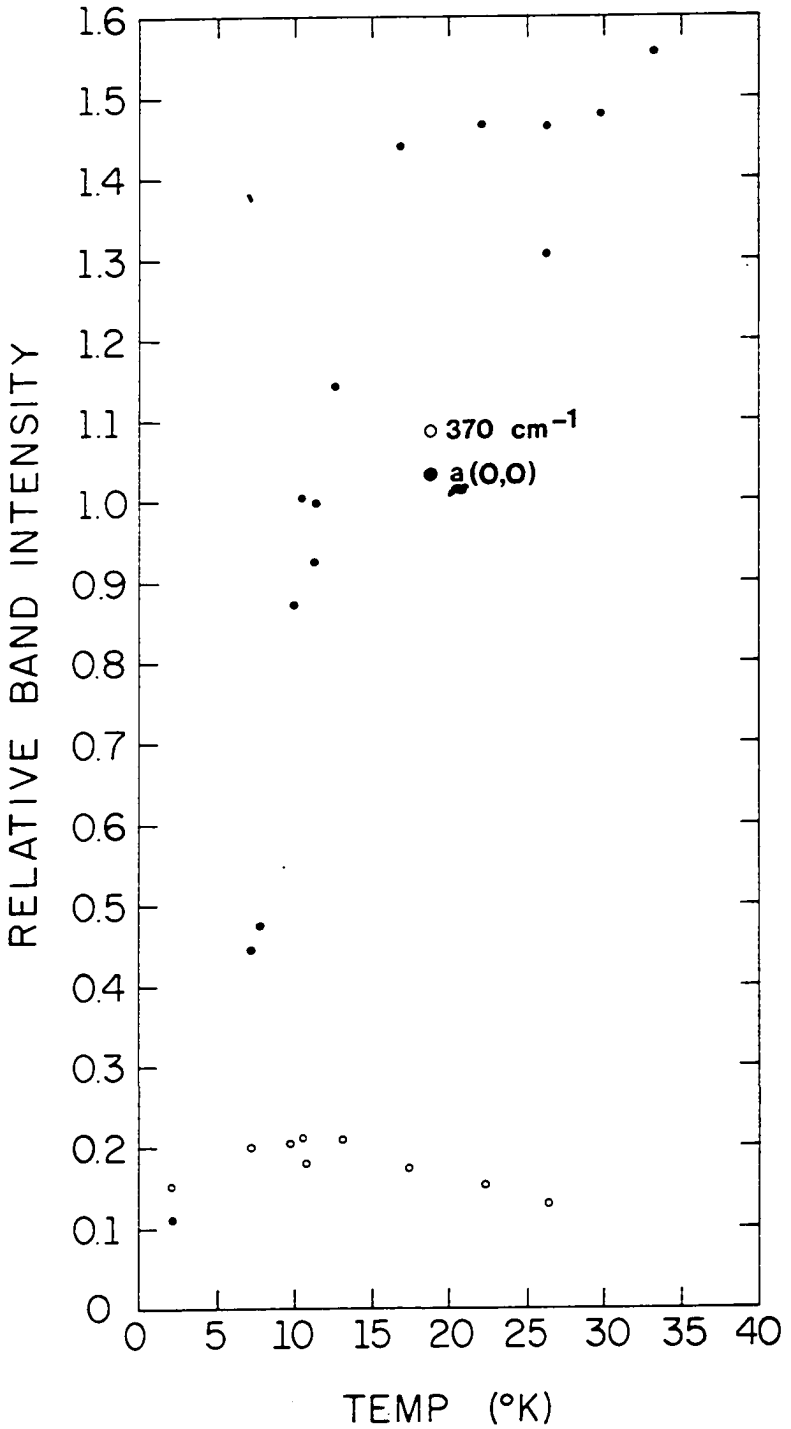

Figure 33. Area of $\underset{\sim}{a}(0,0)$ and 370 cm^{-1} band as a function of temperature for 2.3 μ crystals

Figure 34. $\underset{\sim}{a}(0,0)$ full width-half maxima for several pure strain-free naphthalene crystals

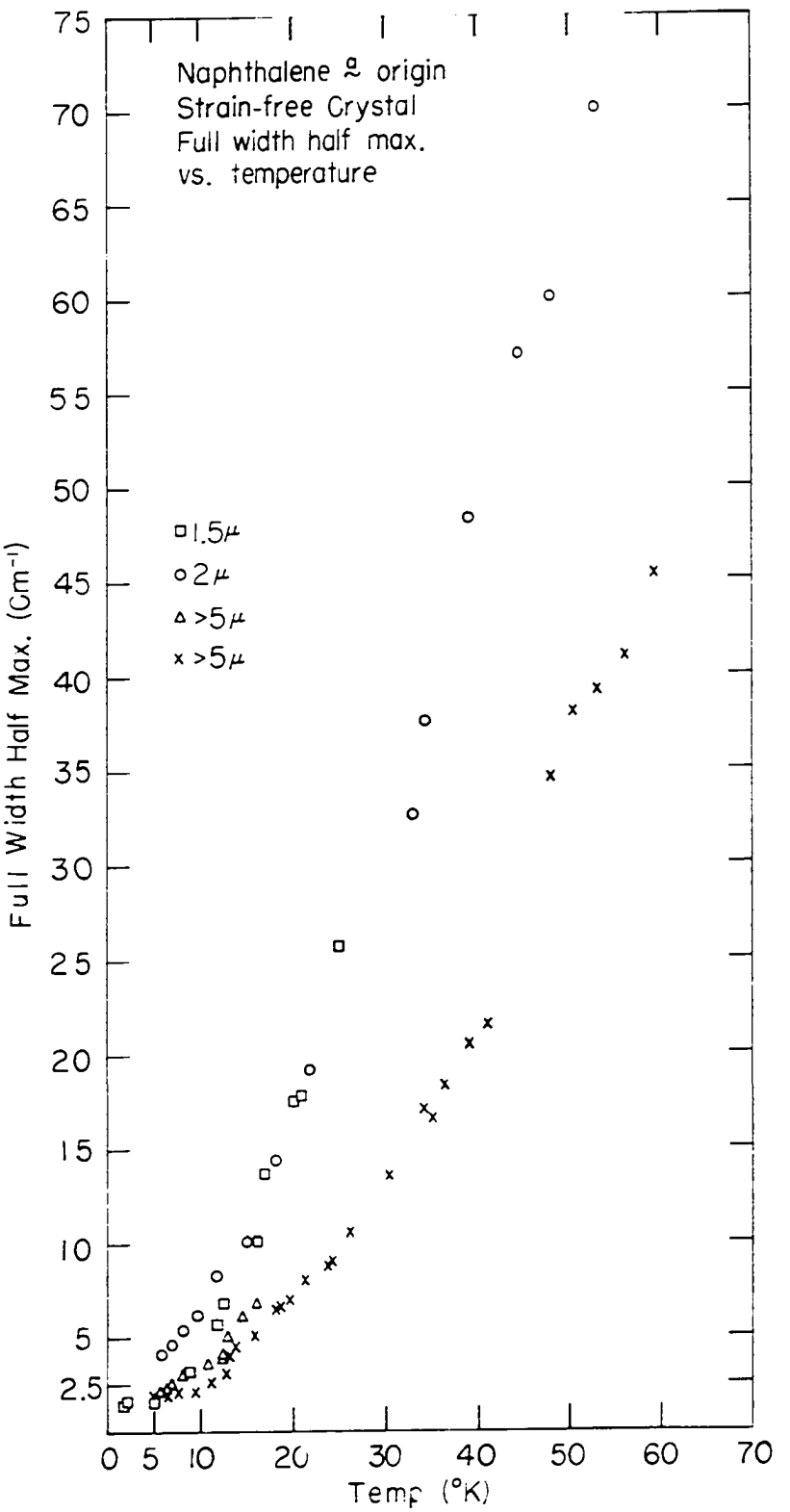
Naphthalene 0 origin
Strain-free Crystal
Full width half max.
vs. temperature
□ 1.5μ
○ 2μ
△ >5μ
× >5μ
Full Width Half Max. (Cm⁻¹)
75
70
65
60
55
50
45
40
35
30
25
20
15
10
5
2.5
0
5
10
20
30
40
50
60
70
Temp (°K)

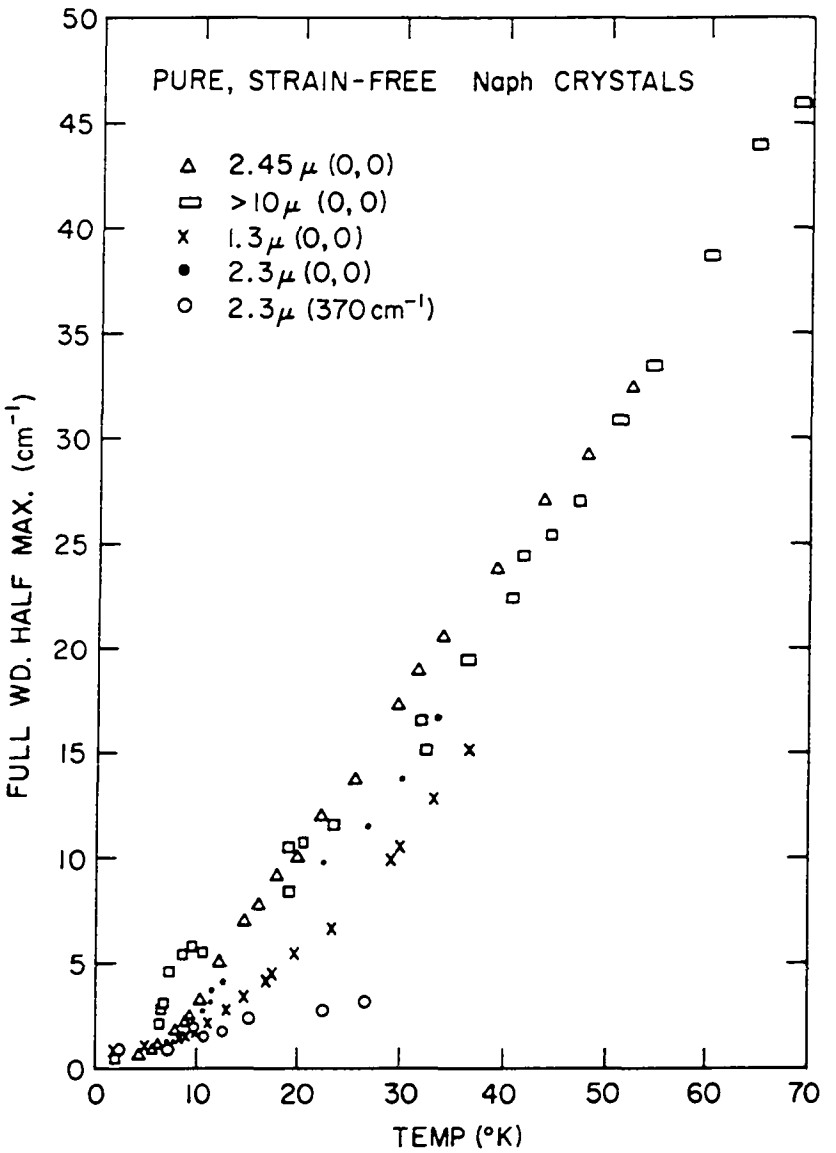

Figure 35. $\tilde{a}(0,0)$ full width-half maxima for several pure strain-free naphthalene crystals

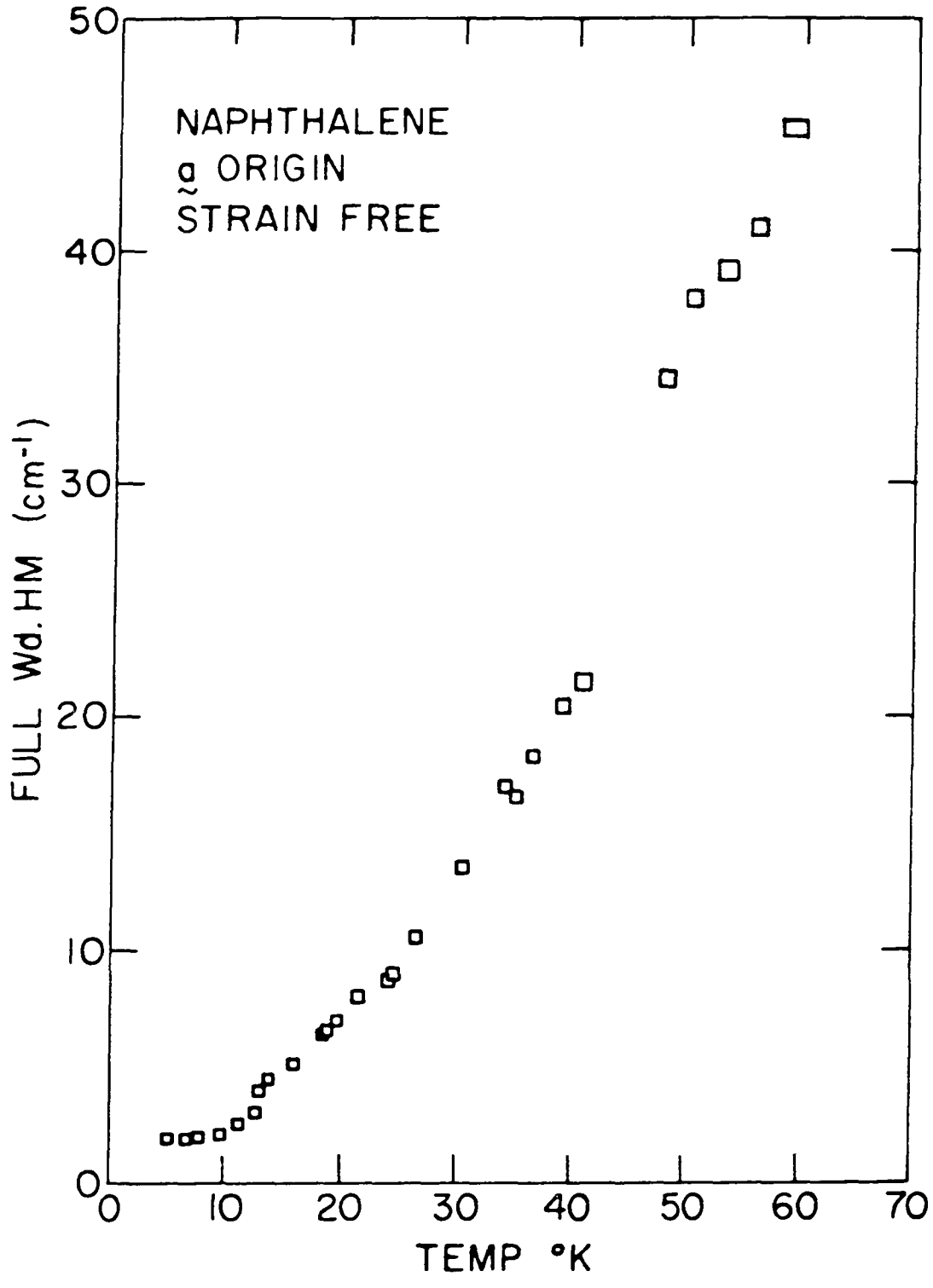

Figure 36. $\underset{\sim}{a}(0,0)$ full width-half maxima for >5 μ pure strain-free naphthalene crystal

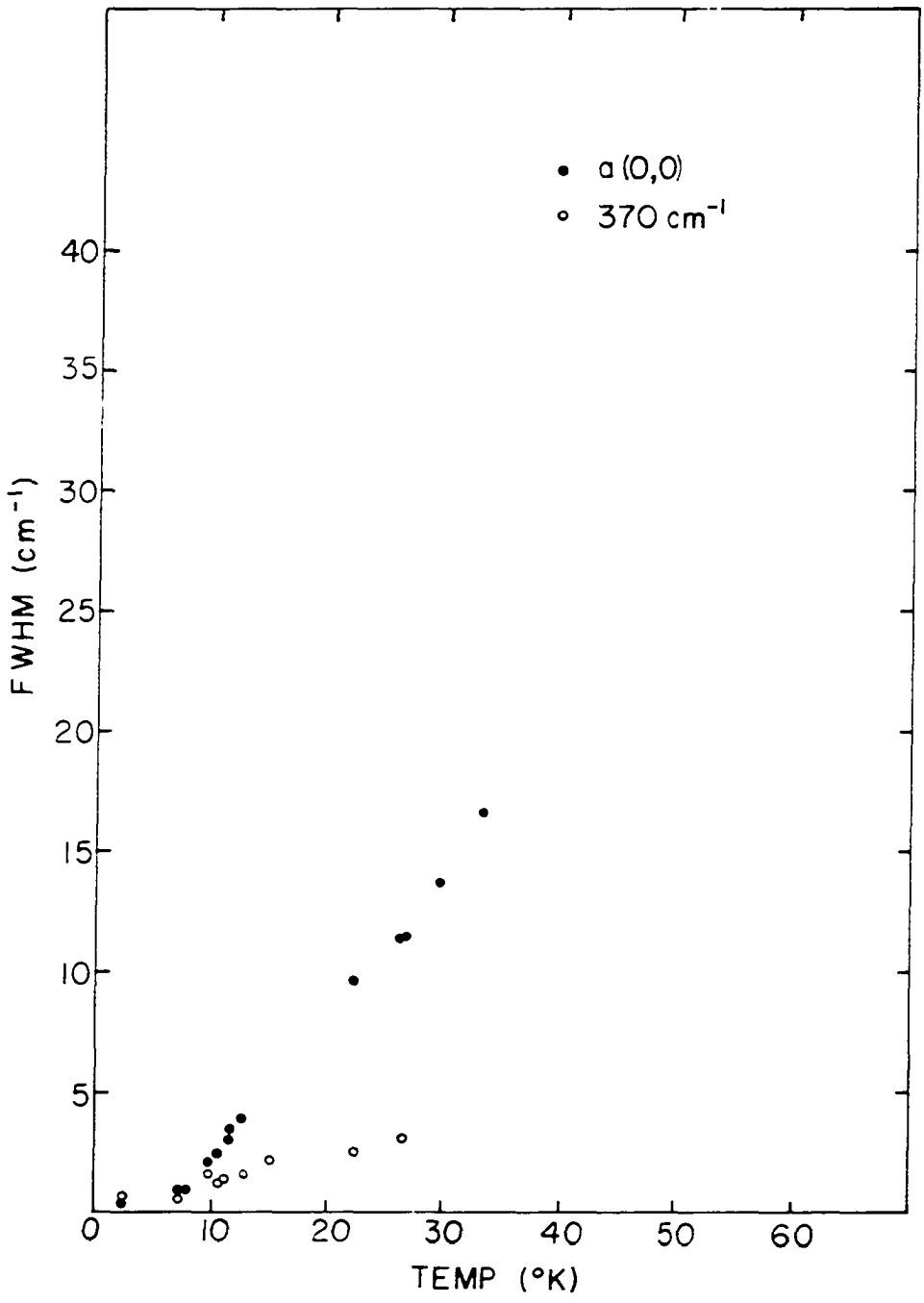

Figure 37. Comparison of FWHM of $\underset{\sim}{a}(0,0)$ and 370 cm^{-1} bands in pure, strain-free naphthalene crystal

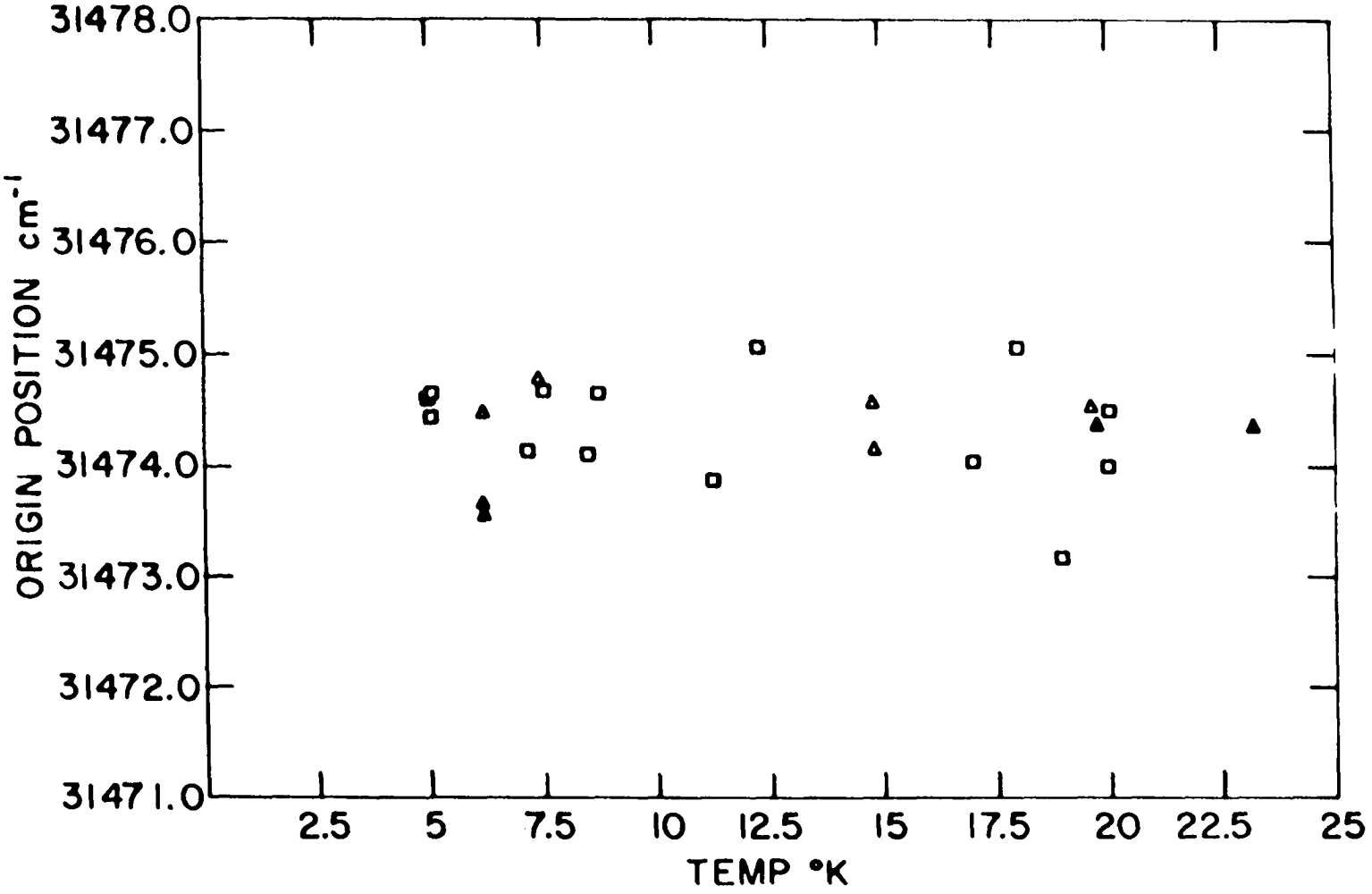

Figure 38. Energy shift of $\underset{\sim}{a}(0,0)$ vs temperature for two perfect crystals

temperature (66). From 2°-77°K, for data at the limit ($\sim$0.1 cm^{-1}) experimental uncertainty of the Jobin-Yvon spectrometer, there is no shift of the $\underset{\sim}{a}(0,0)$ band maxima (Figure 38).

Band shapes

Returning to Figures 26-29, another obvious feature of the bands is their asymmetry. There are several mathematical expressions which yield asymmetric band shapes, e.g., asymmetric Lorentzians, or the sum of two Voigt functions. It is, however, almost certainly not correct to use functions like these to fit single crystal transmission (or absorption) data with the hope of gaining meaningful physical information. The computer plots are most instructive here since asymmetric band shapes occur naturally in the classical theory for transmission through a thin slab. Even the small bumps on the low energy side of some of the experimental bands are qualitatively reproduced by the computer plots. Especially dangerous is the procedure of fitting transmission bands for large oscillator strength transitions ($f \gtrsim 0.1$) by model band shapes and subsequently inferring absorption profiles, since the computer generated spectra as well as Ferguson's experiment data indicate the true absorption profile may be very different. For the naphthalene $\underset{\sim}{a}(0,0)$ band ($f \sim 10^{-6}$) the absorption should be very similar

to transmission but the $\underset{\sim}{b}(0,0)$ computer plots ($f \sim 10^{-4}$) for small γ show a good deal of structure in the (1-R-T) band, and bear no relation to Gaussian or Lorentzian band shapes.

Strained, pure crystals

An obvious check on the interpretation of the data in Figures 38 and 39 would be to measure the temperature dependence of the area of the $\underset{\sim}{a}(0,0)$ band for a strained but chemically pure crystal. Figure 39 shows there is no increase in intensity with temperature for a crystal affixed by two opposite edges to a solid support. Figure 39 also shows the effect of affixing only one edge of a crystal; a factor of two increase in band area is seen. A striking change is seen in the curves for FWHM vs temperature for the strained crystal, Figure 40a and b, as compared to unstrained, Figures 34-36. At $\sim 4°K$ the band is already 3-4 times as broad as for the strain-free case, and proceeds to broaden with temperature approximately as $T^{\frac{1}{2}}$. Interestingly, Toyozawa has proposed, for ionic systems, that a linear $T^{\frac{1}{2}}$ dependence should be indicative of strong exciton-phonon coupling and large effective mass, i.e., of a localized exciton. This mechanism and strain broadening are most likely unrelated.

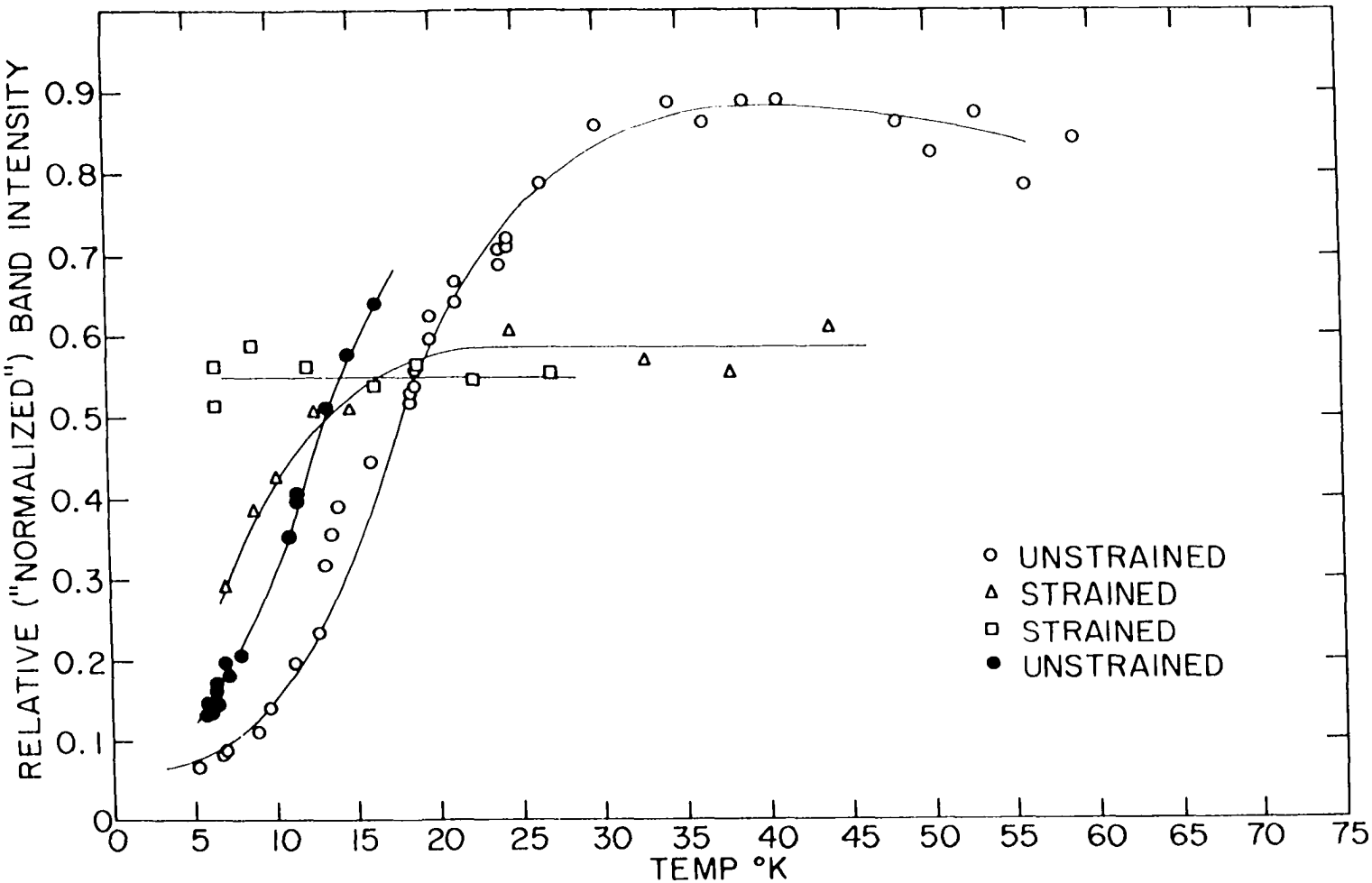

Figure 39. Temperature dependence of $\underset{\sim}{a}(0,0)$ area in pure crystals

▲ Strained-one side attached, □ strained-both sides attached vs unstrained (●,○)

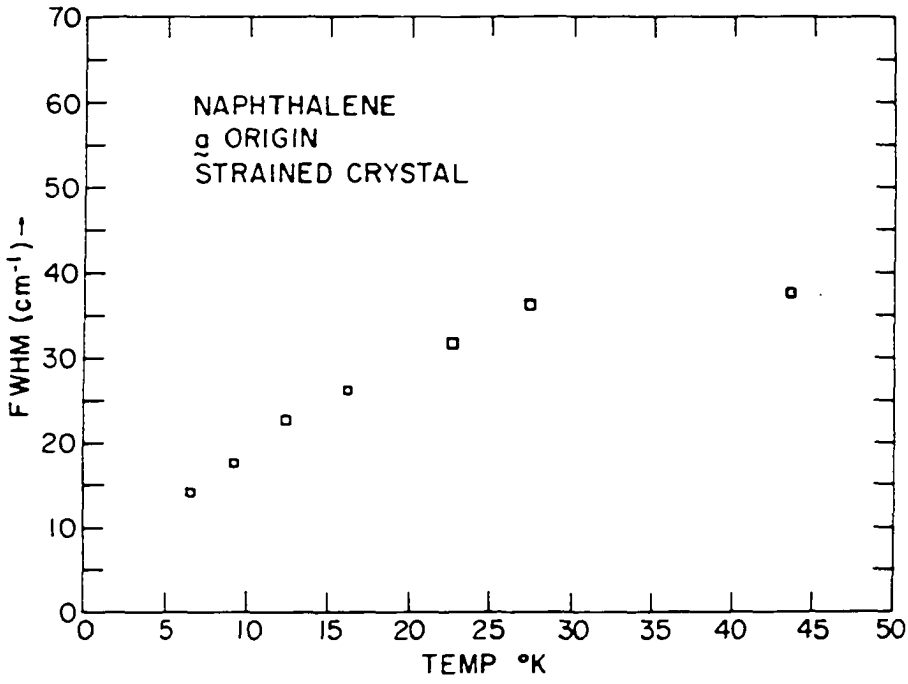

(a)

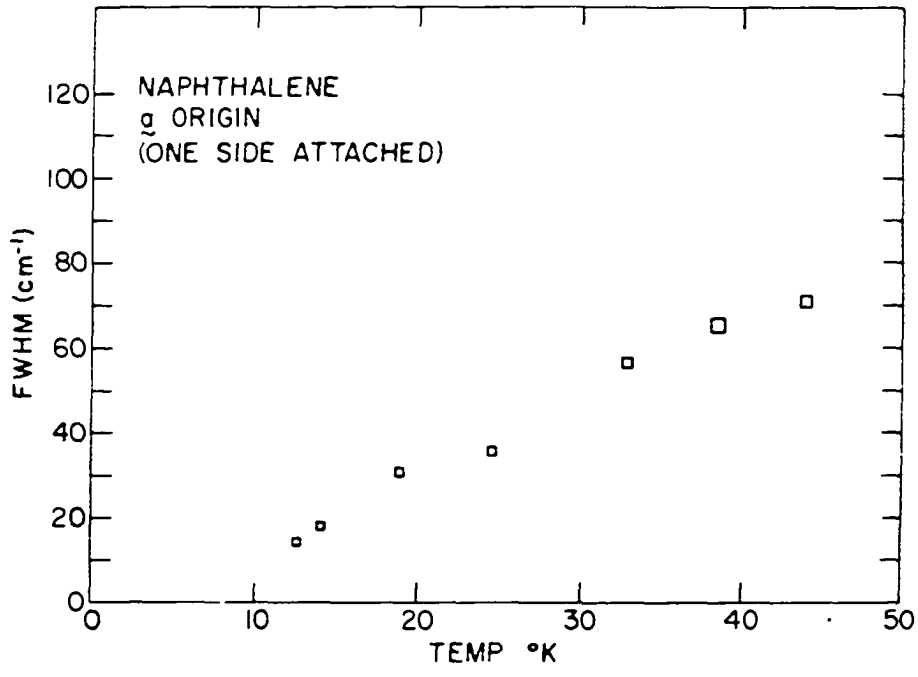

(b)

Figure 40. FWHM behavior in pure, strained crystals

Doped Crystals

Some preliminary temperature dependent studies were performed on crystals doped with either β-methylnaphthalene (βMN) or anthracene.

β-methylnaphthalene

β-methylnaphthalene (βMN) was chosen as a dopant because it is known to incorporate in naphthalene in high mole percents and, secondly, it is a well-characterized shallow trap, lying about 300 cm^{-1} below the naphthalene $\underset{\sim}{a}(0,0)$ in energy. The temperature dependence of a crystal heavily doped with βMN ($\gtrsim$ 0.1%) is shown in Figure 41. As in the highly strained case, there is no increase in area under the a(0,0) band. However, the FWHM data show a temperature dependence similar to that of the pure, strain-free crystals, although the band is significantly broader at 4°K. Figures 42 and 43 show the temperature dependent behavior for a crystal of concentration $\sim 10^{-4}$ mole/mole βMN. There is an approximate factor of five increase in relative band intensity as compared to ~10-25 for pure crystals of the same order of thickness. Again, the FWHM behavior is close to that of the pure crystals except that the band is initially broader.

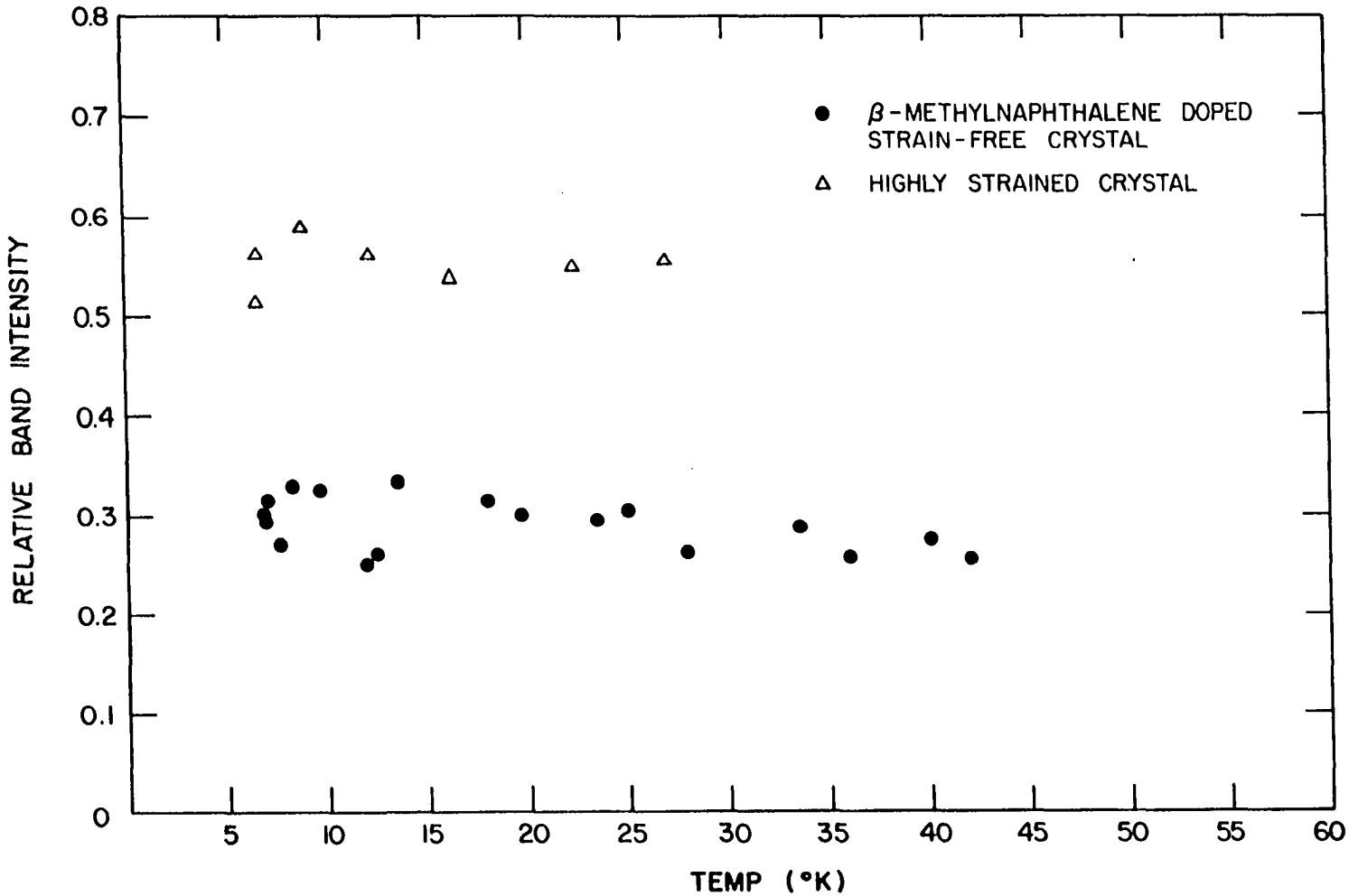

Figure 41. Comparison of heavily doped and highly strained crystals

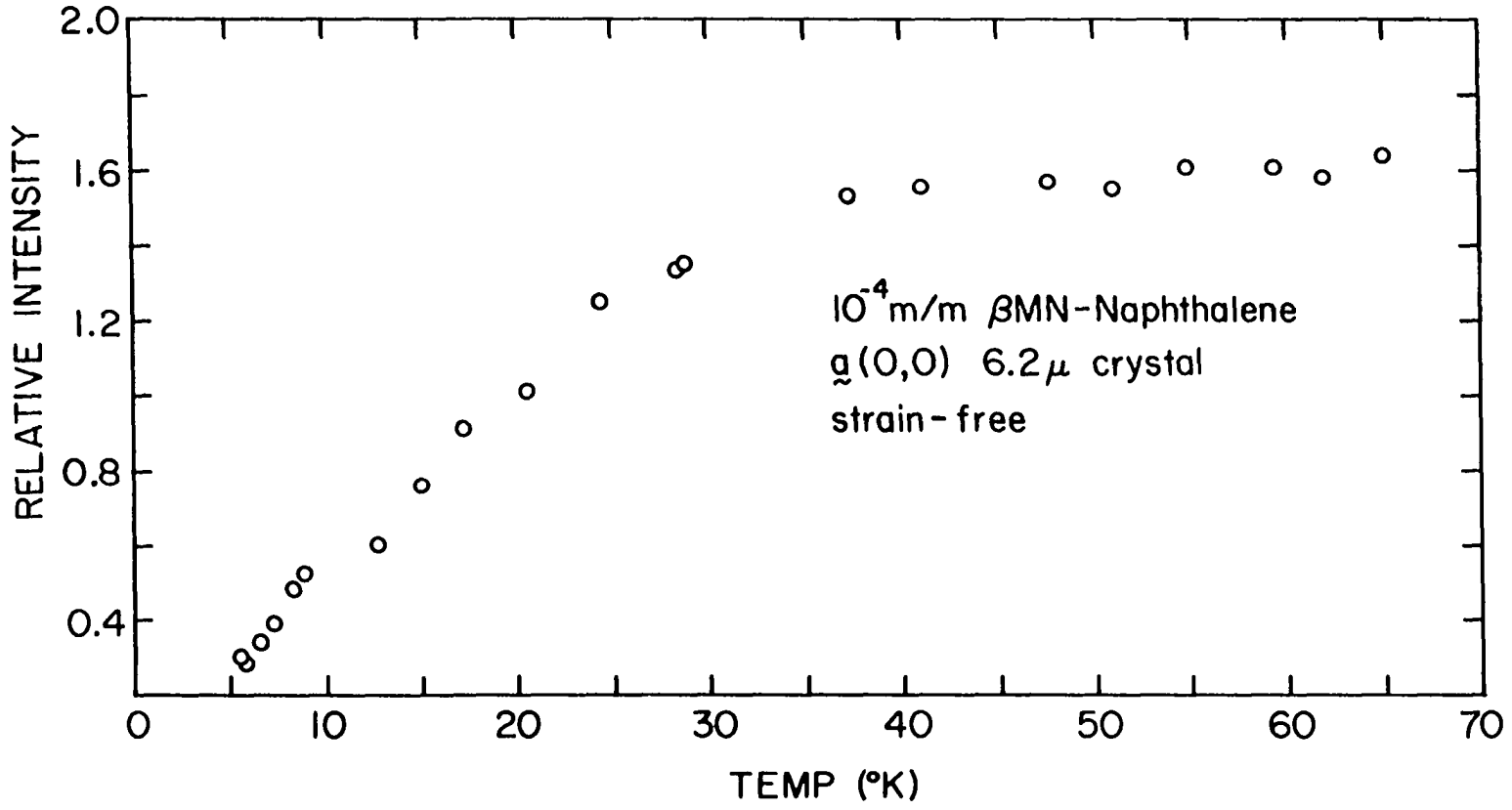

Figure 42. a(0,0) area increase in 10^{-4} m/m βMN doped naphthalene crystal

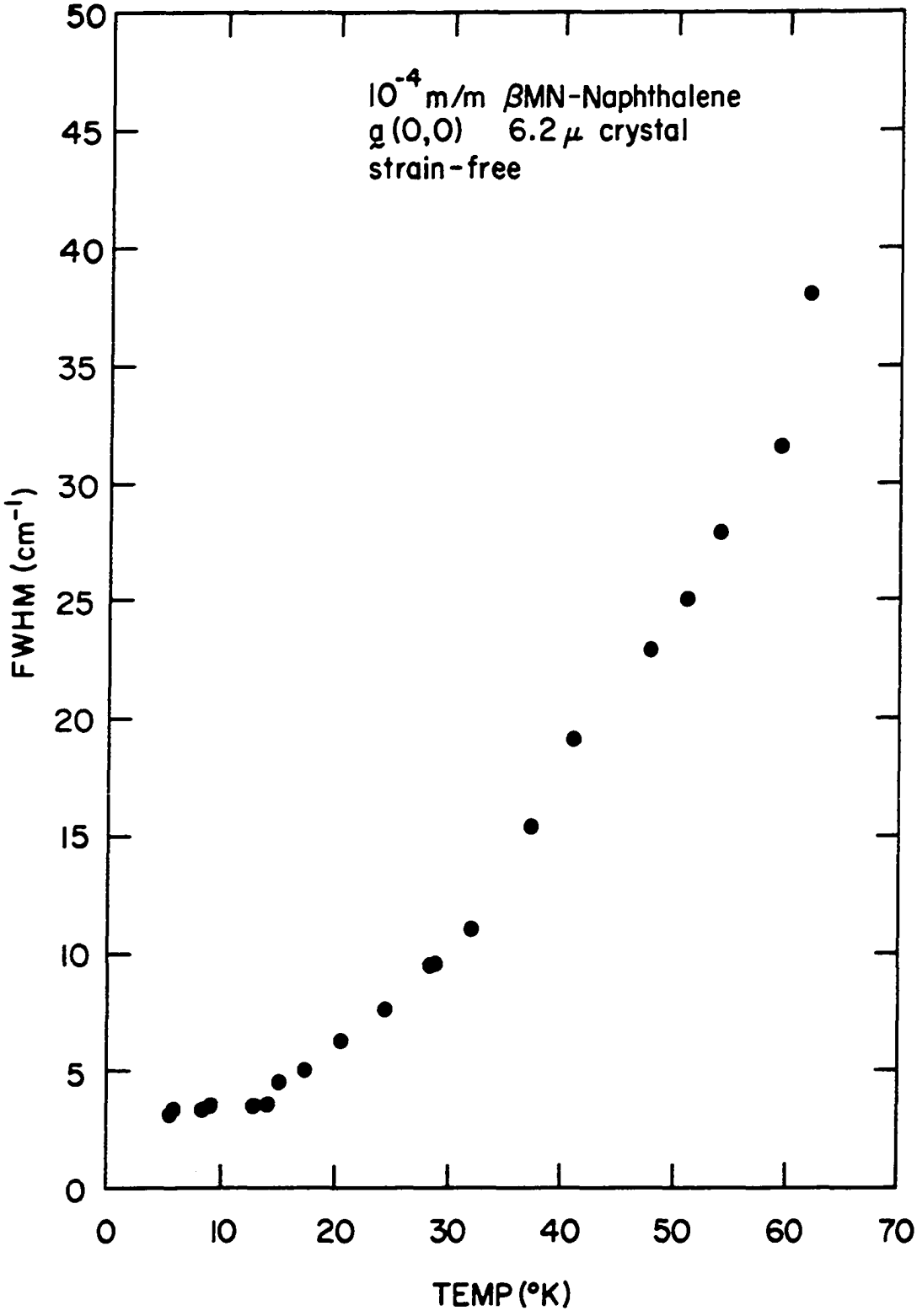

Figure 43. FWHM behavior for 10^{-4} m/m βMN doped naphthalene crystal

Anthracene

Anthracene forms a deep trap system in naphthalene lying about 4,000 cm^{-1} below $\underset{\sim}{a}(0,0)$. Unfortunately, in mixed crystals grown from solid solutions, 10^{-4} mole/mole anthracene appears to be the maximum concentration obtainable in sublimation flakes regardless of the concentration of anthracene in the solid solution. Interestingly, a number of crystals from different batches, but all of $\sim 10^{-4}$ m/m anthracene concentration yielded data points that fell on one smooth curve, showing an approximate x2 increase in relative band intensity vs temperature (Figure 44). For these six crystals then, chemical impurity concentrations appear to be the determining variable as opposed to, say, slightly different growth conditions between batch or variations in internal strain with mounting. Data for one crystal from the doped batches of the so-called "perfect" growth habit (hexagonal) is also shown. This crystal is most probably actually lower in anthracene concentration, since as mentioned in the Experimental section, concentrations determined were averages. FWHM data for the seven crystals are shown in Figure 45. While the preliminary anthracene data suggests an analytical technique for low level concentration determination, the method as described in this dissertation seems rather cumbersome for routine use, although possibly polariton effects might be used to monitor the quality of special high purity single crystals.

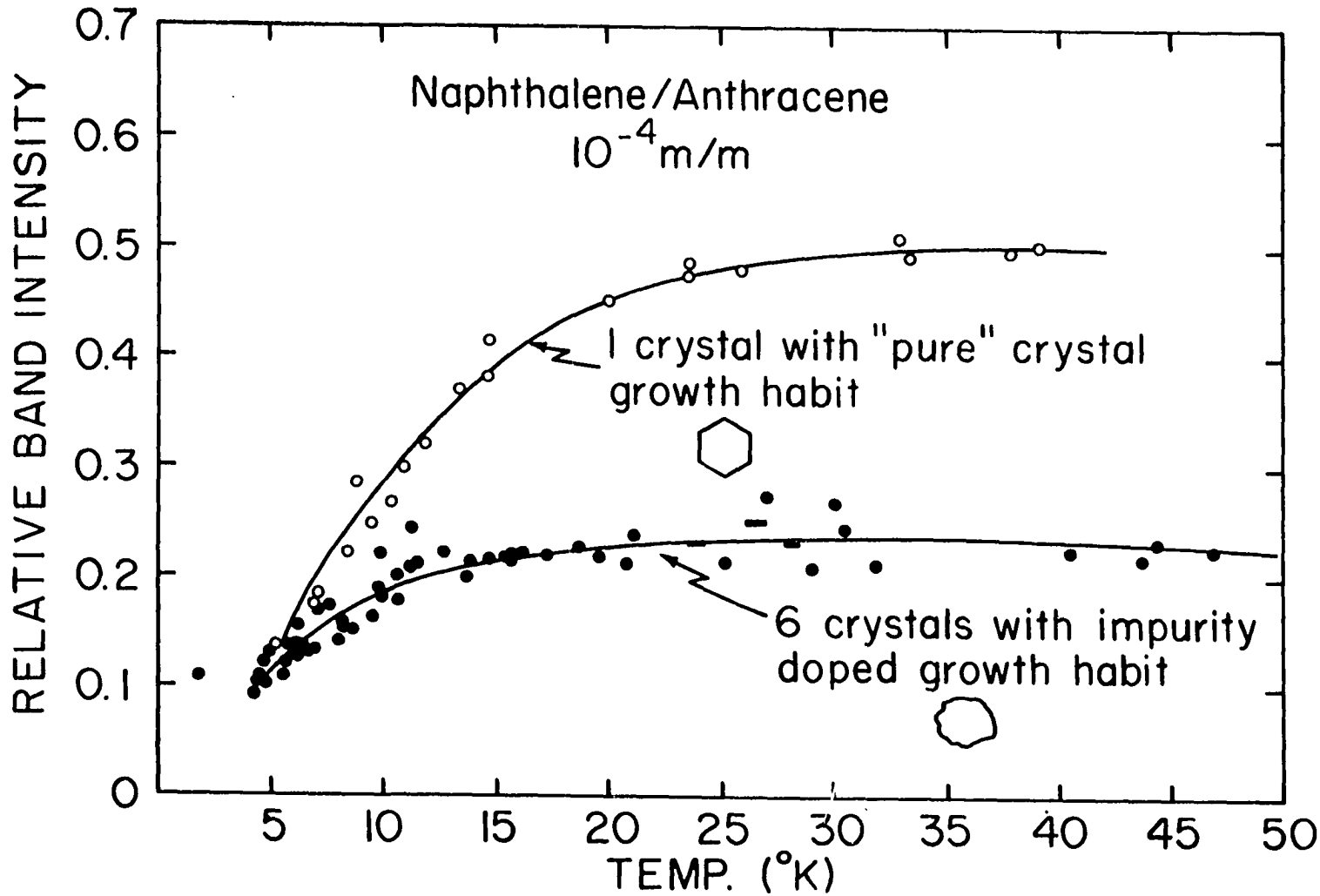

Figure 44. g(0,0) area increase with temperature for anthracene doped naphthalene crystals

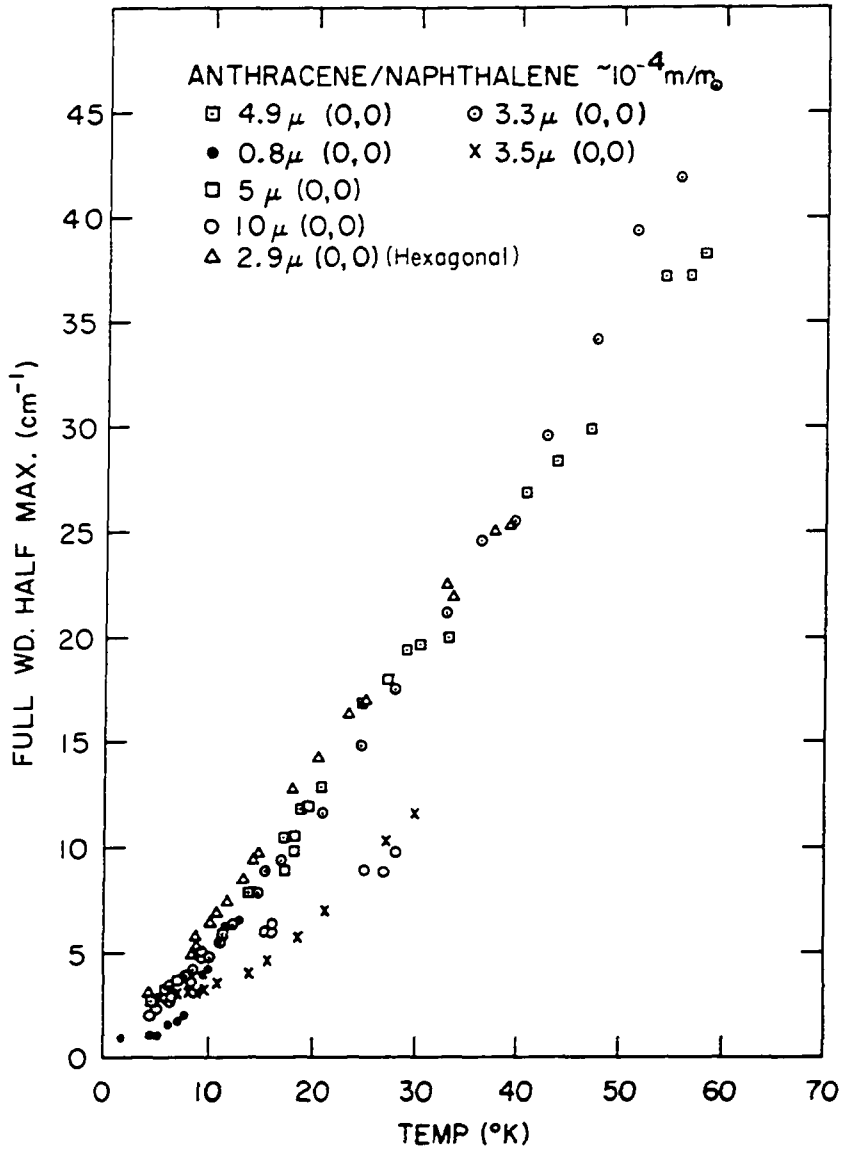

Figure 45. FWHM behavior for anthracene doped naphthalene crystals

Comparison of strained and doped crystal data for an admittedly rather small number of samples leads to the tentative conclusion that strain has a much larger effect on the system than impurity doping, especially if one compares the FWHM behavior. For the severely strained crystals the system appears to have been altered rather fundamentally. Broude and others have studied the effect of strain on molecular crystal absorption bands (281). Broude found for naphthalene that for a crystal grown in a thin quartz cell the $\underset{\sim}{a}(0,0)$ and $\underset{\sim}{b}(0,0)$ Davydov components were separated by only 90 cm^{-1}.

Depolarization spectra

Filinski has pointed out in several papers (280, 281, 282) that polariton effects reported by other workers on semiconductor systems may be due, in part, to depolarization effects. Briefly, Filinski postulates that even in a perfect crystal some photons will lose their polarization and $\vec{k}$ sense in otherwise elastic collisions. Thus, even if no inelastic collisions take place, by detecting polarized light in a small solid angle one may monitor what appears to be a drop in transmission intensity as the temperature increases. (All scattering processes are assumed to increase with temperature). Unfortunately, the dimensions of our cryostat make small solid angle of collection inevitable.

Since in our best polarized crystals $\underset{\sim}{a}(0,0)$ is completely absent at ~4°K, we assume the depolarization effect is small at low temperatures. In order to obtain some feeling for the magnitude of the effect over the temperature range corresponding to our polariton data, several crystals were run using two polarizers, one before and one after the sample. Bands were run with the polarizers aligned parallel for maximum polarization and then the rear polar (between sample and light source) was rotated 90° to minimum transmission intensity. Results varied between crystals but in all cases some depolarized light did come through at the $\underset{\sim}{a}(0,0)$ and $\underset{\sim}{b}(0,0)$ resonances. An interesting observation is that the depolarization spectra look very much like reflectance spectra, Figures 46 and 47. At present we have no rationale for this. It appears that using the depolarization effect one can more accurately locate the energies of broad bands such as $\underset{\sim}{b}(0,0)$, since a sort of second derivative curve is produced. Data for two of the depolarization studies are shown in Figures 46 and 47. For a 6.6 μ crystal (which displayed poor polarization) depolarized light leaked through in the same sense as in the polarized spectrum, i.e., there is a decrease in transmission intensity at the $\underset{\sim}{a}(0,0)$ resonance. As would be expected, the two sets of data for the 6.6 μ crystal ordinary transmission and depolarization show nearly identical increases of relative

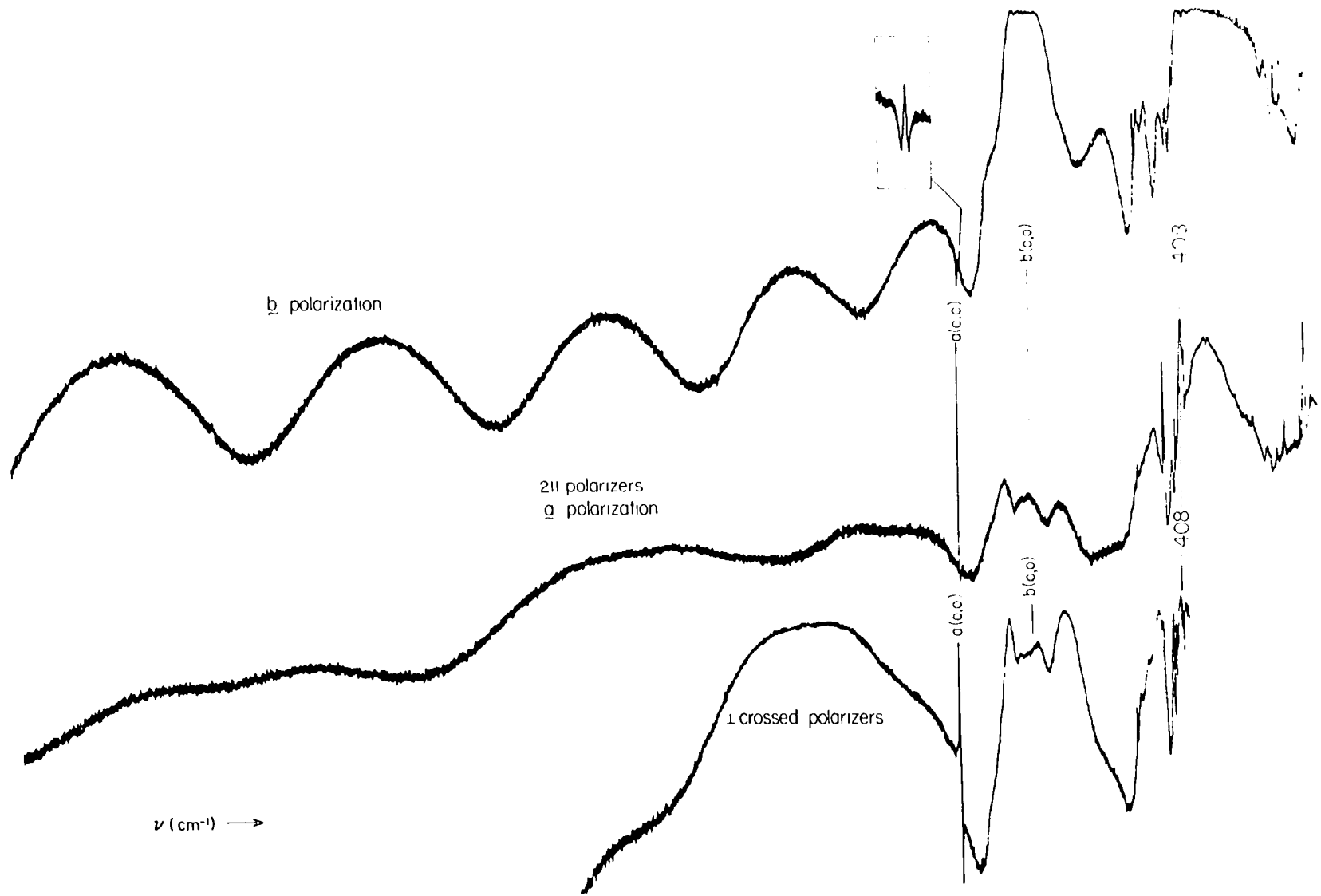

Figure 46. Depolarization effect in $S_{0\leftarrow 1}$ naphthalene spectrum

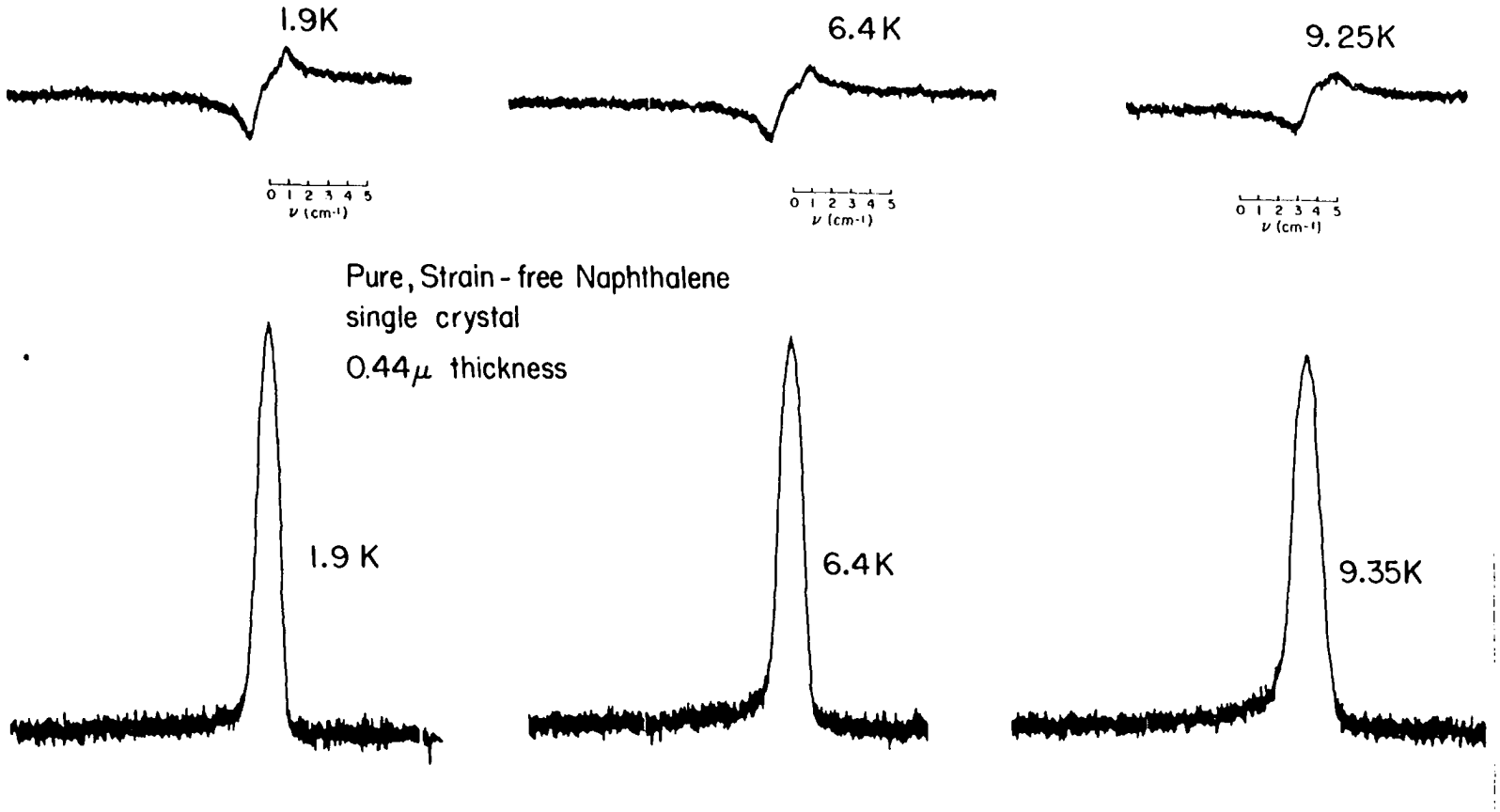

Figure 47. Depolarization effect in perfect crystal $\underset{\sim}{a}(0,0)$ as function of temperature

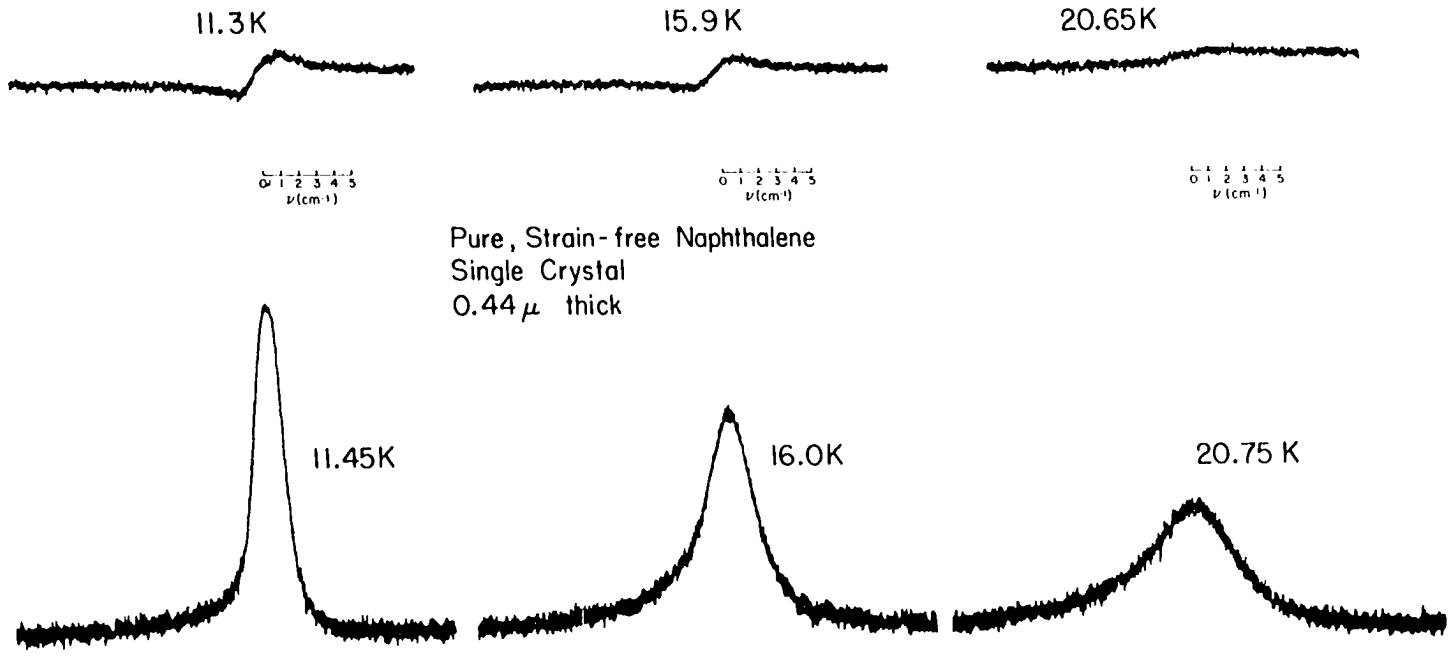

Figure 47. (Continued)

band intensity with temperature. A decrease in depolarized transmission intensity should be a measure of crystal imperfection since apparently real absorption is taking place. On the other hand, if the depolarized intensity increased, this would be a measure of elastic scattering events which destroy polarization sense (but do not change k sense very much, at least in our experimental set-up). For the 0.44 μ crystal showing better polarization the data are ambiguous since it becomes difficult to determine the actual area under the band profiles. It appears that the amount of depolarization decreases.

Emission Experiments

Several (∿2-15°K) emission experiments were done to monitor the presence of βMN in both pure and doped sublimation flakes. The technique appears promising for thinner crystals (∿0.5-2.0 μ). In all cases βMN emission was detected. For crystals doped with 10^{-4} m/m the βMN lines were by far dominant in intensity. For the purest naphthalene, βMN lines were about half as intense as the naphthalene emission lines. In all cases the βMN lines are approximately a factor of ten sharper than those of naphthalene (∿0.5 cm^{-1} *vs* 5 cm^{-1}). This agrees with the trend noted by Colson *et al.* (30) and by Wolf and Von Propste (283). However, the βMN widths reported here are the narrowest to date. These

emission experiments confirm the findings (80,283) that even with repeated purification procedures a small amount of βMN remains in sublimation flakes. We estimate this residual amount to be $\sim 10^{-6}$ m/m.

Exciton-phonon coupling parameters

As mentioned in Chapter 2, several authors have attempted to extract exciton-phonon coupling strengths and active phonon frequencies from Urbach rule treatments of the low energy band edge in absorption (80-86). However, for the naphthalene band profiles recorded here no linear relationship between log K and frequency appears to exist. The handling of raw data itself presents some problems in that the lamp base line (roughly linear) and the overlapping $\underset{\sim}{b}(0,0)$ band at higher temperatures must be subtracted out. Even at the lowest temperatures, where the lamp base line and $\underset{\sim}{b}(0,0)$ are not contributing (i.e., for band ~ 1 cm^{-1} in FWHM) no linear relationship exists. It appears that most of the reported work has been done at higher temperatures (20-298°K) and with crystals which were affixed to a solid support and therefore should be considered as data for the large γ regime. Strain has been shown in our experiments to bring about drastic changes in the pure crystal absorption (transmission) spectra. Strain can be characterized by a large γ, implying strong damping of the polariton wave. Previous explanations have used a parameter σ to fit

temperature dependent data; σ being a measure of the slope of low energy edge as a function of temperature. It is obvious that γ (or actually $1/\gamma$) is equivalent to σ. But γ has the advantage of being physically meaningful in the polariton treatment. Further these results imply that it may be unnecessary to postulate any explicit phonon mechanisms to explain the Urbach rule. Especially for the previously published experimental data, the extraction of a phonon frequency from the σ values seems questionable when one considers the largest scattering mechanism is induced strain. Further, there is no reason to believe the low energy edges of transmission curves for molecules of large oscillator strengths ($f \sim 0.1\text{-}0.001$) reveal very directly the shape of the true absorption since reflection in these cases is a very large correction.

Secondly, we have considered the procedure of Dissado (123,124) for obtaining the phonon modes active in exciton-phonon scattering from experimental band broadening data. As discussed in Chapter 2, it is possible to derive a temperature dependent line width depending essentially on the phonon occupation number $\vec{n}_{\vec{q}s}$ of one (or more) active phonon modes. Dissado has used a formalism similar to this to fit experimental data for anthracene and phenanthrene (123,124). Figure 48 shows the temperature dependence for three active phonons

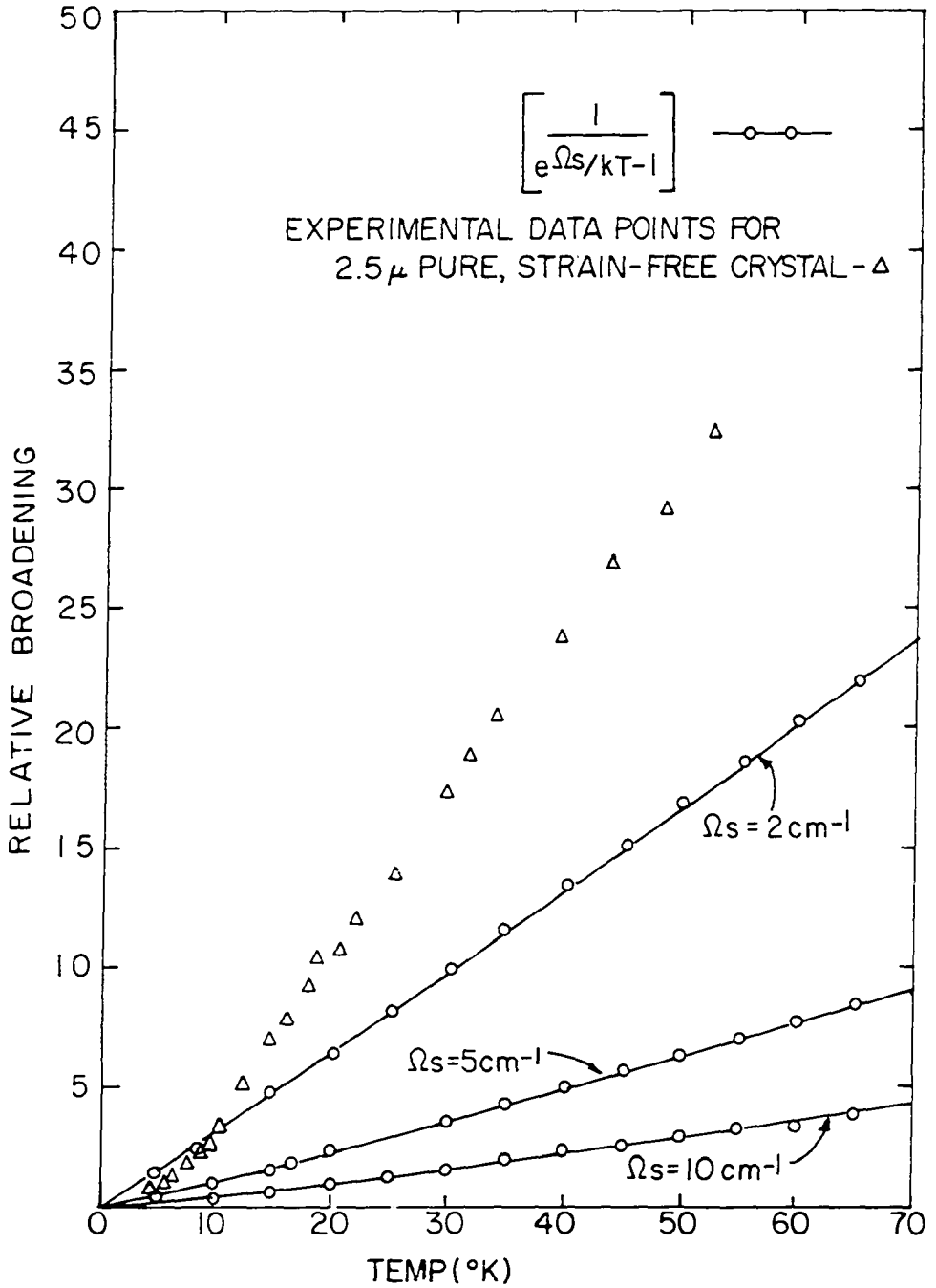

Figure 48. Comparison of experimental band broadening to phonon occupation number curves

(2, 5, 10 cm^{-1}) and a representative experimental curve for naphthalene. It is obvious from the figure that no choice of one (or the sum of several) phonon modes will provide a good fit to the experimental data. It appears that for the anthracene and phenanthrene data the fit looks much better because there are fewer than ten data points from 0° to 300°K with arrow bars approximately the size of a postage stamp on the scale of Figure 48.

CONCLUSIONS

The experimental work presented here demonstrates that in systems for which the oscillator strengths may be considered weak, it is still possible to observe polariton effects due to the temperature dependent nature of the damping, $\gamma(T)$. The temperature increase in absorption intensity in the $\underset{\sim}{a}(0,0)$ band with increasing temperature is certainly the main and most significant result reported in this dissertation. It appears as another feature of the polariton treatment that all transmission bands will show some degree of asymmetry. The asymmetry is seen most clearly in the a origin but is also noted for the b origin (in very thin crystals) by Prikhot'ko and Soskin (276).

Furthermore, it seems obvious that at present no adequate theoretical treatment exists to describe exciton-phonon or polariton-phonon interactions well enough to account for the band-broadening behavior observed when the low temperature region is carefully studied. What is needed as much as a rethinking of the theory is more good (i.e., strain-free, high purity) crystal data at low temperatures.

The marked effects demonstrated for strain and doping should provide a warning with respect to the reliability of even fairly recent experimental results for such quantities as band widths, broadenings, or even Davydov splittings.

Lastly, the computer spectra generated, although admittedly only approximations to the more complicated naphthalene system, have proved extremely helpful in visualizing the experimental effect of increasing $\gamma(T)$ for bands of small ($f \sim 10^{-6}$) and larger ($f \sim 10^{-3}$) oscillator strengths for crystals of varying thicknesses. It cannot be stressed too strongly that the true shape of the absorption curves is given by A = 1-T-R. These curves have no simple of symmetric shape. The true absorption, except at higher temperatures (large gammas) and for weak oscillator strengths cannot be approximated by any regular shape function which as Gaussian, Lorentzian or Voigt profiles.

REFERENCES

1. D. P. Craig and S. H. Wamsley, Excitons in Molecular Crystals (W. A. Benjamin, New York, 1968).

2. A. S. Davydov, Theory of Molecular Excitons (McGraw-Hill, New York, 1962).

3. G. W. Robinson in Annual Review of Physical Chemistry, edited by H. Eyring, C. J. Christensen and H. S. Johnson (Annual Reviews Inc., Palo Alto, California, 1970) vol. 21.

4. R. Kopelman in Excited States, edited by E. C. Lim (Academic Press, New York, 1975).

5. A. S. Davydov, Usp. Fiz. Nauk 82, 393 (1964) [transl.: Sov. Phys.-Uspekhi 82, 145 (1964)].

6. G. Fischer in Transfer and Storage of Energy by Molecules, edited by G. M. Burnett, A. M. North and J. N. Sherwood (John Wiley & Sons, London, 1974).

7. H. C. Wolf in Solid State Physics, edited by F. Seitz and D. Turnbull (Academic Press, New York, 1959) vol. 9.

8. R. S. Knox, Theory of Excitons (Academic Press, New York, 1963).

9. M. R. Philpott in Advances in Chemical Physics, edited by I. Prigogine and S. A. Rice (John Wiley & Sons, New York, 1972) vol. 23.

10. J. Frenkel, Phys. Rev. 37, 17, 1276 (1931).

11. V. L. Broude, W. S. Medvedev and A. F. Prokhot'ko, Zh. Eksp. Teor. Fiz. 21, 665 (1951).

12. D. S. McClure, J. Chem. Phys. 23, 1575 (1955).

13. D. P. Craig and P. C. Hobbins, J. Chem. Soc., 2309 (1955).

14. A. S. Davydov, Zh. Eksp. Teor. Fiz. 18, 210 (1948).

15. R. M. Hochstrasser and P. N. Prasad in Excited States, edited by E. C. Lim (Academic Press, New York, 1974) vol. 1.

16. D. Fox and O. Schepp, J. Chem. Phys. 23, 767 (1955).

17. D. P. Craig and J. R. Walsh, J. Chem. Phys. 25, 588 (1956).

18. V. M. Agranovich, Zh. Eksp. Teor. Fiz. 37, 340 (1959) [transl.: Sov. Phys.--JETP 10, 307 (1960)].

19. P. R. Rimbey, Ph.D. thesis, University of Oregon, 1974 (unpublished).

20. B. R. Johnson and W. T. Simpson, J. Chem. Phys. 65, 4246 (1976).

21. M. R. Philpott, J. Chem. Phys. 58, 588, 595, 639 (1973).

22. M. G. Sceats and S. A. Rice, Chem. Phys. Lett. 44, 425 (1976).

23. D. P. Craig and L. A. Dissado, Proc. Roy. Soc. 325A, 1 (1971).

24. J. Schroeder and R. Silbey, J. Chem. Phys. 55, 5418 (1971).

25. J. S. Avery, Theor. Chim. Acta 39, 281 (1975).

26. H. Winston and R. S. Halford, J. Chem. Phys. 17, 607 (1949).

27. J. Hoshen, R. Kopelman and J. Jortner, Chem. Phys. 10, 185 (1975).

28. E. Glockner and H. C. Wolf, Chem. Phys. Lett. 27, 161 (1974).

29. P. Argyrakis, E. M. Monberg and R. Kopelman, Chem. Phys. Lett. 36, 349 (1975).

30. S. D. Colson, D. M. Hanson, R. Kopelman and G. W. Robinson, J. Chem. Phys. 48, 2215 (1968).

31. H.-K. Hong and R. Kopelman, Phys. Rev. Lett. 25, 1030 (1970).

32. N. V. Rabin'kins, E. I. Rashba and E. F. Sheka, Fiz. Tverd. Tela. 12, 3569 (1971) [transl.: Sov. Phys.--Solid State 12, 2898 (1971)].

33. A. Matsui, K. Tomioka, Y. Oeda and T. Tomotika, Sur. Sci. 37, 849 (1973).

34. G. C. Morris and M. G. Sceats, Chem. Phys. 1, 259 (1973).

35. G. S. Pawley in Transfer and Storage of Energy by Molecules, edited by G. M. Burnett, A. M. North and J. N. Sherwood (John Wiley & Sons, London, 1974) vol. 4.

36. O. Schnepp and N. Jacobi in Advances in Chemical Physics, edited by I. Prigogine and S. A. Rice (John Wiley & Sons, New York, 1972) vol. 22.

37. G. Venkataraman and V. L. Sahni, Rev. Mod. Phys. 42, 409 (1970).

38. M. Sanquer and J. C. Messager, Mol. Cryst. Liq. Cryst. 20, 107 (1973).

39. Bonadeo and G. Taddei, J. Chem. Phys. 58, 979 (1973).

40. P. Weulersse, J. Phys. (Paris) 31, 387 (1970).

41. E. R. Bernstein, J. Chem. Phys. 52, 4701 (1970).

42. R. T. Bailey in Transfer and Storage of Energy by Molecules, edited by G. M. Burnett, A. M. North and J. N. Sherwood (John Wiley & Sons, London, 1974) vol. 4.

43. P. N. Prasad, S. D. Woodruff and R. Kopelman, Chem. Phys. 1, 173 (1973).

44. M. Sanquer and J. Meinnel, C. R. Acad. Sci. Ser. B 274, 1241 (1972).

45. M. Suzuki, T. Yokoyama and M. Ito, Spectrochim. Acta, Part A, 24, 1091 (1968).

46. S. D. Colson and B. P. Klein, Chem. Phys. Lett. 34, 17 (1975).

47. I. I. Kondilenko, P. A. Korotkov and G. S. Litvinov, Opt. Spectrosk. 32, 535 (1972) [transl.: Opt. Spectrosc. 32, 280 (1972)].

48. R. Kopelman, J. Chem. Phys. 57, 3202 (1972).

49. P. N. Prasad and R. Kopelman, J. Chem. Phys. 58, 5031 (1973).

50. M.B.M. Harryman, P. A. Reynolds, J. W. White and J. Kjens in Proceedings of International Conference on Phonons, Rennes, 1971, edited by M. A. Nusimovici (Flammarion, Paris, 1971).

51. D. H. Spielberg, R. A. Arndt, A. C. Damask and I. Lefkowitz, J. Chem. Phys. 54, 2597 (1971).

52. G. S. Pawley and E. A. Yeats, Solid State Commun. 7, 385 (1969).

53. G. J. Small, J. Chem. Phys. 58, 2015 (1973).

54. R. M. Hochstrasser and P. N. Prasad, J. Chem. Phys. 56, 2814 (1972).

55. R. Kopelman, F. W. Ochs and P. N. Prasad, Phys. Status Solidi B 54, K37 (1972).

56. R. Kopelman. F. W. Ochs and P. N. Prasad, J. Chem. Phys. 57, 5409 (1972).

57. E. F. Sheka and I. P. Terenetskaya, Chem. Phys. 8, 99 (1975).

58. G. W. Pawley, Discussions Faraday Soc. No. 48, 125 (1969).

59. G. S. Pawley and S. J. Cyvin, J. Chem. Phys. 52, 4073 (1970).

60. G. S. Pawley, Acta Cryst. Sect. A 30, 585 (1974).

61. P. N. Prasad and R. Kopelman, J. Chem. Phys. 58, 126 (1973).

62. A. S. Davydov, Izv. Akad. Nauk SSSR Ser. Fiz. 34, 483 (1970) [transl.: Bull. Acad. Sci. USSR, Phys. Ser. 34, 416 (1970)].

63. A. S. Davydov and A. A. Serikov, Phys. Status Solidi B 44, 127 (1971).

64. A. Suna, Phys. Status Solidi B 45, 591 (1971).

65. A. Nakamura, J. Chem. Phys. 64, 185 (1976).

66. I. B. Levinson and E. I. Rashba, Rep. Progr. Phys. 36, 1499 (1973).

67. Y. Toyozawa in Proceedings of the 4th International Converence on Ultraviolet Radiation, edited by E. E. Koch, R. Haensel and C. Kunz (Pergamon, Oxford, 1974).

68. P. M. Chaikin, A. F. Garito and A. J. Heegen, Phys. Rev. B 5, 4966 (1972).

69. I. Vilfan, Phys. Status Solidi B 59, 351 (1973).

70. H. Sumi, J. Phys. Soc. Japan 38, 825 (1975).

71. R. A. Bari, Phys. Rev. Lett. 30, 790 (1973).

72. P. Gosar and I. Vilfan, IJS Rep. R564 (Int. Josef Stafan, Yugoslavia) (1969).

73. M. Z. Zgierski, Phys. Status Solidi B 55, 451 (1973).

74. A. Jurgis and E. Silins, Phys. Status Solidi B 53, 735 (1972).

75. M. Z. Zgierski, Phys. Status Solidi B 61, 393 (1974).

76. M. Z. Zgierski, Phys. Status Solidi B 62, 51 (1974).

77. A. S. Davydov and N. I. Kislukla, Phys. Status Solidi B 59, 465 (1973).

78. A. S. Davydov and B. M. Nitsovich, Fiz. Tverd. Tela. 9, 2230 (1967) [transl.: Sov. Phys.--Solid State 9, 1749 (1967)].

79. M. R. Philpott, Prov. Phys. Soc. (London), Solid State Physics 1, 42 (1968).

80. A. S. Krochuk and E. V. Smishko, Opt. Spectrosk. 39, 1098 (1975) [transl.: Opt. Spectrosc. 39, 631 (1975)].

81. K. Cho and Y. Toyozawa, J. Phys. Soc. Japan 30, 1555 (1971).

82. H. Kishi, Y. Ishii and A. Matsui, Solid State Commun. 10, 787 (1972).

83. H. Sumi and Y. Toyozawa, J. Phys. Soc. Japan 31, 342 (1971).

84. J. D. Dow and D. Redfield, Phys. Rev. B 5, 594 (1972).

85. K. Tomioko, H. Amimoto, T. Tomotika and A. Matsui, J. Chem. Phys. 59, 4157 (1973).

86. M. G. Sceats and S. A. Rice, Chem. Phys. Lett. 25, 9 (1974).

87. M. S. Brodin, S. V. Marisova and S. O. Shturkhets'ka, Ukr. Fiz. Zh. 13, 353 (1968).

88. S. Fischer and S. A. Rice, J. Chem. Phys. 52, 2089 (1970).

89. G. C. Morris, S. A. Rice, M. G. Sceats and A. E. Martin, J. Chem. Phys. 55, 5610 (1971).

90. V. K. Dolganov, K. P. Meletov and E. F. Sheka, Izv. Akad. Nauk SSSR Ser. Fiz. 39, 1900 (1975) [transl.: Bull. Acad. Sci. USSR, Phys. Ser. 39, 102 (1975)].

91. G. V. Klimusheva and K. V. Yaremko, Opt. Spectrosk. 31, 243 (1971) [transl.: Opt. Spectrosc. 31, 130 (1971)].

92. M. Z. Zgierski, Acta Phys. Polon. 36, 159 (1969).

93. E. I. Rashba, Fiz. Tverd. Tela. 12, 1801 (1970) [transl.: Sov. Phys.--Solid State 12, 1426 (1970)].

94. A. S. Krochuk, M. V. Kurik and E. V. Smishko, Opt. Spectrosk. 30, 442 (1971) [transl.: Opt. Spectrosk. 30, 243 (1971)].

95. I. I. Abram and R. Silbey, J. Chem. Phys. 63, 2317 (1975).

96. G. C. Morris and M. G. Sceats, Chem. Phys. 1, 1207 (1973).

97. G. C. Morris and M. G. Sceats, Chem. Phys. 3, 332 (1974).

98. G. C. Morris and M. G. Sceats, Chem. Phys. 3, 342 (1974).

99. D. M. Burland, J. Chem. Phys. 59, 4283 (1973).

100. M. V. Kurik and L. I. Tsikora, Fiz. Tverd. Tela. 11, 2624 (1969) [transl.: Sov. Phys.--Solid State 11, 2116 (1969)].

101. V. A. Onishchuk, Ukr. Fiz. Zh. 15, 2007 (1970).

102. S. F. Fisher in International Conference on Luminescence, Leningrad, 1972, edited by F. Williams (Plenum Press, New York, 1973).

103. M. Z. Zgierski, Acta Phys. Polon. A 37, 833 (1970).

104. M. Z. Zgierski, Acta Phys. Polon. A 40, 29 (1971).

105. S. D. Colson, T. C. Netzel and J. M. Van Pruyssen, J. Chem. Phys. 62, 606 (1975).

106. S. D. Colson, Chem. Phys. Lett. 44, 431 (1976).

107. M. Z. Zgierski, Phys. Status Solidi B 57, 405 (1973).

108. S. D. Colson and B. W. Gash, Chem. Phys. 1, 182 (1973).

109. S. D. Woodruff, P. N. Prasad and R. Kopelman, J. Chem. Phys. 60, 2365 (1974).

110. M. R. Philpott, J. Chem. Phys. 51, 2616 (1969).

111. V. K. Dolganov and E. F. Sheka, Fiz. Tverd. Tela. 12, 1450 (1970) [transl.: Sov. Phys.--Solid State 12, 1138 (1970)].

112. A. S. Davydov and A. A. Serikov, Phys. Status Solidi 42, 603 (1970).

113. M. R. Philpott, J. Chem. Phys. 47, 2534, 4437 (1967).

114. V. L. Broude, E. I. Rashba and E. F. Sheka, Phys. Status Solidi B 19, 395 (1967).

115. V. L. Broude, L. M. Umarov and E. F. Sheka, Phys. Status Solidi B 78, 325 (1976).

116. A. A. Serikov, Phys. Status Solidi B 44, 733 (1971).

117. F. B. Slobodskoi and E. F. Sheka, Fiz. Tverd. Tela. 15, 1270 (1973) [transl.: Sov. Phys.--Solid State 15, 860 (1973)].

118. A. Witkowski, Acta Phys. Polon. 30, 431 (1966).

119. P. Reineker in Excitons, Magnons and Phonons in Molecular Crystals, Proceedings of the International Symposium, edited by A. B. Zahlan (Cambridge University Press, Cambridge, 1968).

120. A. Nitzan and J. Jortner, J. Chem. Phys. 58, 2412 (1973).

121. V. K. Dolganov and E. F. Sheka, Fiz. Tverd. Tela. 15, 836 (1973) [transl.: Sov. Phys.--Solid State 15, 576 (1973)].

122. D. P. Craig and L. A. Dissado, Chem. Phys. 14, 89 (1976).

123. L. A. Dissado, Chem. Phys. 8, 289 (1975).

124. L. A. Dissado, Chem. Phys. 33, 57 (1975).

125. T. A. Krivenko, A. V. Leidenmann and E. I. Rashba, Fiz. Tverd. Tela. 17, 137 (1975) [transl.: Sov. Phys.--Solid State 17, 78 (1975)].

126. N. N. Kristofel, Opt. Spectrosk. 35, 307 (1973) [transl.: Opt. Spectrosc. 35, 179 (1973)].

127. H.-K. Hong, Chem. Phys. 1, 348 (1973).

128. M. K. Grover and R. Silbey, J. Chem. Phys. 52, 2099 (1970).

129. S. Takeno, J. Chem. Phys. 46, 2481 (1967).

130. I. S. Osad'ko, Fiz. Tverd. Tela. 13, 1178 (1971) [transl.: Sov. Phys.--Solid State 13, 974 (1971)].

131. P. N. Prasad, Chem. Phys. Lett. 37, 195 (1976).

132. H. Sumi, J. Phys. Soc. Japan 32, 616 (1972).

133. H.-K. Hong and R. Kopelman, J. Chem. Phys. 58, 2557 (1973).

134. R. P. Groffand, R. E. Merrifield and P. Avakian, Chem. Phys. Lett. 5, 168 (1970).

135. J. Fourny, M. Schott and G. Delacote, Chem. Phys. Lett. 20, 559 (1973).

136. M. Trlifaj in International Conference on Luminescence, Leningrad, 1972, edited by F. Williams (Plenum Press, New York, 1973).

137. A. Suna, Phys. Rev. B 1, 1716 (1970).

138. G. Klein, R. Voltz and M. Schott, Chem. Phys. Lett. 19, 391 (1973).

139. M. Trlifaj, Izv. Akad. Nauk SSSR Ser. Fiz. 37, 307 (1973) [transl.: Bull. Acad. Sci. USSR, Phys. Ser. 37, 73 (1973)].

140. A. Bergman, B. Bergman and J. Jortner, Isr. J. Chem. 10, 471 (1972).

141. A. Inoue, K. Yoshihara and S. Nagakura, Bull. Chem. Soc. Japan 45, 1973 (1972).

142. R. C. Powell and R. G. Kepler, Mol. Cryst. Liq. Cryst. 11, 349 (1970).

143. N. E. Gaecintov in Organic Molecular Photophysics, edited by J. B. Birks (Wiley, London, 1973).

144. H. Port and H. C. Wolf, Z. Naturforsch. A 30A, 1290 (1975).

145. A. S. Gaevskii, K. I. Nelipovich and A. N. Faidish, Izv. Akad. Nauk SSSR Ser. Fiz. 39, 2264 (1975) [transl.: Bull. Acad. Sci. USSR, Phys. Ser. 39, 35 (1975)].

146. V. L. Broude, V. K. Dolganov, F. B. Slobodskoi and E. F. Sheka, Izv. Akad. Nauk SSSR Ser. Fiz. 37, 311 (1973) [transl.: Bull. Acad. Sci. USSR, Phys. Ser. 37, 77 (1973)].

147. K. E. Mauser, H. Port and H. C. Wolf, Chem. Phys. 1, 74 (1973).

148. S. Rackovsky, Mol. Phys. 26, 857 (1973).

149. A. V. Solov'ev and N. D. Kurmei, Izv. Acad. Nauk SSSR Ser. Fiz. 39, 1882 (1975) [transl.: Bull. Acad. Sci. USSR, Phys. Ser. 39, 85 (1975)].

150. M. T. Lewellyn, A. A. Zewail and C. B. Harris, J. Chem. Phys. 63, 3687 (1975).

151. R. C. Powell and Z. G. Soos, J. Lumin. 11, 1 (1975).

152. S. H. Tedder and S. E. Weber, Chem. Phys. Lett. 31, 611 (1975).

153. R. P. Groff and R. E. Merrifield, Chem. Phys. Lett. 5, 168 (1970).

154. T. S. Rahman and R. S. Knox, Phys. Status Solidi B 58, 715 (1973).

155. M. Trlifaj, Czech. J. Phys. 22, 832 (1972).

156. R. W. Munn, J. Chem. Phys. 58, 3230 (1970).

157. V. M. Agranovich and Yu. V. Konobeev, Phys. Status Solidi B 27, 435 (1968).

158. Y. Takahashi and M. Tomura, J. Phys. Soc. Japan 29, 525 (1970).

159. M. Drew and D. F. Williams, J. Chem. Phys. 54, 1844 (1971).

160. R. C. Powell and R. G. Kepler in International Conference on Luminescence, Leningrad, 1972, edited by F. Williams (Plenum Press, New York, 1973).

161. F. Vogel and N. Geacintov, Izv. Akad. Nauk SSSR Ser. Fiz. 37, 484 (1973) [transl.: Bull. Acad. Sci. USSR, Phys. Ser. 37, 24 (1973)].

162. M. D. Cohen, E. Klein and Z. Ludmer, Chem. Phys. Lett. 37, 611 (1976).

163. V. Ern, A. Suna, Y. Tomkiewicz, P. Avakian and R. P. Groff, Phys. Rev. B 5, 3222 (1972).

164. R. Braun and H. Killesreiter, Phys. Status Solidi B 48, 201 (1971).

165. M. V. Kurik and Yu. P. Piryatinskii, Fiz. Tverd. Tela. 13, 2877 (1971) [transl.: Sov. Phys.--Solid State 13, 2421 (1972).

166. G. Vaubel and H. Baessler, Mol. Cryst. Liq. Cryst. 12, 47 (1970).

167. R. Kopelman, Phys. Rev. Lett. 34, 1506 (1975).

168. R. Kopelman, E. M. Monberg, F. W. Ochs and P. N. Prasad, J. Chem. Phys. 62, 292 (1975).

169. R. C. Powell, Phys. Rev. B 2, 1207 (1970).

170. Z. G. Soos and R. C. Powell, Phys. Rev. B 6, 4035 (1972).

171. R. C. Powell and Z. G. Soos, Phys. Rev. B 5, 1547 (1972).

172. R. C. Powell, J. Chem. Phys. 58, 920 (1973).

173. R. P. Hememger, R. M. Pearlstein and K. Lakatos-Lindenberg, J. Math. Phys. 13, 1056 (1972).

174. M. Trlifaj, Czech. J. Phys. 23, 250 (1973).

175. P. Reineker, Z. Physik. 261, 187 (1973).

176. D. M. Hanson, Chem. Phys. Lett. 11, 175 (1971).

177. H. Haken and G. Strobl, Z. Physik. 262, 135 (1973).

178. H. Haken and P. Reineker, Z. Physik. 249, 253 (1972).

179. H. Haken and E. Schwarzen, Opt. Commun. 9, 64 (1973).

180. P. P. Schmidt, Mol. Cryst. 5, 185 (1968).

181. M. Pope, J. Burgos and N. Wotherspoon, Chem. Phys. Lett. 12, 140 (1971).

182. L. Peter and G. Vaubel, Phys. Status Solidi B 48, 587 (1971).

183. H. C. Wolf and K. W. Benz, Pure Appl. Chem. 27, 439 (1971).

184. A. Bergman, M. Levine and J. Jortner, Phys. Rev. Lett. 18, 593 (1967).

185. H. B. Rosenstock, Phys. Rev. 187, 1166 (1969).

186. C. P. Heidersdorf, Mol. Cryst. Liq. Cryst. 27, 141 (1974).

187. J. D. Williams and B. P. Clarke, Chem. Phys. Lett. 38, 41 (1976).

188. V. A. Lisovenko and M. T. Shpak, Izv. Akad. Nauk SSSR Ser. Fiz. 39, 2226 (1975) [transl.: Bull. Acad. Sci. USSR, Phys. Ser. 39, 1 (1975)].

189. A. Inoue, J. Phys. Soc. Japan 39, 467 (1975).

190. J. Sworakowski, Pr. Nauk Inst. Chem. Org. Fiz. Politech. Woroclaw 7, 191 (1974).

191. H. Port and H. C. Wolf in Triplet States, Proceedings International Symposium; Beirut, Lebanon, edited by A. B. Zahlan, London, Cambridge, 1967).

192. S. H. Tedder, Chem. Phys. 14, 455 (1976).

193. A. Witkowski and M. Z. Zgierski, Phys. Status Solidi B 56, 755 (1973).

194. F. Anrich and J. Marquard, Chem. Phys. Lett. 11, 167 (1971).

195. M. Higuchi, T. Nakayama and I. Itohi, J. Phys. Soc. Japan 40, 250 (1976).

196. U. P. Wild, H. Känzig and U. B. Ranalder, Helv. Chim. Acta 45, 2724 (1972).

197. H. Kolb and H. C. Wolf, J. Magn. Resonance 7, 374 (1972).

198. V. A. Andreev and V. I. Sugakov, Fiz. Tverd. Tela. 17, 1963 (1975) [transl.: Sov. Phys.--Solid State 17, 1285 (1975)].

199. V. I. Sugakov, Fiz. Tverd. Tela. 15, 2042 (1973) [transl.: Sov. Phys.--Solid State 15, 1362 (1973)].

200. H. Kolb and H. C. Wolf, Z. Naturforsch. A 27, 51 (1972).

201. M. D. Fayer and C. B. Harris, Chem. Phys. Lett. 25, 149 (1974).

202. M. J. Buckley and A. H. Francis, Chem. Phys. Lett. 23, 582 (1973).

203. C. E. Swenberg and N. E. Geacintov in Organic Molecular Photophysics, edited by J. B. Birks (Wiley, London, 1973) vol. 1.

204. U. P. Wild, Top. Curr. Chem. 55, 1 (1975).

205. P. Avakian, Pure Appl. Chem. 37, 1 (1974).

206. P. Avakain and A. Suna, Mater. Res. Bull. 6, 891 (1971).

207. P. Avakian and R. E. Merrifield, Mol. Cryst. 5, 37 (1968).

208. P. E. Shipper, Mol. Phys. 29, 501 (1975).

209. M. S. Brodin, M. A. Dudinskii and S. V. Marisova, Izv. Akad. Nauk SSSR Ser. Fiz. 36, 1047 (1972) [transl.: Bull. Acad. Sci. USSR, Phys. Ser. 36, 946 (1972)].

210. M. S. Brodin, M. A. Dudinskii and S. V. Marisova, Opt. Spectrosk. 34, 1120 (1973) [transl.: Opt. Spectrosc. 34, 651 (1973)].

211. G. C. Morris and M. G. Sceats, Mol. Cryst. Liq. Cryst. 25, 339 (1974).

212. J. Hoshen and R. Kopelman, J. Chem. Phys. 61, 330 (1974).

213. J.-M. Turlet and M. R. Philpott, J. Chem. Phys. 62, 4260 (1975).

214. B. Fischer and H. J. Queisser, C. R. C. Crit. Rev. Solid State Sci. 5, 281 (1975).

215. H. J. Gaehrs and F. W. Willig, Phys. Status Solidi A 27, 355 (1975).

216. U. Hiromu and S. Ichimura, J. Phys. Soc. Japan 41, 1974 (1976).

217. J. J. Hopfield, Phys. Rev. 112, 1555 (1958).

218. J. J. Hopfield, J. Phys. Soc. Japan 21, Suppl. 21, 77 (1966) (Proceedings of the Eighth International Conference on the Physics of Semiconductors, Kyoto, 1966).

219. V. M. Agranovich in Optical Properties of Solids, edited by F. Abeles (North Holland, Amsterdam, 1972).

220. D. L. Mills and E. Burstein, Rep. Prog. Phys. 37, 817 (1974).

221. J. J. Hopfield in Elementary Excitations, edited by A. A. Maradudin and G. F. Nardelli (Plenum Press, New York, 1969).

222. A. S. Davydov, Preprint ITP-75-51E, Institute for Theoretical Physics, Kiev, USSR (1975).

223. A. S. Davydov, Prepring ITP-75-96E, Institute for Theoretical Physics, Kiev, USSR (1975).

224. U. Fano, Phys. Rev. 103, 1202 (1956).

225. S. I. Pekar, Zh. Eksp. Teor. Fiz. 33, 1022 (1957) [transl.: Sov. Phys.--JETP 6, 785 (1958)].

226. S. I. Pekar, Zh. Eksp. Teor. Fiz. 34, 1176 (1958) [transl.: Sov. Phys.--JETP 7, 813 (1958)].

227. S. I. Pekar, Zh. Eksp. Teor. Fiz. 36, 451 (1959) [transl.: Sov. Phys.--JETP 9, 314 (1959)].

228. J. Ferguson, Chem. Phys. Lett. 36, 316 (1975).

229. J. Ferguson, Z. Physik. Chemie (Frankfurt) 101, 45 (1976).

230. Polaritons: Proceedings of the First Taorimina Research Conference on the Structure of Matter, Taorimina, Italy (1972), edited by E. Burstein and F. D. DiMartini (Pergamon Press, New York, 1974).

231. Light Scattering by Phonon-Polaritons, edited by R. Claus, L. Merten and J. Brandmuller, Springer Tracts in Modern Physics 75 (Springer-Verlag, Berlin, 1975).

232. K. L. Kliewer and R. Fuchs in Advances in Chemical Physics, edited by I. Prigogine and S. A. Rice (Wiley, New York, 1974) vol. 27.

233. R. Fuchs, K. L. Kliewer and W. J. Pardee, Phys. Rev. 150, 589 (1966).

234. K. L. Kliewer and R. Fuchs, Phys. Rev. 150, 573 (1966).

235. K. L. Kliewer and R. Fuchs, Phys. Rev. 144, 495 (1966).

236. V. M. Agranovich and Yu. V. Konobeev, Fiz. Tverd. Tela. 3, 360 (1961) [transl.: Sov. Phys.--Solid State 3, 260 (1961)].

237. V. M. Agranovich and V. L. Ginsberg, Spatial Dispersion in Crystal Optics and the Theory of Excitons (Wiley Interscience, New York, 1966).

238. V. M. Agranovich and V. I. Rupasov, Fiz. Tverd. Tela. 18, 801 (1976) [transl.: Sov. Phys.--Solid State 18, 459 (1976)].

239. M. R. Philpott, J. Chem. Phys. 60, 1410, 2520 (1973).

240. M. R. Philpott, Chem. Phys. Lett. 24, 418 (1974).

241. M. R. Philpott, Chem. Phys. Lett. 30, 387 (1975).

242. M. R. Philpott, Phys. Rev. B 14, 3471 (1976).

243. M. R. Philpott, J. Chem. Phys. 65, 3599 (1976).

244. A. S. Davydov and A. A. Serikov, Phys. Status Solidi B 56, 357 (1973).

245. S. Permogorov and V. Travnikov, Phys. Status Solidi B 78, 389 (1976).

246. H. Sumi, J. Phys. Soc. Japan 41, 526 (1976).

247. W. C. Tait and R. L. Weiher, Phys. Rev. 166, 769 (1968).

248. W. C. Tait and R. L. Weiher, Phys. Rev. 178, 1404 (1969).

249. W. C. Tait, Phys. Rev. B 5, 648 (1972).

250. M. R. Philpott and P. G. Sherman, Phys. Rev. B 12, 5381 (1975).

251. M. R. Philpott and J.-M. Turlet, J. Chem. Phys. 64, 3852 (1975).

252. G. S. Kovener, R. W. Alexander, Jr. and R. J. Bell, Phys. Rev. B 14, 1458 (1976).

253. M. F. Bishop, A. A. Maradudin and D. L. Mills, Phys. Rev. B 14, 4744 (1976).

254. A. A. Maradudin and W. Zierau, Phys. Rev. B 14, 484 (1976).

255. J. Lagois and B. Fischer, Sol. State Commun. 18, 1519 (1976).

256. J. Voigt, Phys. Status Solidi B 64, 549 (1974).

257. A. A. Delyukov and G. V. Klimusheva, Fiz. Tverd. Tela. 16, 3255 (1974) [transl.: Sov. Phys.--Solid State 16, 2116 (1975)].

258. F. I. Kreingol'd and V. L. Makarov, Fiz. Tverd. Tela. 17, 472 (1975) [transl.: Sov. Phys.--Solid State 17, 297 (1975)].

259. A. Bosacchi, B. Bosacchi and S. Franchi, Phys. Rev. Lett. 36, 1086 (1976).

260. M. S. Brodin, M. A. Dudinskii, S. V. Marisova and E. N. Myasnikov, Phys. Status Solidi 74, 453 (1976).

261. J. Lagois and B. Fischer, Phys. Rev. Lett. 36, 680 (1976).

262. F. DiMartini, G. Giuliani, P. Mataloni, E. Palange and Y. R. Shen, Phys. Rev. Lett. 37, 440 (1976).

263. S. L. Robinette and G. J. Small, J. Chem. Phys. 65, 837 (1976).

264. S. A. Rice and J. Jortner in Physics and Chemistry of the Organic Solid State, edited by D. Fox, M. M. Lakes and A. Weissberger (Interscience Publishers, New York, 1967) vol. III.

265. R. E. Peierls, Ann. Physik. 13, 905 (1932).

266. G. H. Wannier, Phys. Rev. 52, 191 (1963).

267. R. P. Feynman in The Feynman Lectures, Addison-Wesley, Reading, Mass., 1964, vol. II.

268. E. E. Koch, A. Otto, and K. L. Kliewer, Chem. Phys. 3, 362 (1974).

269. F. W. Byron and R. W. Fuller, Mathematics of Classical and Quantum Physics, Addison-Wesley, Reading, Mass., 1970, vol. II.

270. A. S. Davydov, Theory of Molecular Excitons [transl.: Plenum Press, New York, 1971].

271. L. Merten and G. Borstel, Z. Naturforsch. 27a, 1792 (1972).

272. R. R. Alfano and T. G. Giallorenzi, Opt. Commun. 4, 271 (1971).

273. D. L. Johnson and P. R. Rimbey, Phys. Rev. B 14, 2398 (1976).

274. S. I. Pekar and M. I. Strashnikova, Zh. Eksp. Teor. Fiz. 68, 2047 (1975) [transl.: Sov. Phys.--JETP 41, 1024 (1976)].

275. D. L. Johnson, submitted to Phys. Rev. Lett.

276. V. Sethuraman, unpublished results.

277. D. P. Craig and L. A. Dissado, unpublished results.

278. A. F. Prikhot'ko and M. S. Soskin, Opt. Spectrosk. 13, 522 (1962) [transl.: Opt. Spectrosc. 13, 291 (1962)].

279. D. S. McClure and O. Schnepp, J. Chem. Phys. 23, 1575 (1955).

280. D. P. Craig, L. E. Lyons and J. R. Walsh, Mol. Phys. 4, 97 (1961).

281. V. L. Broude, Opt. Spectrosk. Suppl. 2, 49 (1963) [transl.: Opt. Spectrosc. Suppl. 2, 25 (1966)].

282. I. Filinski, Phys. Stat. Solidi b 49, 577 (1972).

283. I. Filinski, results presented at the Taorimina Conference, 1976, unpublished.

284. I. Filinski in Molecular Spectroscopy of Dense Phases, Proceedings of the 12th European Congress on Molecular Spectroscopy, Strasbourg, France, July 1975, edited by M. Grosmann, S. G. Elkomos and J. Ringeissen (Elsevier, Amsterdam, 1976).

285. H. C. Wolf and A. Von Propste, Z. Naturforsch. 18A, 724 (1963).

ACKNOWLEDGMENTS

It's a pleasure to acknowledge the people whose help has made this dissertation possible. First, I must thank my research advisor, Dr. Gerald J. Small, for many helpful and enjoyable discussions and for all his help and encouragement. The enthusiasm he brought to the project helped make the polariton work a success.

Drs. Kenneth Kliewer, Peter Rimbey and David Johnson generously shared their insights into the polariton problem and Dr. Kliewer provided the programs which made the computer calculations possible. Dr. V. Sethuraman kindly provided assistance with the exciton-photon theory which appears herein, and in the course of our acquaintance he has often managed to teach me some physics. Lastly, my typist, Sue Musselman, must be thanked for a splendid job.

The following people also helped: Dr. Jerome Ostenson, Dr. John Hayes, Richard Palmer, Larry Barr, Lenore Nordyke, Bruce Golden, Roger Clark, Robert Eades, Dr. Richard Kniseley, Dr. John McClelland, John Richard, Denny Salisbury, Denny Lindeman, Aggie Oh, Victor Chen, Wen-Fang Hwang, Phillip Fanwick, Dr. Don S. Martin, Merl Frette, Gary Johnson, Ilo M. Severs, Gary Wells, Thomas Johnson, Harry Amenson, Jerry Hand, Harold Hall, Edgar Moore, Charles Patterson, Ida Sachan, and Thomas Weller.

Last, but not least, I want to thank Marie, Tim, Ron, Pat and the other folks at The Quarter Stove for fixing me all those good lunches.

Thanks everyone.